Estimation of Ecological Risk of Oil Spills in Ice-Covered Waters: A Surface Slick Model Coupled with a Food-Web Bioaccumulation Model

By

© Guilherme Dias Bernardino de Oliveira

A thesis submitted to the School of Graduate Studies

in partial fulfillment of the requirements for the degree of

Master of Engineering

Faculty of Engineering and Applied Science
Memorial University of Newfoundland

October 2019

St. John's, Newfoundland, Canada

Abstract

The limited knowledge on the Arctic environment and ecology leads to uncertainties in case of oil spills resulting from shipping and oil and gas activities enabled by a more accessible Arctic, as ice retreats due to climate changes. The behavior of oil in ice-covered waters is also not fully understood and, although models have been developed and adapted to ice conditions, gaps in knowledge still exist. The present work aims at the definition of the ecological risk posed by an oil spill in the Arctic by the implementation of two methodologies, introduced on Chapters 3 and 4. On the first part, the fate of surface oil slicks formed after an oil spill in ice-infested waters is examined and improvements are suggested to existing transport and weathering algorithms in order to represent all processes as a function of ice coverage. In addition, a new algorithm is proposed to model the phenomenon of oil entrainment in ice, a process so far neglected in current models. On the second part, a fugacity-based food-web bioaccumulation model is proposed to determine the ecological risk introduced by oil spills to a hypothetical Arctic food web consisting of three species' representative of the Arctic ecosystem characterizing three trophic levels linearly related. This is done in three steps: first, the model estimates the distribution of a toxic component of oil – namely naphthalene – in the multimedia environment; then, the transfer of contaminant throughout the food web is predicted; lastly, the bioaccumulation potential and the ecological risk profile are defined as a function of respectively the Bioconcentration Potential (BCF) and the Risk Quotient (RQ). The present thesis thus provides a complete picture of an oil spill scenario in ice-covered waters, and emphasis is given in the implications of such events to the unspoiled Arctic ecosystem.

Acknowledgements

I would like to express my gratitude to my supervisors Dr. Faisal Khan and Dr. Lesley James for all support and availability during my research, guiding and directing my work. Also, for the extraordinary opportunity given to participate on the 2017 NTNU-MUN INTPART, an experience that was very meaningful to me and of great importance to my academic and professional development.

I also would like to thank all members of C-RISE who somehow contributed to this thesis with their knowledge and expertise, friendly helping me whenever I needed.

Finally, I thank my parents José Antonio and Maria Cristina, as well as my brother Fellipe, who have always been supportive to all my decisions and provided me with all resources I ever needed in my studies and in my life.

Table of Contents

List of Tables

List of Figures

List of Abbreviations and Symbols

AMAP	Arctic Monitoring Assessment Programme
BCF	Bioconcentration Factor
DAMSA	Danish Maritime Safety Administration
OSCAR	Oil Spill Contingency and Response
PAH	Polycyclic Aromatic Hydrocarbons
PEC	Predicted Exposure Concentration
PISCES 2	Potential Incident Simulation, Control and Evaluation System
PNEC	Predicted No Effect Concentration
RQ	Risk Quotient
SINTEF	*Stiftelsen for industriell og teknisk forskning* (Norwegian) – The Foundation for Scientific and Industrial Research
SMHI	Swedish Meteorological and Hydrological Institute

Chapter 1: Introduction and Overview

1.1 Background

The behavior of oil when spilled in the sea has long been investigated by researchers seeking a better understanding of its fate after an accident occurs. Research in this area is of great importance for companies and governmental agencies that need reliable information on where the oil is travelling to and how environmental pressures such as wind and ocean currents will affect its fate. This information will subsidize emergency response actions and the accuracy of this information is highly dependent on adequate prediction models, which must consider the particularities of different spill scenarios.

Despite the extensive understanding of transport and fate of oil when spilled in open waters, the behavior of oil in ice-infested waters and the consequences of an oil spill in those environments are still not well understood. Predicting the interaction of oil with ice remains as a challenge for modelers due to the lack of data for validation of existing algorithms and models, as well as to the incipient state of knowledge of the Arctic environment.

As climate change makes parts of Arctic regions ice-free for longer periods and therefore more accessible to ships throughout the year (Yang et al., 2015), the Arctic Ocean and its marginal seas become important routes for marine traffic, increasing the risk of oil spills as a result of accidents. Also, it is estimated that up to 30% of undiscovered gas and

13% of undiscovered oil reserves are in the Arctic (Kjær, 2014), making it the next frontier for the oil and gas industry.

Accidents may occur in the form of collision between vessels, between vessels and icebergs or sea ice, well blowouts in drilling or production operations, leakage on risers and subsea pipelines or structures, fueling operations, loading and offloading of oil tankers, amongst a variety of other possible scenarios that represent great potential for oil pollution in the pristine Arctic environment (Arctic Council, 2015).

Due to the harsh nature of the Arctic environment, the likelihood of accidents is expected to be higher than in temperate and tropical regions, given factors such as (Arctic Council, 2015):

- Presence of ice in various forms (first-year, multi-year, icebergs, etc.)
- Extremely cold temperatures, leading to icing of structures and hazardous wind chills;
- Severe weather events such as polar lows;
- Low visibility due to constant fog and snow;
- Darkness during the winter.

From the consequence's perspective, an oil spill in the Arctic also introduces some complicating aspects when compared to spills in other locations. From an ecological standpoint, the Arctic is a very sensitive region due to its simple trophic structure, low ecological diversity and highly seasonal ecosystems (Yang et al., 2015). As a result, it displays a low resilience to external disturbances, hence oil pollution can impact severely its fragile ecological equilibrium. In addition, the remoteness imposes great challenges in

terms of spill response logistics, which may lead to delayed emergency response actions resulting in larger contaminated areas. The harsh nature of the Arctic environment also represents a barrier for oil spill response in terms of deployment of recovery equipment in severe weather or in high ice concentrations, meaning that emergency response actions are not feasible in many cases. Lastly, oil spilled in cold ice-covered waters may persist longer than in temperate climates (Yang et al., 2015) as weathering processes such as evaporation, dispersion and biodegradation occur at slower rates.

A framework of algorithms adapted for ice conditions and in their original forms have been proposed by some authors to model oil fate in the Arctic (Afenyo et al., 2015; Yang et al., 2015; Arneborg et al., 2017; Fingas & Hollebone, 2015), but no emphasis has been put on the different possible outcomes of an oil spill given different ice conditions. Another aspect that has been neglected is the influence of encapsulation and entrainment of oil in ice on the overall fate of the oil slick. The uptake of oil by the ice sheets above it can be a major source of oil removal from the water column and the ice floes can act as real reservoirs, storing a considerable part of the spilled oil inventory and taking it to locations far from the original spill site. This mode of transport cannot be predicted by conventional models designed for spills in open waters.

Fugacity-based models have been explored by Yang et al. (2015) and Afenyo et. al. (2016) to estimate the fate of oil in ice-infested waters, and the applicability of the methodology for predicting the mass balance of more soluble oil components, namely, polycyclic aromatic hydrocarbons (PAH) in the environment has been demonstrated. The fugacity approach is a methodology that enables the calculation of transport and

transformation rates, tendency for accumulation and concentration profiles of contaminants in the environment (Mackay, 1979). It translates the escaping tendency of chemicals from a phase into a framework of mathematical relationships that can be used to describe in a simple fashion the partitioning of contaminants in a multi-phase environment. Every relevant environmental process can be described mathematically and accounted for in the calculations and one can include as many environmental media as required for the analysis.

As an extension of the fugacity approach, food-web bioaccumulation models can be defined using its concepts to investigate the uptake of chemicals from water or sediment by organisms and its transfer throughout trophic levels in a given food web. Here, fish and other organisms are regarded as additional bulk phases in the multimedia evaluative environment and processes like uptake from water though gills, uptake from food, metabolism and growth dilution are included in the calculations. Bioaccumulation is described in terms of bioconcentration and biomagnification, which are the uptake by respiration from water and by food, respectively (Mackay, 2001). Models can be developed to simulate chemical uptake by organisms from any food web, from simple and linear to more complex branched structures, and species can be included as many as deemed relevant for the study.

The fugacity concept is not new and has been extensively applied to study the distribution of chemicals in the environment, yet to date only a few works have made use of this approach to model oil fate in ice covered waters and to access environmental risk of oil-in-ice events. Moreover, the application of food-web bioaccumulation models using fish and other organisms as bulk phases for multimedia oil spill modeling in ice covered

waters has been little explored in literature, although represents a valuable tool for ecological risk assessment.

1.2 Objectives

The present work aims at demonstrating the environmental outcome of oil spills in ice-infested waters as a function of sea ice coverage. This is done through the integration of two different modeling approaches: First, the surface oil slick fate is modeled using a set of modified transport and weathering algorithms adapted for the conditions under investigation, that is, oil in ice. On the second part, a multimedia fugacity model is integrated in the context to simulate the mass balance of low-concentration and more soluble oil components in the selected environmental compartments. A food-web model is then applied to define how the oil will be transferred throughout three trophic levels, having fish representing the highest level and therefore the target of the analysis. Given the partition of oil in the evaluative environment, the risk profile is deducted as a function of concentration in water and bioaccumulation in fish. In summary, the objectives of this thesis are:

- Improve oil-in-ice models and study the influence of different ice coverages in oil transport and weathering processes;
- Determine the level of risk posed by oil spills in ice-covered waters to the Arctic ecosystem.

1.3 Thesis Outline

This thesis is written in a manuscript format and is structured in five chapters as described below:

Chapter 1 introduces the research done and describes the concepts of oil spill fate modeling to be developed in the thesis, as well as the main objectives of the work.

Chapter 2 provides a literature review on the key elements of the thesis, including the state of knowledge of oil spill transport and weathering modeling in ice-infested waters and the algorithms applied, an overview of multimedia fugacity models and of food-web bioaccumulation models.

Chapter 3 presents the methodology for the surface oil transport and weathering model in ice-infested waters and demonstrates the application of the developed model to a real spill, providing a discussion emphasizing the different outcomes given different ice conditions, along with the conclusions from this part of the work.

Chapter 4 presents the multimedia fugacity model proposed to accomplish the main goal of the thesis: determine the partition of oil components in the environment and the transfer of the contaminant in the food web, as well as define the environmental risk associated with the oil release for different ice conditions. In this Chapter it is also described how this part integrates the first part of the work (Chapter 3) in the broader picture of the thesis.

Chapter 5 summarizes the overall results accomplished by the research, including concluding remarks and recommendations for future works.

Chapter 2: Literature Review

Several models have been developed to simulate changing oil properties and the transport of slicks after oil is released in the sea. Some models are focused on weathering properties of oil in the environment, others on slick transport, whereas some would give a more complete picture of oil fate, encompassing both weathering and transport aspects, thus providing a more realistic simulation. Also, some models include a module for simulating environmental outcomes of oil spills in selected valued ecosystem (Johnsen et. al., 2012).

For ice-covered waters, different approaches have been developed to incorporate ice dynamics and cold-water characteristics into the models, both by adding an ice drift model to the calculations and by adapting existing algorithms to ice conditions. The presence of ice alters all transport and weathering processes, most of which will occur at lower rates than in ice-free and warmer waters. Many authors have focused in the spreading of oil in and under ice (Brandvik et al., 2006), although important processes such as natural dispersion, evaporation, emulsification and entrainment in ice have received less attention and are therefore not well understood in ice conditions.

In order to produce realistic outputs, oil spill models are often combined with hydrodynamic and meteorological models, which provide information on wind, ocean currents and waves used as input for the oil transport and weathering model (French-McCay et al., 2017). In ice-infested waters, these models are also integrated by an ice drift model, employed to simulate ice drift rates, ice coverage and thickness (French-McCay et

al., 2017). The accuracy of the integrated oil-in-ice model will be highly dependent on the quality of data generated by the ice model, as the oil will be mainly transported with ice for medium to high ice concentrations. However, predicting ice movement is challenging due to the highly dynamic nature of sea ice. According to Brandvik et al., 2006, our limited ability to model the behavior of ice represents a key problem in oil modeling in ice-covered waters.

Furthermore, the oil transport and weathering algorithms used in open-waters models need calibration and modifications to be able to represent the behavior of oil in the presence of ice. Consequently, the importance of each process in the context of ice-infested waters will differ from that in temperate and tropical waters, as well as the partition of contaminants in the different environmental compartments.

Fugacity-based models in ice infested waters have been explored by Yang et al. (2015) and Afenyo et al. (2016a) to predict the partition of oil's toxic components in evaluative environments including ice cover as a compartment in the analysis. The applicability of this methodology for Arctic environments has been demonstrated and it represents a promising approach for environmental assessment in ice-covered waters.

The next sub-chapters will explore the existing knowledge on surface oil slick transport and weathering and on fugacity-based models for multimedia oil-in-ice modeling.

2.1 Surface Oil Transport and Weathering in Ice-Infested Waters

Afenyo et al. (2015) carried out an extensive review on fate and transport of oil spills in ice-infested waters, highlighting key factors for each process and identifying the

available algorithms for oil-in-ice modeling. According to the authors, not many models are available for ice-covered waters to date, as an example of the Oil Spill Contingency and Response (OSCAR) model, from SINTEF. Developed by the Swedish Meteorological and Hydrological Institute (SMHI) and the Danish Maritime Safety Administration (DAMSA), the Seatrack Web model can also simulate oil spills in ice-infested waters, using a set of modified oil transport and weathering algorithms.

When oil is spilled in the sea, it quickly forms a slick on the surface, which increases in size and undergoes a series of processes that will result in change in its position and in physicochemical properties, the former regarded as transport and the latter as weathering. All processes occur simultaneously and are inter-dependent, that is, changes in one process will influence all other processes involved. For example, the evaporation of oil will result in increase in viscosity. This increase in viscosity will reduce both the spreading and the natural dispersion rate.

The presence of ice retards the rate in which weathering processes occur and spreading of oil is limited by the ice floes, which act as natural barriers against the gravity-viscous spreading forces. The ice concentration, the type of ice present and the water temperature will play a major role on the prediction of oil fate and, along with information on oil properties and spill scenario, will determine how the oil slick will behave in the ocean. Venkatesh et al. (1990) suggested three classes of ice concentration for modeling purposes: $C<30\%$ for low concentrations; $30\% \leq C \leq 80\%$ for medium concentrations; and $C>80\%$ for high concentrations. In general, the following set of information is required as input for modeling oil spills in ice-infested waters:

- Type of ice present: first year ice, multi-year ice, land fast ice, pack ice, brash ice, slush ice;
- Concentration of ice in water;
- Oil properties: density, viscosity, boiling point, oil/water interfacial tension. Additional parameters may be required depending on the type of analysis performed;
- Spill scenario: spill volume (for instantaneous release), spill flow rate and duration (for continuous release), spill source (subsea, water surface, on or under ice, on leads or polynyas);
- Meteorological and oceanographic conditions: wind and current speed and direction, wave heights, water and ambient temperature.

When developing a model, one can select as many processes as deemed appropriate for the conditions under analysis. Depending on the context and the objectives of the model, some processes will be more important whereas some will not be relevant, and specialized judgement should be made when selecting the processes to be included in the analysis.

Overall, the processes that oil undergoes when spilled in the sea can be classified in two categories: transport and weathering. Transport processes are those that will result in change in the oil slick position defining its trajectory in the ocean after the release but won't affect its physicochemical properties. Oil is transported by ocean currents, winds and waves as well as under gravitational spreading forces, and transport processes include advection, spreading, sedimentation, natural dispersion and, for ice-covered waters,

encapsulation and entrainment in ice. Weathering processes are regarded as those responsible for the change in physicochemical properties of oil under the action of temperature, wind, waves and degradation driven by bacterial and sunlight activity. It encompasses the processes of evaporation, emulsification, dissolution, biodegradation and photo-oxidation.

The next sub-sections will explore in more details the processes relevant for oil slick transport and weathering in ice-infested waters: advection, spreading, natural dispersion, entrainment in ice, evaporation and emulsification. The processes of sedimentation, dissolution, biodegradation and photo-oxidation are not relevant for the fate of surface oil but are considered under the context of the fugacity modeling, explored in section 2.2.

2.1.1 **Advection**

Advection is the process in which oil is transported by winds and ocean currents and can be expressed as the combination of velocities, as Eq. (2.1) below.

$$\frac{dx}{dt} = U_{current} + 0.035\, U_{wind} \tag{2.1}$$

Where x is the coordinate of the center of mass of the oil, $U_{current}$ is the depth-averaged current velocity and U_{wind} is the wind velocity 10 m above water surface. A component accounting for turbulent diffusion can be added to the equation, although its effect can be neglected in most cases. In order to account for advective transport of oil, some models include a hydrodynamic module that produces forecasts used as input for the oil spill modeling (Afenyo et al., 2015).

In ice-infested waters, oil will mainly move with ice for ice concentrations above 30% and will move freely as if in open waters for concentrations below that. If the velocity difference between ice and water exceeds a threshold, typically of magnitude of 0.2 m/s, oil will move with the water current instead (Arneborg et al., 2017). Experimental results from Buist et al. (1987) indicated that oil in pack ice does not drift relative to the surrounding ice floes and that ice floes drift at approximately 3% of the wind speed at 10 m above the sea level.

2.1.2 **Spreading**

Spreading is a self-driven transport process by which oil slicks increase in area under the action of gravitational, viscous and surface tension forces. According to Fay (1969), oil spreads progressively according to three phases: gravity-inertia, gravity-viscous and viscous-surface tension. On the first phase, when the slick is thick, it spreads as a result of competing forces of gravity (stronger, acting outwards) and inertia (acting against the gravity to prevent the slick from spreading). The slick area continues to increase, and this phase progresses up until the point in which inertia forces are no longer important and the oil viscosity becomes relevant to the process. Then, the gravity-viscous phase, which is the most important spreading regime and the one that lasts the longest, begins. Here, the gravity spreading force is counteracted by the viscosity of oil, which continues to regulate the spreading rate until the slick thickness is small enough for the interfacial tension between oil and water to become important and begin to affect the spreading. Subsequently, the viscous-surface tension is the last spreading phase, when gravity no longer controls the spreading rate. The interfacial tension between oil and water becomes the driver of

spreading until, after a certain time, the oil ceases to spread due to a balance between buoyancy (gravitational) and net interfacial tension forces (Yapa & Chowdhury, 1991).

Fay (1969) proposed a set of three equations to model spreading for each phase:

$$A = 4.1\,(Vg't^2)^{0.5} \quad \rightarrow \quad Gravity - Inertia \tag{2.2}$$

$$A = 6.6\left(\frac{V^2 g'}{\sqrt{\mu/\rho}}\right)^{1/3} t^{0.5} \quad \rightarrow \quad Gravity - Viscous \tag{2.3}$$

$$A = 16.6\left(\frac{\sigma^2 t^3}{\rho\mu}\right)^{1/2} \quad \rightarrow \quad Surface\ tension - Viscous \tag{2.4}$$

Where A is the spill area (m^2); V is the spill volume (m^3); ρ is the water density (kg/m^3); ρ_0 is the oil density (kg/m^3); g is the acceleration of gravity (m/s^2); μ is the dynamic viscosity of water (Pas); σ is the oil/water interfacial tension (N/m); t is the elapsed time (s); and:

$$g' = g\frac{(\rho - \rho_o)}{\rho}$$

It is interesting to note that each of the equations explicitly includes a term for the dominant force acting at a given phase, e.g., the gravity-inertia equation is written as a function only of the density differential between water and oil; the gravity-viscous is a function of both the density differential and the water viscosity; and the surface-tension phase is a function of water viscosity and the interfacial tension between oil and water.

Most models describe the oil spreading in terms of the gravity-viscous phase only, as this is the predominant regime and in many cases the gravity-inertia and the surface tension-viscous phases are not relevant for modeling purposes.

When ice is present, the rate of oil spreading is determined by a combination of factors, including oil viscosity, oil-ice interfacial tension and under-ice topography (Wilkinson et al., 2007), as well as ice concentration. The gravity-inertia phase only lasts for a very short time and surface tension-viscous phase is not present (Yapa & Belaskas, 2010). Experiments conducted by Ross & Energetex (1985) identified a correction factor to be applied to Eq. (2.3) to account for oil viscosity. After some algebra, it can be demonstrated that the inclusion of the correction factor is equivalent to the replacement of the water viscosity, μ, for the oil viscosity, μ_{oil} in the equation. Later, Buist et al. (1987) suggested another correction factor to account for ice concentration. The resulting adjusted equation is then:

$$A = (1 - c)\ 6.6 \left(\frac{V^2 g'}{\sqrt{\mu_{oil}/\rho}} \right)^{1/3} t^{0.5} \tag{2.5}$$

Where c is the ice concentration (%) and μ_{oil} is the dynamic viscosity of oil (Pas). Several algorithms have been developed for modeling oil spread in different ice environments and the work from Afenyo et al. (2015) offers a description of some of the most scientifically accepted and used in current available models. As the majority of spreading models are empirical formulations derived from lab experiments, limitations exist and validation has still not been fully performed in real field conditions.

Gravitational spreading is assumed to cease when the slick thickness reaches a given terminal thickness, at which buoyancy forces acting outwards are in equilibrium with surface tension forces, acting inwards. As the slick area grows, it becomes progressively thinner up until it reaches a minimum value, resulting in the termination of the spreading. It is believed that this final thickness will be a function of oil viscosity, but studies on oil spreading are not conclusive on that matter. In ice-covered waters, terminal thickness will be also a function of ice thickness and coverage, and some studies indicate that the final slick thickness will be greater the higher the ice coverage. Yapa & Chowdhury (1990) obtained an equation to define the minimum slick radius under ice by equating the acting buoyancy force to the net interfacial tension, assuming that the termination of spreading occurs due to a balance between these two forces. Further, Venkatesh et al. (1990) developed a set of four equations to model oil slick thickness. The first and second formulations defined the slick thickness for oil in cold waters and in particle ice, respectively, and both were written as a function of oil viscosity. The third formulation described the slick thickness under ice, and it was defined as a function of the overlying ice thickness only. Finally, the fourth equation was intended to model the slick thickness in high ice concentrations in terms of ice thickness and of a ratio between oil and seawater densities. Nazir et al. (2007) used a final value of 0.01 cm in his work for the open water case.

2.1.3 **Natural Dispersion**

If waves or other turbulence sources are present on the sea surface, natural dispersion of oil – also known as entrainment in water – may occur. In natural dispersion,

oil droplets are driven permanently or temporarily into the water column by the action of turbulence in the sea surface generated by tidal sea currents, wind-drift currents and waves, being the latter two caused by winds (Delvigne & Sweeney, 1988). If small enough, usually less than 0.02 mm, droplets remain in suspension whereas if greater than approximately 0.05 mm they quickly rise back to the surface, returning to the slick or spreading out as a film (Afenyo et al., 2015). Although any turbulence in the sea may potentially lead to oil dispersion, according to Liungman & Mattsson (2011), turbulent mixing generated by wind shear is unlikely to break up oil slicks, thus the main mechanism that enables natural dispersion in the sea is breaking waves.

Natural dispersion is, along with evaporation, the most important mechanism in the prediction of the lifetime of an oil slick on the sea surface (Reed et al., 2009) and is controlled by several factors including oil slick thickness, oil viscosity, oil-water interfacial tension and wave height, which is a function of wind speed. The degree in which each of these factors influence the rate of natural dispersion is still not fully understood, yet a number of formulations have been proposed to model the entrainment of oil particles into the water column. A review of natural dispersion models was carried out by Fingas (2015), who pointed out several issues about all models available. One important note is that none of the dispersion models include considerations regarding droplet resurfacing.

Delvigne & Sweeney (1988) developed an algorithm that is extensively used in transport and weathering models, where entrainment rate is a function of breaking wave energy and oil droplet diameter:

$$Q = C\ D^{0.57}\ S\ F\ d^{0.7}\ \Delta d \tag{2.6}$$

Where C is an empirical constant dependent on oil type and weathering state; D is the dissipated breaking wave energy per unit surface area (J/m^2); S is the fraction of sea surface covered by oil; F is the fraction of sea surface hit by breaking waves; d is the oil droplet diameter (m); and Δd is the droplet diameter interval (m).

The above equation explicitly considers the influence of droplet diameter in the entrainment rate, although this formulation is only valid for a limited range of oil viscosities and does not address the droplet vertical displacement. Also, ocean surface turbulence is not addressed in the calculations.

Recent studies (Reed et al., 2009; Li et al., 2017; Li, 2017; Johansen et al., 2015) have correlated the permanent entrainment to the droplet rise velocity after the oil has been driven down to subsurface by each breaking wave. When waves break over oil slicks, oil droplets are formed and forced downwards, separating from the slick to a depth determined by the breaking wave energy. The submerged droplets will tend to move upwards back to the surface due to buoyancy forces, with a rise velocity dependent on each droplet's diameter. According to Li (2017), when rise velocity of droplets is less than a certain vertical turbulence velocity – which is a function of wind speed – the droplets will not resurface and therefore will remain permanently entrained in the water column.

A simpler approach proposed by Mackay et. al. (1980) accounts for the changing oil viscosity, the oil-water interfacial tension, the oil slick thickness and the wind speed:

$$D = D_a\, D_b \;=\; \frac{0.11\,(W+1)^2}{1 + 50\mu^{0.5} h\, S_t} \tag{2.7}$$

Where D_a is the fraction of sea dispersed per hour; D_b is the fraction of dispersed oil not returning to the slick; W is the wind speed (m/s); μ is the oil viscosity (cP); h is the slick thickness (m); and S_t is the oil-water interfacial tension (dyne/m).

In Mackay's equation, all the calculated dispersed oil is assumed to entrain permanently and the mechanism of oil droplet formation is not addressed.

In ice-covered waters, the presence of ice in its various forms damps the action of breaking waves (Afenyo et al., 2015), hindering the natural dispersion process and reducing its rate. Liungman & Mattsson (2011) proposed a correction factor to account for ice concentration in dispersion models, as follows.

$$r_{ice} = \begin{cases} 0, & c \geq 0.8 \\ (0.8 - c)/0.5\,, & 0.3 \leq c < 0.8 \\ 1, & c < 0.3 \end{cases} \tag{2.8}$$

Considering the damping effect of ice, the above correction factor results in no dispersion for high concentration and reduced dispersion for medium ice concentration. For low ice concentrations, dispersion rates remain the same as in open waters.

2.1.4 **Entrainment in Ice**

Before examining the mechanism of oil entrainment in ice, it is convenient to elucidate some aspects of sea ice formation, evolution and composition. When ice crystals are formed in the ocean, salt collects in ice pores in the form of small droplets known as brine, which remains as a liquid and may be expelled back to the underlying water or become trapped in pore spaces between ice crystals (National Snow & Ice Data Center). The salinity of ice will highly depend on its temperature profile during ice growth, such

that warmer temperatures will normally result in formation of lower salinity ice (Petrich et al., 2013). After ice is formed though, as temperature increases over time towards summer, the trapped brine drains down to the sea, creating brine channels in the ice structure and reducing its salinity. These brine channels, that can be up to 10 mm wide (Martin, 1979), will be important pathways for oil migration through the ice, from the bottom ice/water interface up to the ice surface.

At high ice concentrations, oil will collect into pools or lenses in under-ice roughness elements. During ice growth season, ice may form a lip around the edge of the oil lens and encapsulate it. Given the cold temperatures over winter, brine channels are not sufficiently developed and therefore oil migration, when present, is limited to the very bottom of the ice (Maus et al., 2015). As ice warms, brine channels increase in number and size enabling upward migration of oil due to its lower density compared to brine. The rate of entrainment in ice will depend on the ice characteristics, as discussed above, as well as the thickness of oil pooled in the under-ice depressions. Thicker oil lenses in contact with overlying ice will exert greater hydrostatic pressure in the ice bottom and, if a developed drainage network is present, will migrate faster and more efficiently than thin oil lenses. Thus, pooling capacity of under-ice roughness is a critical parameter for predicting oil entrainment in ice.

The age of the ice plays an important role when determining the oil movement through it. Multi-year ice is less saline than first year ice, therefore brine channels won't be as abundant and will generally have smaller diameters. Consequently, the available volume for oil to migrate will be limited, meaning that entrainment in multi-year ice is

expected to occur at slower rates than in first-year ice. Also, multi-year ice is thicker than first year ice, thus a longer time is required for oil to surface on the top of the ice. However, storage capacity of under-ice roughness in multi-year ice is greater than in first year ice, consequently oil will generally collect with greater thickness (Afenyo et al., 2015) which will translate into greater entrainment potential. In fact, Maus et al. (2015) pointed out that buoyancy forcing in oil pools under first year ice is insufficient to describe upward migration, and convective mass transfer might be the predominant mechanism of entrainment for that type of ice.

Studies to try quantify oil entrainment in ice have been performed (Martin, 1979; Karlsson et al., 2011; Petrich et al., 2013; Maus et al., 2015) yielding interesting results, although an algorithm that describes the process in terms of its variables is still pending, hence modeling is still not feasible. Some authors claim that there is a porosity threshold for oil to be able to migrate through the drainage network (Karlsson et al., 2011; Petrich et al., 2013), varying from 8 to 15% depending on the type and age of ice. However, Maus et al. (2015) could not determine a porosity threshold in their study. Instead, the authors found other factors such as ice age, pore volume, oil lens thickness and convection more likely to control the process. The work from Petrich et al. (2013) determined an average entrainment capacity of less than 2 L/m^2 in winter and of 5 to 10 L/m^2 in spring. Karlsson et al. (2011) found an entrainment potential of about 1 L/m^2 in cold sea ice. In agreement with Petrich et al. (2013), Wilkinson et al. (2007) estimated a most probable pooling capacity for first year ice of 2 L/m^2. The latter work also found that only about 5% of the total contaminated area under ice is expected to be oil-covered at any single moment. Oil entrainment in ice is dependent on the highly variable pooling capacity of under ice

topography – which is inherently heterogeneous – thus description of this process by simple parameters might not be realistic (Wilkinson et al., 2007).

While the above experiments provided estimative on entrainment capacity of ice covers, oil encapsulation mechanism is still poorly understood and has never been quantified. As connected to the phenomenon of entrainment in ice, a better understanding of encapsulation process is of paramount importance.

The interface between ice and water provides a sheltered environment in constant fluid exchange (Petrich et al., 2013), making it a viable habitat for ecological entities such as algae and plankton that will be associated with brine channels. Moreover, entrainment in ice will be an important route of oil transportation, removing it temporarily from the water surface and releasing it back to the ocean in distances away from the spill site upon ice melt on spring and summer, as well as bringing oil from below the ice to its surface where it becomes accessible to marine birds and mammals. On an experiment performed in the pack ice of Svalbard, Boccadoro et al. (2018) found that oil previously entrained in the ice remained practically unchanged over the 5 months of monitoring, confirming that ice would act as a reservoir, storing the entrained oil and transporting it nearly fresh to other locations, posing an environmental risk for regions that wouldn't be affected by the slick otherwise. In that sense, the quantification of entrainment process is crucial to enhance oil-in-ice models and environmental risk assessment of oil spills in ice-infested waters.

2.1.5 Evaporation

Evaporation is the most important weathering process that oil undergoes when spilled in the sea and is the main process in most oil spill models. In open waters, it accounts for removal of up to 40% of the oil mass, whereas in ice-covered waters it can be drastically reduced due to cold temperatures, increased oil slick thickness (Afenyo et al., 2015) as well as less oil surface area available, since ice floes will be present and part of the oil will be submerged underneath the ice. In the Arctic, prolonged periods of darkness over winter also lead to reduced evaporation rates.

Extensive research has been carried out over the past decades to investigate and properly model evaporative loss from surface oil slicks, though scientists still diverge regarding the complete physicochemical process involved in evaporation. Oil is composed of hundreds of compounds (M. Fingas, 1995) that will show different evaporative loss profiles and will have different mass transfer coefficients, hence measuring evaporation for oil as one single substance is challenging. Fingas (1995) conducted an in-depth review on evaporation models and stressed that most evaporation models are based on water evaporation process, which is air-boundary layer regulated, although oil is not and therefore the mechanism in which it evaporates may differ greatly from that of water. Boundary layer is the interface between the air and a liquid, with a thickness generally of the order of less than 1 mm, which regulates the evaporation of a pure liquid. The saturation of this boundary layer will control the evaporation rate, that is, the liquid will quickly evaporate until the air immediately above it becomes saturated, after which the evaporation slows down. If no wind is present to move the saturated boundary layer away, the

evaporation halts. If a source of turbulence is present, the moisture in the boundary layer will be constantly pushed away and the evaporation will be constant.

Measuring evaporation in water pools is relatively straight-forward but for crude oil evaporation mechanism is complex, since many factors are acting together and a different process may be playing out. Some liquids are not regulated by a boundary layer as they evaporate too slowly to saturate the air immediately above it (Fingas, 2015b). The evaporation of such liquids is likely to be associated with the diffusive movement of molecules inside the liquid towards its surface. In this case, area of the pool and wind speed won't influence evaporation.

In general, two approaches are adopted to model evaporation: the pseudo-component method and the analytical method, the former being a complex and computationally-intensive but more accurate method (Afenyo et al., 2015) in which oil is fractionated in groups of components of same molecular weight and boiling point, resulting in different evaporative rates for each fraction (Nazir et al., 2007). The second approach is more widely used in oil spill models as it provides a simpler method to describe analytically the evaporation process as a function of vapor pressure using distillation data, which are readily available.

The analytical method proposed by Stiver & Mackay (1984) is the most popular and expresses the volume fraction evaporated as:

$$F_E = ln\left[1 + B\left(\frac{T_G}{T}\right)\theta\ exp\left(A - B\frac{T_0}{T}\right)\right]\left[\frac{T}{BT_G}\right] \quad (2.9)$$

Where,

$$\theta = \frac{K_2 A_S t}{V_0} \qquad and \qquad K_2 = 2.5\ x\ 10^{-3}\ W^{0.78}$$

And: F_E = volume fraction evaporated (%); θ = evaporative coefficient; K_2 = mass transfer coefficient for evaporation (m/s); W = wind speed (m/s); V_0 = initial volume of spilled oil (m^3); T_0 = initial boiling point at F_E of zero (K); T_G = gradient of the boiling point; T = ambient temperature (K); A and B are dimensionless constants derived from distillation data; A_S = spill area (m^2); and t = time (s).

Fingas (1995) pointed out that the above formulation only works well until 8 hours after the spill occurred, but after that it overpredicts the evaporation as much as 10%. Furthermore, the proposed equation assumes oil evaporation as boundary layer-regulated and uses constant vapor pressure and boiling point, which does not seem to be the case for complex mixtures of components such as oil.

A simpler approach was proposed by Fingas (2004) in an effort to improve models for liquids in which evaporation is not regulated by a boundary layer. The author conducted a series of experiments to investigate the evaporative behavior of complex mixtures, testing the real influence of parameters used in the equation by Stiver & Mackay (1984) in the rate of evaporation. His findings were that, for those liquids wind speed, area and thickness of the pooled liquid do not control the evaporation process and therefore should not be included in the model. Instead, it appears that a simplistic approach suffices to describe diffusion-regulated evaporation as a function of distillation data, temperature and elapsed time only.

For this new empirical approach, distillation data is used to develop a unique equation for each type of oil, given that each oil is unique in its composition and thus distills at different rates, so different treatment is required. In his experiments, the author found that the distillation percentage at 180^{o} C has good correlation with the parameters in the newly developed equation. One of his findings is that oils and fuels evaporate at two different regimes, because some lighter fuels such as diesel and kerosene have a narrower range of compounds than the majority of more complex oils. For those oils, evaporation is a function of the square root of time. For all the others, the evaporation takes place as the logarithm of time. From the experiments, the following equations were proposed (Fingas, 2004, 2015):

For oils that display a logarithmic behavior:

$$\%\, Evaporated = \, [0.165(\%D) + 0.045(T - 15)] \ln(t) \qquad (2.10)$$

For oils that display a square root behavior:

$$\%\, Evaporated = \, [0.0254(\%D) + 0.01(T - 15)] \sqrt{t} \qquad (2.11)$$

Where %D is the percentage distilled at 180^{o} C; T is temperature (^{o}C); and t is the elapsed time (minutes).

With these equations, Fingas (2004, 2015) described the phenomenon of oil evaporation in terms of simple and readily available parameters. Equations can be developed for any type of oil, as long as distillation data is obtainable. Based on that, the author developed a series of equations for the most common types of oils which can be found in Fingas (2015) and be readily used. The equations describe in a very simple manner

the evaporation in terms of temperature and time only. As an example, the evaporation equation for the Statfjord crude is:

$$\% \, Evaporated = (2.67 + 0.06T) \ln(t) \tag{2.12}$$

Toz & Koseoglu (2018) found good correlation between the equations proposed by Fingas (2015) and the evaporation rates predicted by the oil spill model PISCES 2 for two different spill scenarios simulated at the Bay of Izmir, in Turkey, showing its reliability when compared to existing models.

Evaporation causes an increase in oil viscosity as volatile fractions of oil are lost to the atmosphere. Light oils can change drastically from fluid to viscous and heavy oils can become practically solid (Fingas, 2015). After enough time, some types of oil will form tar balls or tar matts on the sea surface. Sebastiao & Guedes (1995) proposed the following equation to model increase in viscosity due to evaporation:

$$\mu = \mu_0 \exp(C_4 F_E) \tag{2.13}$$

Where μ is the new viscosity (cP), μ_0 is the initial viscosity, C_4 is a constant dependent on the oil type, taken as 10 for crude oil, and F_E is the percent evaporated at a given time.

Currently there is no specific algorithm for modeling oil evaporation in ice conditions, although the algorithm by Fingas (2004, 2015) include the temperature as a dominant parameter, hence reduced evaporation rate in cold environments can still be modeled. Liungman & Mattsson (2011) included an ice correction factor in their equation

for evaporation to account for ice concentration, assuming that only oil on the water surface between floes will experience evaporative loss.

2.1.6 **Emulsification**

Water-in-oil emulsions are formed after oil is spilled in the ocean as water droplets are absorbed into the oil matrix, creating a "mousse" like patch. According to Fingas (2015) emulsification depends on percentage of resins and asphaltenes, which act as natural surfactants and stabilize the water droplets within the oil slick.

Fingas (2015) found four types of water-in-oil emulsions can be formed: stable and meso-stable emulsions, entrained water-in-oil, and unstable types. The four types have unique properties and differ basically in stability of emulsion and water content. Once one type is formed, it is believed that it won't convert to any other type. A thorough description of all types is given in Fingas (2015).

Understanding the mechanism by which water is incorporated by oil slicks and form emulsions entails quantifying energy levels at sea (Afenyo et al., 2015). Also, the physicochemical processes that control the stability of emulsions need to be considered, thus modeling oil emulsification is challenging. Most oil spill models use the formulation from Mackay et al. (1980) to determine the rate of incorporation of water into oil, given by:

$$Y = C_f \left[1 - exp\left(\frac{-2x10^{-6}}{C_f}(1+W)^2 t\right)\right] \tag{2.14}$$

Where Y is the water content (%); C_f is the final water content; W is the wind speed (m/s) and t is time (s). The final water content for crude oils and heavy fuel oil is 0.7 for

the open water case. Mackay's equation describes the water uptake in terms of wind speed and time only besides the final water content constant, which represents a simplification of the complexity involved in the process. The stability of the emulsion is not addressed and therefore the model does not represent the whole physicochemical mechanism by which emulsification occurs.

Currently, there is no specific algorithm to represent mathematically the mousse formation in ice-infested waters. Emulsification may be considerably reduced in high ice concentrations as wind-driven turbulence will be damped by the ice, resulting in limited water uptake by the oil slick. Liungman & Mattsson (2011) included an ice correction factor in their equation for modeling emulsification in the form of (1-c), where c is the ice concentration. Recent experiments from Brandvik et al. (2010a) suggested that the final water content decreases with increasing ice concentration to as low as 0.2 for 90% ice coverage. Based on those experiments, Yang et al. (2015) came up with a relation to represent the emulsification in waters with 90% ice coverage by adapting Eq. (2.14) to this condition. The resulting algorithm is:

$$Y = 0.34C_f \left[1 - exp\left(\frac{-2x10^{-6}}{C_f}(1+W)^2 t\right)\right] - 1.32 \qquad (2.15)$$

Meso and large-scale experiments carried out by SINTEF (Brandvik et al., 2010a and 2010b) showed great variability in the final water content for different ice concentrations, which may indicate the need for a correction in the final water content constant, C_f, to account for ice coverage.

Mousse formation greatly increases the volume of the oil slick and the oil viscosity, as well as its density as water is incorporated to the oil matrix. According to Brandvik & Faksness (2009), oil viscosity increases as a result of internal friction between water droplets and the continuous oil phase as they are stabilized by naturally occurring surface active components of oil such as asphaltenes, waxes and resins. Sebastiao & Guedes (1995) used the Mooney equation to model the increase in viscosity driven by emulsification:

$$\mu = \mu_0 \exp\left[\frac{2.5Y}{(1 - C_f Y)}\right] \tag{2.16}$$

The work by Yang et al. (2015) presented an adapted version of Eq. (2.16) to model the increase in viscosity due to emulsification at 90% ice coverage, based on the experiments by Brandvik & Faksness (2009):

$$\mu = 0.28\mu_0 \exp\left[\frac{2.5Y}{(1 - C_f Y)}\right] - 150 \tag{2.17}$$

2.2 Fugacity-Based Multimedia Fate Modeling

When an organic chemical enters the environment, it will partition between the available phases through diffusive or advective processes seeking to reach an equilibrium distribution in which the chemical potential in all phases is equal. Also, the chemical might undergo transformation as a result of interaction with water, air and other environmental pressures such as sunlight. The transformation and migration of the chemical between phases will be controlled by several factors, or processes, and quantifying these processes is vital to understand the behavior of contaminants in the environment.

The concept of fugacity was first presented in 1901 by G.N. Lewis as an equivalent for chemical potential and represents the "escaping" tendency of a chemical from a medium (Mackay, 2001). Since it correlates linearly to concentration, it consists in a simpler approach to model concentration profiles in a multimedia environment when compared to the use of chemical potential, which is logarithmically related to concentration.

An evaluative environment can be conceived to study the distribution of the chemical and one can include as many phases – or compartments – as deemed relevant for the analysis. In a marine environment, it is convenient to consider water, air, sediment and biotic phases. If Arctic waters are under investigation, ice should be also included as a compartment. Each bulk compartment encompasses sub-compartments consisting of pure and dispersed phases (Yang et al., 2015) that will be included in the calculations by their volume fractions in the bulk phase. For instance, water phase is composed by water, biota and particulate matter. The sum of the volume fractions of each sub-compartment will then constitute the bulk compartment. The chemical will be transferred by diffusive mechanisms from phases with lower to those with greater fugacity capacity for that given substance and equilibrium will be established when fugacity is equal in all phases. In addition, the chemical may be subject to reaction and advective transport between phases, in or out of the considered evaluative environment.

Mackay (1979) introduced a set of models consisting in four levels of increasing complexity to predict intermedia transport, transformation rates, buildup tendency and overall concentration of organic chemicals in multimedia environments, as detailed in the next sub-sections.

2.2.1 **Level I**

Level I defines the simple partition of a substance between phases in a closed environment assuming equilibrium between phases, a constant amount of chemical and no degradative or advective processes. Fugacity is directly and linearly correlated to concentration as stated by Mackay & Paterson (1981):

$$C = f\,Z \tag{2.18}$$

Where C is the concentration (mol/m^3); f is the fugacity (Pa) and Z is the fugacity capacity of a compartment (mol/m^3 Pa). Z values can be defined for all environmental compartments, and a summary is provided in Table 2-1 below.

Table 1-1: Definition of Z values for various phases (Adapted from Mackay, 2001).

Phase	Z Value (mol/m^3 Pa)	Parameter Definition
Pure solute	$Z_P = 1/P^S V$	P^S = vapor pressure (Pa) V = molar volume (m^3/mol)
Air	$Z_A = 1/RT$	R = gas constant = 8.314 Pa m^3/mol K T = temp. (K)
Water	$Z_W = 1/H = C^S/P^S$	C^S = aqueous solubility (mol/m^3) H = Henry's law constant (Pa m^3/mol)
Solid Sorbents	$Z_S = K_P \rho_S / H$	K_P = soil/water partition coeff. (L/kg) ρ_s = density (kg/L)
Biota	$Z_B = K_B \rho_S / H$	K_B = bioconcentration factor (L/kg) = L_B K_{OW} L_B = lipid content of organism ≈ 0.048 K_{OW} = octanol/water partition coefficient

Wania (1997) suggested a Z value for the ice-air interface to be applied when ice cover is included as a compartment, as follows:

$$Z_{ia} = K_{ia}/RT = K_{ia}\,Z_A$$

Where K_{ia} is the ice surface-air partition coefficient (m) and all other parameters as in Table 2-1. The Z value of each bulk compartment will be given by the sum of Z values of all sub-compartments present, considering their volume fractions in the bulk phase.

Considering an evaluative environment consisting of air, water, sediment, ice and biota, for Level I calculations:

$$f_A = f_W = f_S = f_I = f_B \tag{2.19}$$

Where f_A, f_W, f_S, f_I and f_B are fugacities of air, water, sediment, ice and biota, respectively, given in units of pressure (Pa). Assuming that a single fugacity f applies to all compartments and if M is the total amount of chemical in the environment, in moles, V_i is the volume (m3), Z_i is the fugacity capacity (mol/m3 Pa) and C_i is the concentration (mol/m3) for the compartment i, it can be stated that for a Level I calculation:

$$M = \sum V_i C_i = \sum V_i Z_i f_i = f \sum V_i Z_i \tag{2.20}$$

And therefore:

$$f = \frac{M}{\sum V_i Z_i} \tag{2.21}$$

Given the direct relationship between fugacity and concentration (Eq. (2.18)), the concentrations in all phases can be deducted from Eq. (2.21).

2.2.2 **Level II**

On Level II, an emission source at constant rate is added to the system in addition to the loss processes of reaction and advection, although equilibrium is still assumed between phases, thus a single fugacity for all media still applies.

The chemical might be removed from or enter the evaluative environment by advective processes such as ocean currents and wind, but on Level II there is no transport between phases, as they are in equilibrium. Advection is expressed by a flow rate G (m^3/h) and when contaminant is present in the inflow of air or water, it adds up to the emissions as chemical inputs to the evaluative environment. The advective residence time for a given phase will be given by its volume divided by the outflow rate of contaminant. Net accumulation may occur if the inflow of contaminant is greater than the outflow or, if no contaminant is present in the inflow of air or water, the advective outflow will result in loss of chemical from the evaluative environment. Mackay & Paterson (1981) pointed out that information on advective processes is of great regulatory importance, as reduction in local contaminant emissions might not be followed by the same level of reduction in concentrations if the chemical is being advected with winds and currents into the considered environment from unknown emission sources elsewhere.

Reaction processes are those by which the chemical nature of a solute is changed (Mackay, 2001) and they comprise photolysis, hydrolysis, biodegradation and oxidation. It is defined in terms of a first-order rate constant k, which is a function of the reaction half-life τ of the chemical in a given environment and have units of reciprocal time (h^{-1}).

Transformation and transport processes are described through fugacity rate constants, known as D values (mol/Pa h). For the advective transport into and out of a compartment i, the D value is defined as:

$$D_{Ai} = G_i \, Z_i \qquad (2.22)$$

The D value for reaction of a chemical contained in the compartment i is given by:

$$D_{Ri} = K_{Ri}\, V_i\, Z_i \tag{2.23}$$

The analysis of D values provides awareness on the relevance of a process in the context of the environment under study. When multiplied by the fugacity, D values give the rates of transport and transformation processes. Fast processes will have large D values, thus will have a greater relative importance than processes with lower D values, which can often be ignored in the calculations given the long time required for those processes to degrade or transport the chemical.

The emission rate is then given by:

$$E = \sum D_i f_i \tag{2.24}$$

Given a single fugacity applies to all compartments, Eq. (2.23) can be re-written in the following form:

$$f = \frac{E}{\sum D_i} \tag{2.25}$$

2.2.3 **Level III**

The next level accounts for intermedia transport processes such as diffusion, deposition and resuspension, hence the equilibrium assumption is relaxed, meaning that a common fugacity for all compartments no longer applies. Additionally, on Level III each compartment may receive chemical input from phase-specific emission sources, as opposed to the assumption on Level II of one single emission source for the entire evaluative environment. As in real environments equilibrium between phases is often an unrealistic assumption, Level III calculations output more accurate results for the cost of increase in complexity. However, the system remains in steady state as in the two previous

levels, that is, the fugacity in each compartment does not change over time. Emissions maintained constant for a long enough time, for instance, will reach steady state and Level III can be applied (Webster et al., 2005). Also, equilibrium is assumed within the compartments, implying that the bulk phases are homogeneous spatially and the dispersed phases (sub-compartments) within each compartment have the same fugacity.

At steady state, mass conservation applies and the amount of chemical emitted to each compartment should be balanced by the amount transported to another phases and the amount lost through reaction and advection. In general lines, (Webster et al., 2005) postulated that: entering = advected + degraded + transferred. In that sense, considering D_{Ti} as the sum of all D values in the phase i ($D_{Ti} = D_{Ai} + D_{Ri} + \Sigma D_{i-j}$), being ΣD_{i-j} the sum of D values for all intermedia processes from the phase i to j, it can be demonstrated that:

$$E_i + \sum D_{j-i}\, f_j = f_i\, D_{Ti} \tag{2.26}$$

Isolating the fugacity term for the phase i on Eq. (2.26), it follows that:

$$f_i = \frac{\left(E_i + \sum D_{j-i}\, f_j\right)}{D_{Ti}} \tag{2.27}$$

With the formulations above, every process taking place in the environment can be accounted for by the inclusion of D values for as many processes as deemed relevant in the analysis. D values can be estimated for every process in nature, even though uncertainties regarding the rates in which they occur impose limitations to the ability to define these transport parameters. D values can be generally defined by the formulation D = A U Z, where A (m^2) is the surface area between phases, where the exchange of chemical takes

place and U is the rate of transport for the process, given in m/h. A summary of some relevant intermedia D values for an evaluative environment consisting of air, water and sediment is given in Table 2-2.

Table 1-2: Intermedia transfer D values for an evaluative environment consisting of air, water and sediment. (Adapted from Mackay, 2001).

Phase	Process	D Value (mol/Pa h)
Air(1) – Water(2)	Diffusion	$D_V = 1/(1/K_{VA} A_{12} Z_A + 1/K_{VW} A_{12} Z_W)$
	Rain Dissolution	$D_{RW2} = A_{12} U_Q Z_W$
	Wet Deposition	$D_{QW2} = A_{12} U_R Q V_Q Z_Q$
	Dry Deposition	$D_{QD2} = A_{12} U_Q V_Q Z_Q$
	Total D (1-2)	$D_{12} = D_V + D_{RW2} + D_{QW2} + D_{QD2}$
	Total D (2-1)	$D_{21} = D_V$
Water(2) – Sediment(3)	Diffusion	$D_Y = 1/(1/K_{SW} A_{23} Z_W + Y_4/B_{W4} A_{23} Z_W)$
	Deposition	$D_{DS} = A_{23} U_{DP} Z_P$
	Resuspension	$D_{RS} = A_{23} U_{RS} Z_S$
	Total D (2-3)	$D_{23} = D_Y + D_{DS}$
	Total D (3-2)	$D_{32} = D_Y + D_{RS}$

In Table 2-2, K_{VA} is the air-side mass transfer coefficient (m/h); K_{VW} is the water-side mass transfer coefficient (m/h); U_Q is the dry deposition velocity (m/h); U_R is the rain rate (m/h); Q is the scavenging ratio (dimensionless); V_Q is the volume fraction of aerosols in air (dimensionless); Z_Q is the fugacity capacity of aerosols (mol/m^3 Pa); K_{SW} is the water-side mass transfer coefficient over sediment (m/h); Y_4 is the diffusion path length in sediment (m); B_{W4} is the molecular diffusivity in water (m^2/h); U_{DP} is the sediment deposition rate (m^3/m^2 h); U_{RS} is the sediment resuspension rate (m^3/m^2 h); A_{ij} is the

interfacial area between media i and j; and subscripts in Z are A for air, W for water, S for sediment and P for particles in water. Mackay (2001) provides a list of order-of-magnitude values for those and other parameters used in the calculations of D values.

As an example, the mas balance for the same evaluative environment is expressed by (adapted from Mackay, 2001):

- **Air (1):**

$$E_1 + G_{A1}C_{A1} + f_2D_{21} = f_1(D_{12} + D_{R1} + D_{A1}) = f_1D_{T1} \quad (2.28)$$

- **Water (2):**

$$E_2 + G_{A2}C_{A2} + f_1D_{12} + f_3D_{32} = f_2(D_{21} + D_{23} + D_{R2} + D_{A2}) = f_2D_{T2} \quad (2.29)$$

- **Sediment (3):**

$$E_3 + f_2D_{23} = f_3(D_{32} + D_{R3}) = f_3D_{T3} \quad (2.30)$$

Where E_i is the direct emission to the compartment i and the group $G_{Ai}C_{Ai}$ is the advective input, being C_{Ai} the concentration of contaminant in the inflow of air or water.

2.2.4 **Level IV**

The last level is a natural extension of Level III to reflect unsteady-state conditions. It provides the most realistic mass balance of contaminant in the environment amongst all four levels, as no simplifications are necessary on Level IV. The behavior of the chemical can be examined in more details and the effects of changing emissions can be observed over time. Level IV calculations are useful when the goal is to determine how

concentrations will vary and how environmental media will respond to reduction or increase in emissions, as well as to estimate recovery times after the emissions have ceased.

On Level IV, calculations are similar to those from Level III, but now the fugacity is varying with time, thus the equations are written in the differential form. Here, all chemical entering each compartment is either transported to another phase (in the same evaluative environment), lost from the evaluative environment through reaction or advection or accumulate in that given compartment, becoming part of its chemical inventory. The mass balance hence dictates that the rate of inventory change should equal the difference between the rate of chemical entering and leaving the compartment. The mass balance for a compartment i will thus be given by (Mackay, 2001):

$$V_i Z_i \, df_i/dt = I_i + \sum(D_{j-i} f_j) - D_{Ti} f_i \qquad (2.31)$$

Where V_i is the volume of the compartment i, I_i is the input rate, which may be a function of time, and all other parameters as stated before. The group $D_{i\text{-}j}f_j$ represents the chemical input to the given compartment, whereas the group $D_{Ti}f_i$ represents the total output. The left-hand side of Eq. (2.31) represents the rate of change in the inventory of chemical in the compartment, given in mol/h, and can be transformed into concentration through Eq. (2.18).

A system of linear differential equations can be assembled with one equation for each compartment and be solved either analytically or numerically, although numerical methods offer a simpler solution. Mackay (2001) and colleagues developed a series of software to compute the mass balance of contaminants in multimedia environments using

concepts of Levels I, II and III models, and a description of those applications is available in his work.

2.2.5 Food-Web Bioaccumulation Models

The concept of fugacity can be explored to investigate the interaction of organisms with organic contaminants present in the environment by the study of uptake and loss mechanisms taking place at organs and tissues. By the inclusion of biota as a bulk compartment in the fugacity calculations it is possible to analyze the transfer of contaminants between the abiotic and biotic media. The long-term effects of chemical exposure can then be quantified objectively, subsidizing ecological risk assessment and restoration efforts. According to Sharpe & Mackay (2000), food-web bioaccumulation models "may help to identify vulnerable species, assess the potential for effects, and guide monitoring programs".

Hydrophobic organic chemicals are soluble in lipid, thus likely to accumulate in lipidic fraction of organisms in concentrations usually many orders of magnitude higher than that of the surrounding environment. Moreover, the contaminant might be transferred to organisms in upper levels in the food chain by the phenomenon of biomagnification, by which a chemical becomes increasingly concentrated in the food chain from lower to higher trophic levels (Mackay, 2001).

Bioaccumulation encompasses two separate phenomena that are described under this broader concept. In the context of marine ecosystems, bioconcentration is the mechanism whereby chemicals present in the water are absorbed through respiration, and the uptake occurs by diffusive exchange via the organism's gills. It is generally determined

by exposing fish to chemicals in a lab environment where food is not administered (Mackay, 2001) and is defined by a bioconcentration factor (BCF) which is the ratio between the contaminant concentration in the organism and in the water. Biomagnification is a consequence of ingestion of contaminated food, leading to an increase in fugacity from prey to predator. It is more likely to occur for chemicals with high log K_{OW} (>5) which are not readily metabolized (Mackay, 2001), therefore are carried up to higher trophic levels. Bioaccumulation is then the total effect of bioconcentration and biomagnification and is controlled by a balance between chemical uptake and loss in organisms.

The dynamics of bioaccumulation depends on two main uptake processes and four loss processes. Chemical may be taken up by aquatic organisms through exchange with water via gills and food consumption. Gill exchange also results in chemical clearance, which adds up to the loss processes of egestion, metabolism and growth dilution. Each process can be described in terms of a D value, as in Table 2-3. Metabolism and growth dilution are considered as self-elimination processes, as no chemical is exchanged with the environment. Metabolism will lead to internal transformation of chemical controlled by a metabolic rate constant, k_M, determined by the chemical's half-life in the organism. Loss by growth dilution is simply attributed to an increase in the organism's volume, which will result in a lower amount of chemical per body weight, that is, a lower concentration. The mechanisms by which metabolic clearance occur are not well understood given the difficulties to measure metabolic rates. Likewise, growth dilution depends on growth rates which can vary substantially between individuals even from the same species, thus is also challenging to be measured and generalized as a model.

Table 1-3: D values for chemical uptake and clearance processes in aquatic organisms (adapted from Campfens & Mackay, 1997).

Process	D Value (mol/Pa h)	Parameter Definition
Uptake from food	$D_A = E_A G_A Z_A$	G_A = gross food ingestion rate (m^3/h) E_A = gut absortion efficiency (%)
Gill uptake	$D_{WI} = k_1 V_F Z_W$	k_1 = gill uptake rate constant (h^{-1}) V_F = volume of organism (m^3)
Gill elimination	$D_{WE} = k_2 V_F Z_W$	k_2 = gill elimination rate constant (h^{-1}) = $k_1/L_B K_{OW}$
Loss by egestion	$D_E = D_A/Q$	D_A = D value for uptake from food (mol/Pa h) Q = limiting biomagnification factor ≈ 3
Metabolism	$D_M = k_M V_F Z_F$	k_M = metabolic rate constant (h^{-1}) Z_F = Fugacity capacity of organism (mol/m^3 Pa)
Growth dilution	$D_G = Z_F\,(dV_F/dt)$	dV_F/dt = growth rate (m^3/h)

A detailed definition of the parameters from Table 2-3 is available in the work by Campfens & Mackay (1997). Based on the D values presented on Table 2-3, a set of equations can be assembled to model uptake and clearance processes in a single organism, which can then be extended to linear food chains and finally to complex food webs.

For a single organism, the steady-state fugacity in a fish is given by:

$$f_W D_{WI} + f_A D_A \ = f_F(D_{WE} + D_E + D_M + D_G) \tag{2.32}$$

Where f_W, f_A and f_F are the fugacities of water, air and fish, respectively and D values as in Table 2-3. Eq. (2.32) can be re-written isolating the fugacity in fish:

$$f_F = (f_W D_{WI} + f_A D_A)/(D_{WE} + D_E + D_M + D_G) \tag{2.33}$$

By the previous formulations, fugacity in organisms are explicitly expressed in terms of chemical uptake and loss processes. The group $f_W D_{W1}$ controls the uptake from

water, representing the bioconcentration phenomenon, while the group $f_A D_A$ controls the uptake from food, representing biomagnification. In fact, Campfens & Mackay (1997) suggested the dimensionless quantities W and A as "fugacity factors" for uptake through respiration and food ingestion, respectively, define by:

$$W = D_{WI}/(D_{WE} + D_E + D_M + D_G) \tag{2.34}$$

$$A = D_A/(D_{WE} + D_E + D_M + D_G) \tag{2.35}$$

Replacing the fugacity factors in Eq. (2.33), it becomes:

$$f_F = f_W W + f_A A \tag{2.36}$$

Both processes of bioconcentration and biomagnification are thus objectively addressed, and inference can be made on dominant uptake and loss processes as well as on the time required for chemical depuration. Highly hydrophobic chemicals of log K_{OW} greater than 5, for instance, will display high values for A, meaning that uptake occurs mostly by food ingestion and gill uptake will not be significant. If it is desired to follow the change in concentrations over time and observe the long-term behavior of the contaminant in the biotic media, the unsteady-state version of Eq. (2.33) is given by:

$$V_F Z_F \, df_F/dt = f_W D_{WI} + f_A D_A - f_F(D_{WE} + D_E + D_M + D_G) \tag{2.37}$$

The same framework of formulations can be further developed to model chemical transfer in food webs of increasing complexity. The first case is a linear food chain, whereby organisms in each trophic level feed exclusively in organisms at the immediate lower level. It is possible thus to treat each organism as a single bulk compartment

interacting only with the water and with organisms one trophic level lower. The structure of the food chain will be defined according to the ecosystem under investigation, but general guidelines can be applied to most cases. The food chain will start with simple organisms such as phytoplankton, which are likely to be in equilibrium with water, hence food uptake and egestion can be neglected and water fugacity applies (Campfens & Mackay, 1997). From more simple organisms, the food chain progressively increases in complexity, moving to invertebrates, fish and so on. The model can include as many trophic levels as deemed relevant for the analysis without increasing complexity in the calculations. The steady-state mass balance for a three-level linear food chain starting from an organism in equilibrium with water will be then:

$$f_1 = f_W D_{WI1}/(D_{WE1} + D_{M1} + D_{G1}) = f_W W_1 \quad (2.38)$$

$$f_2 = (f_W D_{WI2} + f_1 D_{A2})/(D_{WE2} + D_{E2} + D_{M2} + D_{G2}) = f_W W_2 + f_1 A_2 \quad (2.39)$$

$$f_3 = (f_W D_{WI3} + f_2 D_{A3})/(D_{WE3} + D_{E3} + D_{M3} + D_{G3}) = f_W W_3 + f_2 A_3 \quad (2.40)$$

Where subscripts 1, 2 and 3 represent trophic levels in the food chain, from the lowest to the highest. A diagram is showed in Figure 2-1 to visually represent the food chain structure.

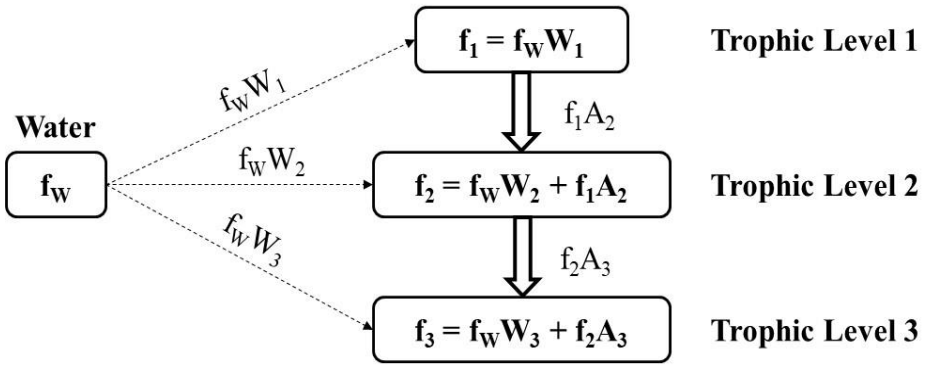

Figure 1-1: Linear food chain structure. Dashed arrows represent uptake by respiration and solid arrows represent uptake by food consumption (adapted from Campfens & Mackay, 1997).

The system of equations representing the food chain can then be combined with the equations for the abiotic media and be solved by numerical methods. The entire multimedia environment can thus be modeled, and concentration profiles can be determined for each biotic and abiotic compartment separately, enabling an in-depth analysis of all relevant aspects of contaminant distribution in the environment.

Moving forward, the linear food chain structure can be expanded to represent general food webs, where organisms from upper trophic levels may consume organisms from any trophic level equal or below its own level, including themselves. This approach is the most realistic, as in nature dietary habits rarely consists of only one species.

A matrix consisting of N equations for N species mutually interacting can be obtained based on the following equation, where the organism i respire in water and/or sediment:

$$D_{WIi}(x_W f_W + x_S f_S) + \sum(D_{Aji} f_j) = f_i(D_{WEi} + D_{Mi} + D_{Gi} + \sum D_{Ei}) \quad (2.41)$$

Re-writing Eq. (2.41) as a function of f_i and applying the fugacity factors defined in Eqs. (2.34) and (2.35), it becomes:

$$f_i = \sum(A_{ji} f_j) + W_i(x_W f_W + x_S f_S) \tag{2.42}$$

If the three-level linear food chain represented by Eqs. (2.38 – 2.40) is generalized to include branched feeding, the following matrix represents the general food web:

$$\begin{bmatrix} (1-A_{11}) & -A_{21} & -A_{31} \\ -A_{12} & (1-A_{22}) & -A_{32} \\ -A_{13} & -A_{23} & (1-A_{33}) \end{bmatrix} \begin{bmatrix} f_1 \\ f_2 \\ f_3 \end{bmatrix} = \begin{bmatrix} W_1(x_{1W} f_W + x_{1S} f_S) \\ W_2(x_{2W} f_W + x_{2S} f_S) \\ W_3(x_{3W} f_W + x_{3S} f_S) \end{bmatrix} \tag{2.42}$$

Where subscripts in the matrix A represent the consumption of organism j by organism i. Campfens & Mackay (1997) pointed out that the matrix can be solved by Gaussian elimination subroutine and that it can be shown that the linear food chain described by Eqs. (2.38 – 2.40) is a special case of this general matrix in which all A_{ji} values are zero, except for A_{12} and A_{23}.

Food-web bioaccumulation models represent an invaluable tool to predict biotic response to contaminant exposure in an ecosystem level, describing in details important processes of chemical exchange between organisms and between organisms and the abiotic media. It can be used to define priority species that are more sensitive to contaminants, thus more susceptible to impacts, as well as to predict possible human risk potential given the consumption of contaminated food. However, the reliability of the analysis is highly dependent on the accuracy of the selected parameters, and uncertainties regarding the methods of estimation of those parameters should be addressed properly. Many transport rates and organism properties such as feeding rates are of difficult quantification, thus care

must be taken to ensure that parameters with higher sensitivity to the model outputs are estimated with accuracy. Additionally, judgement on which processes to include in the calculations must be based on scientific evidence and relevance for the analysis. On one hand, the inclusion of processes that are not relevant may lead to unnecessary increase in complexity, consequently greater computational capacity is required for the model. On the other hand, the absence of a significant process may imply in biased and erroneous predictions.

Chapter 3: The Influence of Different Ice Conditions on the Fate and Transport of Surface Oil Slicks

Abstract: As some regions of the Arctic become ice-free for extended periods throughout the year, its resources become more accessible and its waters turn into routes for marine traffic. Due to the lack of knowledge on the Arctic environment, developing this area brings about a whole new range of risks and amongst them is the risk of oil spills. Oil spill models have been developed and adapted for Arctic conditions, but some of the main transport and weathering processes are still poorly understood in ice conditions. The present work proposes improvements to existing transport and weathering algorithms in order to describe these processes as a function of ice coverage. In addition, a simplistic formulation is introduced to model oil entrainment in ice, a process so far neglected in oil-in-ice models. The outputs of the model show good agreement with results from field experiments conducted by SINTEF at the Barents Sea in 2009.

3.1 Introduction

Increased marine traffic and growing interest in Arctic resources from the industry and governments pose risks to that environment (Nevalainen et al., 2016). The development of tools to understand the interactions between oil and ice is of vital importance in the planning of such activities. Risk management and emergency

preparedness in Arctic activities will be highly reliant in accurate information on oil behavior in those environments (French-McCay et al., 2017).

Ongoing research seeks understanding of the mechanisms that control the behavior of oil when ice is present and algorithms have been developed or adapted to ice conditions, but some key processes are still not well understood (Afenyo et al., 2016b). Oil movement through the ice, i.e., encapsulation and subsequent entrainment in ice, are currently not included in oil spill models due to the lack of algorithms to describe these processes, even though experiments have been conducted to investigate it (Martin, 1979; Karlsson et al., 2011; Petrich et al., 2013; Maus et al., 2015). Knowledge on other important transport and weathering processes such as natural dispersion, evaporation and emulsification are also limited even for open waters, and the presence of ice complicates even further modeling efforts. The access to ice-covered waters is still very restricted and only a few exploration developments have been possible in the Arctic, hence case studies of real oil spills in those environments are scarce (Nevalainen et al., 2016). In addition, field experiments involving oil release face severe regulatory control and, in most cases, environmental agencies do not grant a permit for those activities. In this context, oil-in-ice models are highly reliant in lab-scale experiments and validation in realistic field conditions represents a challenge (Wang et al., 2008). Given the difficulties regarding validation of existing models, it is important that research moves forward in this field, bringing new perspectives from different works and generating more data to cross-validate previous and newly developed models.

Oil spill models are frequently referred to as transport and weathering models. Transport processes are those responsible for the change in position of an oil slick due to winds, ocean currents, waves and to internal forces acting over the slick such as gravity and viscous forces. These processes do not alter oil chemical properties (Afenyo et al., 2015) and included in this category are advection, spreading, natural dispersion and, in ice-covered waters, entrainment in ice. Weathering processes are those by which oil properties such as density and viscosity are changed over time as the surface slick undergoes transformations due to evaporation, emulsification, dissolution, biodegradation and photo-oxidation (Reed et al., 1999; Afenyo et al., 2015). Emulsification is a consequence of the incorporation of water droplets into the oil matrix, and leads to increase in volume, density and viscosity. Evaporation is the loss of lower-weight fractions of oil to the atmosphere, also contributing to the increase in viscosity of oil. Other weathering processes include dissolution of soluble fractions of oil, the action of microorganisms that biodegrade the oil and photo-oxidation led by direct sunlight over the oil slick.

When modeling the short-term fate of oil when spilled in the ocean, some processes are more important over some others that may be important in a later moment but not in the time frame of the analysis, thus the majority of models include only the most relevant processes for the scenario under investigation (Nazir et al., 2007). Biodegradation and photo-oxidation in the Arctic, for instance, may not play an important role in the fate of oil slicks as they occur in very slow rates or may not occur at all. Overall, modeling of advection, spreading, natural dispersion, evaporation and emulsification suffice to describe the fate of oil slicks in most scenarios, but other processes may be included in the analysis, according to its objectives. Biodegradation and dissolution, for instance, may be relevant

if the goal is to assess long-term environmental outcomes of oil spills (Afenyo et al., 2016b).

In the present work, an analysis of the fate of oil spills in Arctic conditions is carried out considering the following processes: spreading, natural dispersion, entrainment in ice, evaporation and emulsification. The effects of advection can be introduced by the combination of the oil spill model with a hydrodynamic or an ice model, therefore are not considered in this analysis. Dissolution, biodegradation and photo-oxidation are not dominant processes acting over surface slicks in Arctic waters, thus are also not included in the model. The final goal of this study is to express each transport and weathering process relevant for Arctic waters as a function of ice coverage and investigate the influence of changes in ice conditions in oil fate in the Arctic. The remainder of this work is organized as follows. Section 3.2 will provide details on the methodology applied to achieve the goals of the research. On Section 3.3, the results are presented, and the most relevant aspects are discussed. Finally, Section 3.4 concludes the study, pointing out future research directions and suggesting improvements to bridge the identified gaps in knowledge.

3.2 Methodology

The proposed methodology is structured in two main parts and corresponding sub-sections. On the first part, all information relevant for the analysis is collected. That encompasses the identification of chemical properties of the oil relevant for the model, spill characteristics such as volume spilled and source of release and the definition of the

environmental background for the modeling, which involves collecting parameters such as wind speed and ambient temperature and ice conditions at the spill site.

On the second part, details are given on the model development as for the assumptions made, the selection of processes and algorithms and how the equations are solved to give a final output as a function of ice concentrations. The flowchart on Figure 3-1 visually presents the proposed methodology.

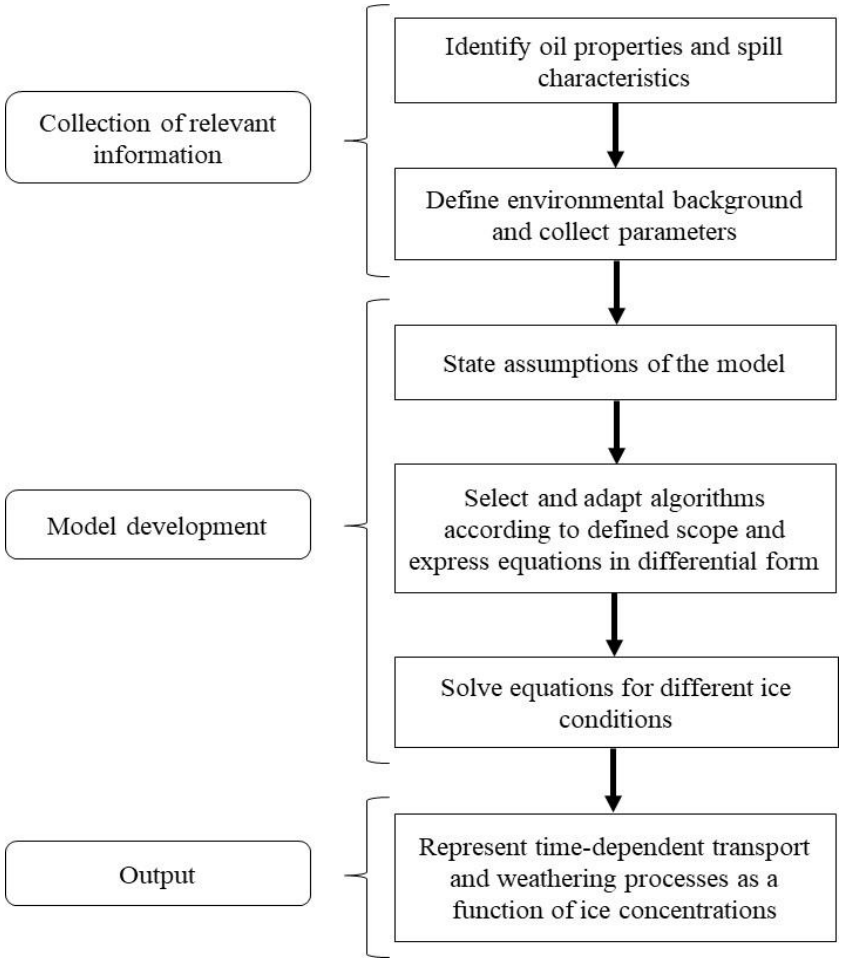

Figure 3-1: Proposed methodology for oil spill fate modeling in ice-infested waters.

3.2.1 Collection of Relevant Information

The first stage of any modeling effort is the collection of applicable input parameters for the simulation to be performed. The type of information required will depend on the scenario under investigation, the algorithms or other tools used in the model and, most importantly, the targeted goals of the analysis. Some models may be interested solely in the spread behavior of oil in the ocean, for which only a small set of parameters may be required. Sometimes however, the objective of the model might be to assess environmental risk of a given release, and for those cases much more detailed input is needed. For the present model, the required input parameters are separated in two different classes: oil properties/spill characteristics and environmental parameters.

3.2.1.1 Oil properties and spill characteristics

Oil is characterized by several key parameters that will determine its hydraulic and thermodynamic behavior and influence the way it is transported and weathered when spilled at the sea. Properties such as oil density, viscosity, solubility and interfacial tension carry important information on how oil may interact with water and ice and are used as input for the model.

Spill characteristics are the conditions in which the oil spill took place, that is, if it is an instantaneous or continuous release, a subsea leak or blowout or a surface release. If it is a continuous release, information on duration and flow rate of the spill are required in order to predict its fate. If, instead, an instantaneous release is the object of the analysis, information on the total volume of the spill may suffice.

The input parameters required for the present model are:

Oil Properties:

- Type of oil;
- Oil density (Kg/m^3);
- Oil viscosity (Pas);
- Oil/saltwater interfacial tension (N/m).

Spill Characteristics:

- Release mode (continuous or instantaneous);
- If release is continuous: spill duration (hours/days) and release rate (m^3/h);
- If release is instantaneous: total spilled volume (m^3);
- Release source (surface, subsea).

Some models may require information on the release path (well blowout, subsea pipeline leakage, surface release from ships, among others), which may be used for underwater plume hydrodynamic calculations, but these aspects are not on the scope of the present work.

3.2.1.2 **Environmental Background and Parameters**

The meteorological and oceanographic conditions in which the spill takes place are crucial to determine how oil will interact with the surrounding environment. Parameter requirements may include ambient and water temperature, wind and ocean current speed

and direction, seawater density and viscosity. If ice is present, information on type of ice and ice coverage will play a major role in determining oil slick fate.

If a hydrodynamic or an ice model is coupled with the oil spill model, information on currents, winds and ice drift will be constantly updated based on the forecasts generated by those models, meaning that the met-oceanographic input to the oil spill model will be changing over time, rather than be specified a priori.

In the current model, hydrodynamic or ice drift models are not used, thus ocean currents are not given consideration. Wind speed is considered constant in time and therefore specified as a single discrete input parameter. Surface waves are considered wind-driven phenomena in the model, hence are not directly addressed. Ice concentration is also considered constant over each simulation, although this parameter is allowed to vary for different simulations in order to study its influence on the oil fate. The environmental input parameters required for the model are:

- Ambient temperature (^{o}C);
- Wind speed (m/s);
- Water density (Kg/m^{3});
- Water viscosity (Pas);
- Ice type (first year ice, multi-year ice, land fast ice, pack ice, brash ice, slush ice);
- Ice concentration (%).

For the present work, the ice field is assumed to be composed of first year pack ice, provided that this is a common type of ice found both static in the Arctic and drifting onto sub-arctic regions.

3.2.2 Model Development

The model developed in the present work is structured in three steps: first, the assumptions of the model are stated and clarified. Second, appropriate algorithms to describe the processes identified as representative of the scenario under study are selected and adapted and represented in the differential form. Finally, the system of differential equations is solved for a range of ice concentrations. The output of the model is then the graphic representation of time-varying transport and weathering processes as a function of ice concentration.

3.2.2.1 Assumptions of the Model

As most oil transport and weathering processes are not fully understood and are described in terms of algorithms derived empirically from lab-scale experiments, oil spill models rely in a set of assumptions, or simplifications, in order to predict a given scenario. The developed model bases upon the following assumptions:

1. Oil slick spreads in a radial pattern. Elongation of slick due to wind, currents and due to the process of resurfacing of temporarily entrained droplets behind the leading edge of oil are not accounted for.
2. The oil slick area on the spreading model is taken as the contaminated zone and slick thickness is assumed to be distributed uniformly over the whole

contaminated area. Discontinuities within the oil slick may exist but are not accounted for.

3. Ice concentration is considered constant throughout the whole ice field where the oil spill takes place. Discontinuities in ice coverage are also not accounted for.
4. Oil is assumed to be advected with the ice in medium to high ice concentrations, that is, the model does not account for relative movement between the oil slick and the ice. In low ice concentration, oil is assumed to move as in open waters.
5. It is assumed that oil pooled underneath the ice will remain there for enough time to be encapsulated and migrate up through brine channels.
6. All the oil that is not between the ice floes is assumed to spread and be retained under ice. No spread of oil on top of ice sheets is considered.
7. The processes of evaporation and emulsification are considered statistically independent.
8. The initial oil slick thickness is assumed to be 0.01 m, as suggested by Afenyo et al. (2016b).
9. The oil spreading is expected to cease when the slick thickness decreases to 0.01 cm, as suggested by Nazir et al. (2007).
10. Oil evaporation is not considered as being strictly air-boundary layer regulated.
11. Wind speed, ambient temperature, oil density and oil/water interfacial tension are assumed constant.

3.2.2.2 **Selection and Adaptation of Algorithms**

In this section, the algorithms selected for the model are explored and a brief discussion is carried out on the applicability of each algorithm to the scenario studied, adaptations required for the current model and existing limitations.

As mentioned before, the following processes are deemed representative of the scenario modeled in the present work: spreading, natural dispersion, entrainment in ice, evaporation and emulsification.

3.2.2.2.1 **Spreading**

Many formulations were suggested by different authors to describe spreading mechanism when ice is present. A description of the available algorithms to model oil spreading in ice conditions is provided by Afenyo et al. (2015). Most algorithms will be applicable for specific ice conditions, e.g., spreading on and under broken ice. In the current work, a more generalist approach was implemented, using the adapted version of the equation by Fay (1969), proposed by Buist et al. (1987).

In this algorithm, the implementation of an ice factor means that it can be applied for all ice concentrations simply by the adjustment of the factor. In fact, Fingas & Hollebone (2003) recommended the use of this equation to model oil spreading in pack ice. In high ice concentrations (>80%) the spreading will be substantially retarded and, by the inclusion of the ice factor this reduction can be modeled. The algorithm selected to model oil spreading in the present work is then:

$$A = (1 - c)\, 6.6 \left(\frac{V^2 g'}{\sqrt{\mu_{oil}/\rho}} \right)^{1/3} t^{0.5} \qquad (3.1)$$

Where A is the increasing slick area (m^2); c is the ice concentration (%); V is the total volume of the oil slick (m^3); μ_{oil} is the oil viscosity at a given time (Pas); ρ is the water density (Kg/m^3); t is the elapsed time (s) and g' is given by:

$$g' = g \frac{(\rho - \rho_o)}{\rho}$$

Where g is the acceleration of gravity (m/s^2), ρ is the water density (Kg/m^3) and ρ_o is the oil density (Kg/m^3).

In the proposed spreading model, the area of spreading is considered as the contaminated area, as shown in Figure 3-2 below.

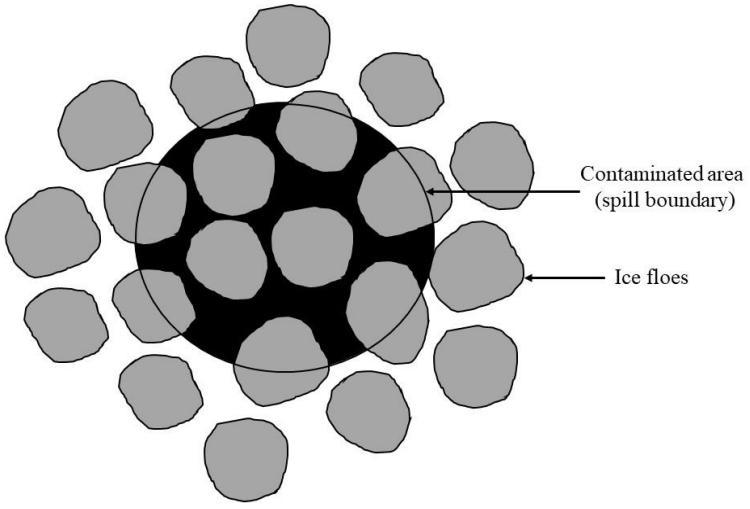

Figure 3-2: Spreading area in the present model (Adapted from Arneborg et al., 2017).

Eq. (3.1) is expressed in the differential form in the formulation by Arneborg et al. (2017):

$$\frac{dA}{dt} = \frac{1}{2}\frac{k^2 V^{4/3}}{A} \tag{3.2}$$

Where all parameters are as before, and:

$$k = (1-c)\ 6.6\ \left(\frac{g'}{\sqrt{\mu_{oil}/\rho}}\right)^{1/3} \tag{3.3}$$

As a consequence of oil spreading, slick thickness decreases. The work by Arneborg et al. (2017) introduced a differential equation to model the rate of slick thickness change due to oil spreading, considering the opposite effect caused by weathering processes, as follows:

$$\frac{dh}{dt} = \frac{1}{A}\frac{dV}{dt} - \frac{h^2}{V}\frac{dA}{dt} \tag{3.4}$$

Where h is the slick thickness (m) and other parameters as in the previous formulation. In the present work, for simplification oil spreading is assumed to cease when the slick thickness reaches a terminal value of 0.01 cm, as suggested by Nazir et al. (2007).

3.2.2.2.2 **Natural Dispersion**

In the present work, natural dispersion – or entrainment in water – is modeled using the formulation by Mackay et. al. (1980). In order to account for ice concentration, the original equation is modified to include an ice correction factor as proposed by Liungman & Mattsson (2011). The differential equation including the proposed ice factor is:

$$\frac{dD}{dt} = r_{ice} \frac{0.11\,(W+1)^2}{1 + 50\mu^{0.5} h\, S_t} \tag{3.5}$$

Where dD/dt is the rate of oil entrainment in water; W is the wind speed (m/s); μ is the oil viscosity (cP); h is the slick thickness (m); S_t is the oil-water interfacial tension (dyne/m); and r_{ice} is given by:

$$r_{ice} = \begin{cases} 0, & c \geq 0.8 \\ (0.8 - c)/0.5\,, & 0.3 \leq c < 0.8 \\ 1, & c < 0.3 \end{cases} \tag{3.6}$$

With Eqs. (3.4) and (3.5) the presence of ice is addressed in the entrainment model. It is expected that for high ice concentrations the natural dispersion will be negligible as waves will be dampened by ice, assuming that entrainment in water is a wave-driven process. By applying the ice correction factor, the natural dispersion goes to zero for high ice concentrations (≥ 80%), is reduced for medium ice concentrations (> 30% and < 80%) and remains unchanged for low ice concentrations (≤ 30%).

3.2.2.2.3 **Entrainment in Ice**

To date, only few works were dedicated to the study of oil entrainment in ice (Martin, 1979; Karlsson et al., 2011; Petrich et al., 2013; Maus et al., 2015), consequently the physical understanding of this process is limited. A mathematical representation of the phenomenon has yet to be developed, reason why most models do not include this process in their scope.

In the present study, a simplistic formulation is attempted to account for oil entrainment in ice based on the findings from Wilkinson et al. (2007) and Karlsson et al.

(2011). According to the first work, oil is expected to be present in about 5% of the underside of sea ice within the contaminated area. The latter work estimated an entrainment capacity of about 0.001 m^3/m^2 in cold sea ice, present during winter and fall. The latter authors highlighted that higher entrainment volumes can be expected during spring and summer in warmer ice, as brine network is more well developed.

The proposed formulation describes oil entrainment as a function of increasing slick area, entrainment capacity per area and expected under-ice oil coverage, taken here as the probability of finding oil in a given point within the contaminated area. It follows that:

$$V_E = A\ E\ C_o \tag{3.7}$$

Where V_E is the volume of oil entrained in ice; A is the slick area at any given time; E is the entrainment capacity of the under-ice topography, taken here as 0.001 m^3/m^2; and C_o is the percent of contaminated area covered by oil under the ice, taken as 0.05. Accounting for the slick area growth over time and replacing the parameters by the suggested values, the differential form of Eq. (3.6) becomes:

$$\frac{dV_E}{dt} = 5x10^{-5}\ \frac{dA}{dt} \tag{3.8}$$

The suggested formulation provides an estimative of the amount of oil taken up by the ice cover, which might be significant at high ice coverages. Oil entrainment in ice adds up to evaporation and natural dispersion as loss processes and may play a major role in oil transport at high ice concentrations where both previous processes are severely retarded or may not occur. It is important to note though that this is a simplistic approach that seeks a better understanding of the overall oil mass balance in ice-infested waters and does not

address the complexity of the encapsulation and entrainment mechanism. Also, no consideration is made in regard to the time necessary for the oil pooled underneath the ice to migrate up through the brine channels. It is assumed that all the oil that becomes eventually trapped at the underside of ice roughness features remains there for enough time to become encapsulated and entrain into the ice cover.

3.2.2.2.4 **Evaporation**

In the present work, the evaporation phenomenon is not considered as being strictly air-boundary layer regulated, meaning that oil does not evaporate by the same mechanism as water. Instead, the model proposed by Fingas (2004, 2015) is used, for which temperature and time are the only parameters required. In his work, the author found that oils evaporate by two different regimes. Some lighter fuel oils evaporate as a function of the square root of time, whereas all other oils will evaporate as a function of the logarithm of time. Considering this aspect, the author developed a series of equations to describe the evaporative behavior of a range of different types of oils, each formulation exclusive for a given oil.

For the present study, Troll crude is selected as the oil type for the modeling effort. Given that only the oil present at the sea surface between ice floes will be subject to evaporation, an ice correction factor is added to the equation to account for ice concentration. The equation proposed by Fingas (2004, 2015) for Troll crude including the ice factor follows:

$$\%Ev = (1 - c)\,(2.26 + 0.045T)\ln(t) \tag{3.9}$$

Where %Ev is the percentage of oil evaporated; c is the ice concentration (%); T is the ambient temperature (°C); and t is the elapsed time (minutes). Writing Eq. (3.8) in the differential form, it becomes:

$$\frac{d(\%Ev)}{dt} = (1 - c)\,(2.26 + 0.045T)\,t^{-1} \tag{3.10}$$

After testing both the presented equation and the algorithm proposed by Stiver & Mackay (1984), this study found a more direct correlation with experimental results in Arctic conditions through the algorithm by Fingas (2004, 2015), which is therefore used for the proposed model.

As volatile fractions of oil evaporate, the remaining oil experiences an increase in viscosity. This viscosity increase can be modeled using the formulation by Sebastiao & Guedes (1995):

$$\mu = \mu_0 \exp[C_4(\%Ev)] \tag{3.11}$$

Where μ is the new viscosity (cP); μ_0 is the initial viscosity; C_4 is a constant dependent on the oil type, taken as 10 for crude oil; and %Ev is the percent evaporated at a given time.

3.2.2.2.5 **Emulsification**

The algorithm adopted in the current work to model oil-in-water emulsions is an adapted version of the broadly used equation by Mackay et al. (1980). Liungman & Mattsson (2011) suggested an ice correction factor to account for ice concentration, given the lower rate of emulsification observed in ice-infested waters. Also, in meso-scale

experiments carried out by SINTEF (Brandvik et al., 2010a), the final water content of the formed emulsions were approximately 0.7, 0.6 and 0.3 for ice concentrations of 30%, 70% and 90% respectively.

The present work makes use of the ice correction factor suggested by Liungman & Mattsson (2011), as well as proposes the adjustment of the final water content, C_f, in Eqs. (3.12) and (3.13) below to account for ice concentration, according to the final water content values reached on the experiment from Brandvik et al. (2010a). It then follows that:

$$Y = C_f \left[1 - exp\left(\frac{-2x10^{-6}}{C_f}((1-c)\,W+1)^2 t\right)\right] \tag{3.12}$$

Where Y is the water content (%); W is the wind speed (m/s); c is the ice concentration (%); t is the elapsed time (s); and C_f is the final water content, taken here as 0.7 for low ice concentrations (≤30%), 0.6 for medium ice concentrations (>30% and <80%), and 0.3 for high ice concentrations (≥80%), according to the definition from Venkatesh et al. (1990). The differential form of Eq. (3.10) is:

$$\frac{dY}{dt} = 2x10^{-6}\,[(1-c)\,W+1]^2\left(1-\frac{Y}{C_f}\right) \tag{3.13}$$

This approach offers an improvement to the conventional emulsification equation that does not account for the presence of ice. The use of an ice correction factor in Eqs. (3.12) and (3.13) enables the algorithm to model the emulsification process for different ice conditions, considering that in higher concentrations the final equilibrium water content will take longer to be reached. In addition, the categorization of the final water content

constant into three ice concentration ranges (low, medium and high) results in water content profiles that agree better with oil-in-ice experiments.

Analogous to evaporation, emulsification also results in increase in viscosity as water droplets are absorbed into the oil slick. Yang et al. (2015) proposed an adapted version of the algorithm introduced by Sebastiao & Guedes (1995) to represent this increase in viscosity due to emulsification at 90% ice coverage, which is also adopted in the present work:

$$\mu = 0.28\mu_0 \exp\left[\frac{2.5Y}{(1 - C_f Y)}\right] - 150 \tag{3.14}$$

Sebastiao & Guedes (1995) suggested that increase in viscosity resulting from evaporation and emulsification are additive, hence statistically independent, implying that the overall viscosity increase can be modeled simply by the sum of both contributions to it. Thus, the algorithm describing the increase in viscosity is given by the combination of Eqs. (3.10) and (3.13), in the differential form:

$$\frac{d\mu}{dt} = C_4 \frac{d(\%Ev)}{dt} + \frac{0.07\mu}{(1 - C_f Y)^2} \frac{dY}{dt} \tag{3.15}$$

Brandvik & Faksness (2009) pointed out that emulsification is the main contributor for increase in viscosity. According to the authors, emulsification leads to viscosity changes in the order of 10^3 or 10^4, whereas evaporation alone only promotes changes in the order of 10^2.

3.2.2.2.6 **Volume Balance**

Oil will be lost from the slick to the atmosphere, ice cover and water column as a result of evaporation, entrainment in ice and natural dispersion, respectively. These loss processes progress with time, eventually leading to the complete depletion of oil from the sea surface. When ice is present, the slick's lifetime at sea will increase given that, the higher the ice concentration, the slower the loss processes. The oil loss rate, or volume variation rate, will be a function of evaporation, natural dispersion and entrainment in ice as in Eq. (3.16) below:

$$\frac{dV}{dt} = -V\frac{dD}{dt} - \frac{dV_E}{dt} - V\frac{d(\%Ev)}{dt} \tag{3.16}$$

Where V is the volume of oil at a given time and dD/dt, dV_E/dt and d(%Ev)/dt are given respectively by Eqs. (3.5), (3.8) and (3.10).

3.2.2.3 **Solution of System of Equations for Different Ice Conditions**

After compiling all the algorithms proposed for the model, the system of differential equations is solved using the software MATLAB Simulink. In the present Thesis, the student version was used. The model consists in five differential equations intended to model the five processes included in the scope of the study (Eqs. (3.2), (3.5), (3.8), (3.10) and (3.13)) in addition to one equation to model the increase in viscosity due to evaporation and emulsification (Eq. (3.15)), one to represent the oil slick volume loss (Eq. (3.16)), and one to compute the slick thickness decrease due to gravitational/viscous spreading (Eq. 3.4).

The system of eight differential equations is solved numerically using the MATLAB solver ode45, a built-in function that makes use of fourth and fifth-order Runge-Kutta methods to solve numerically systems of equations (Nazir et al., 2007). The equations are solved simultaneously in order to account for the interdependence between the processes. More details on the model's algorithms and solution of equations are given on Appendix I.

Since all equations are written as a function of ice concentration, it is possible to vary this parameter and study the implications of this variation for each process. The equations are solved for ice concentrations of 30%, 70% and 90% representing low, medium and high ice concentrations respectively.

3.2.3 Output – Representation of Time-Dependent Processes as a Function of Ice Concentration

The last part of the work – and the final output of the model – is the representation of transport and weathering processes as a function of different ice concentration over a time span of 5 days. All processes are plotted against time and different curves are obtained for three ranges of ice coverage.

Each transport and weathering process can then be analyzed in terms of varying ice concentrations, and comparison with previous works can be made. The main goal is to investigate the different outcomes in oil fate and transport processes given different ice conditions.

3.3 Model Application and Validation

The presented model was applied to a real spill scenario to demonstrate the applicability of the methodology and to attempt to validate it. On May/2009, SINTEF carried out a large-scale experiment – from this point on, referred to as FEX2009 – releasing 7 m^3 of crude oil on the pack ice at the marginal ice zone in the Barents Sea northeast of Hopen Island, where ice concentrations varied between 60% and 70%. After the oil was released on May 15th, 2009 the ice coverage increased to approximately 70 – 90%. The experiment was later reported in the work by Brandvik et al. (2010a), where the authors compared its results with those from a previously performed meso-scale weathering experiment in different ice conditions at SINTEF SeaLab. In the present work, the large-scale experimental results will be compared to the outputs of the proposed model.

The type of oil released was Troll B crude, a naphthenic oil with properties listed in Table 3-1. The oil was released over a period of 30 minutes under temperatures that varied between -2^{o}C and -10^{o}C, seawater temperature around -1.8^{o}C, wind speed between 5 and 10 m/s, peaking at 15-20 m/s during a passing low pressure, and ice drift up to 100 cm/s. Very limited relative movement of ice floes was observed. The spreading oil slick was monitored and weathering profiles were determined for evaporative loss, slick water content and increase in viscosity. According to the authors, oil drifted with the ice, which is in agreement with conclusions from previous studies at medium to high ice concentrations.

The oil was released over a period of 30 minutes and, since this is less than the time step of 1 hour defined for the model, the release is assumed to be instantaneous. The oil

was discharged at the sea surface between ice floes, and as so a surface spill is assumed. Also, for modeling purposes, the wind speed is considered constant at 10 m/s and the ambient temperature is fixed at -2^{o}C. Table 3-2 summarizes the environmental conditions used as input for the model.

Table 3-1: Properties of Troll B crude oil.

Property	Value
Density	885 Kg/m^3
Viscosity	0.0235 Pas
Oil/water interfacial tension	0.0226 N/m

Table 3-2: Environmental parameters used as input for the model.

Environmental Parameter	Value
Ambient temperature	-2^{o}C
Wind speed	10 m/s
Water density	1025 Kg/m^3
Water viscosity	0.00188 Pas

As suggested by Afenyo et al. (2016b), the initial oil slick thickness is taken as 0.01 m and, for a spill of 7 m^3, this thickness is equivalent to an initial spill area of 700 m^2. The initial value of oil entrainment in ice, as connected to the spreading process, is 0.035 m^3. Initial values of evaporative loss, water content and entrainment in water are taken as zero.

3.3.1 Outputs of the Model and Comparison with Experimental Results

After running the model with the algorithms presented in Section 3.2.1 and input parameters defined for the case study, each process was plotted against time with separate curves for the three defined ice coverages.

3.3.1.1 **Spreading**

Regardless of ice concentration, the model predicted a rapid increase in slick area on the first hours after the release, as buoyancy forces are more intense when the oil slick is thick. After the first day, spreading rate decreased drastically and the slick area moved towards a semi-constant equilibrium. Figure 3-3 shows oil spreading profiles for the ice concentrations under investigation, as well as a plot of oil spreading results from the SINTEF FEX2009 experiment, published in the work from French-McCay et al. (2017). The curves show that oil slick area increases with decreasing ice concentration, which was a predicted result according to previous studies. The final spreading area varied in about one order of magnitude from low to high ice coverages at the end of the simulations.

The FEX2009 curve displays a more gradual and linear increase and appears to be developing towards an equilibrium after the third day, although the increase in area does not seem to be ceasing. As the experiment lasted for 5 days only and no monitoring of the oil slick was done after that period, no information is available on the spreading progress after the fifth day, as well on the termination of the process, that is, the terminal area.

Comparing the experimental results (FEX2009) with the model outputs, it can be observed that the model slightly underpredicted the area at the fifth day, considering that the experiment took place in an ice concentration of 70 to 90%. Taken the 70% curve as reference though, the model predicted a slick area of the same order of magnitude as the area observed in the experiment, which can be considered a satisfactory result. Although the 70% curve can be considered a good predictor for the conditions under study, the 30% curve compared the best with the FEX2009 curve, reaching a final area very similar to that

from the experiment. This may be indication of a need for calibration of the ice correction factor, as the low ice concentration model predicted better spreading in medium to high ice concentration. In this respect, it is important that as data becomes available from real spills, models are validated and updated to provide more realistic and reliable outputs. Another difference that stands out between the experimental result and the simulations is that the modeled curves are somewhat plateauing after the second day, whereas the FEX2009 curve remains increasing, though in a lower rate. This is mainly because the spreading algorithm used in the model only accounts for the gravitational spreading, that is, the mechanism by which the oil slick increases in area as a result of buoyancy, viscous and surface tension forces. It does not account for the effect of ocean currents, waves and winds in the increasing area, which will ultimately dictate the fate of the oil slick once the gravitational spreading ceases. Therefore, it is expected that these oceanographic forces will result in a continued spreading effect on the oil slick that is not predicted by the model.

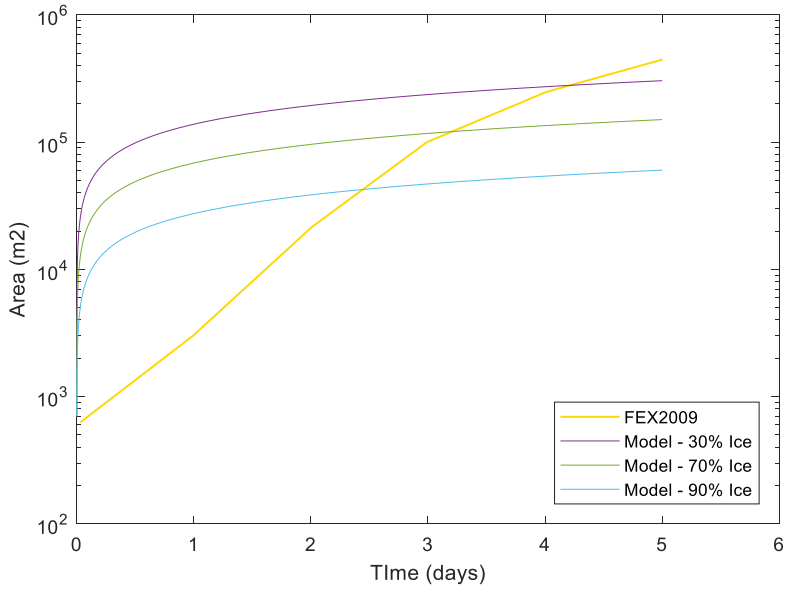

Figure 3-3: Modeled and experimental results for oil spreading.

Figure 3-4 displays the modeled decrease in oil slick thickness due to spreading process. The work from Brandvik et al. (2010b) does not include considerations on the slick thickness, therefore comparison is not provided. Ice concentration had a high influence on the thickness profile over the simulation time. The minimum thickness of 0.01 cm was reached on the second day of simulation for the low ice concentration case, whereas for medium and high ice concentrations this terminal thickness was not reached over the time span of the simulation.

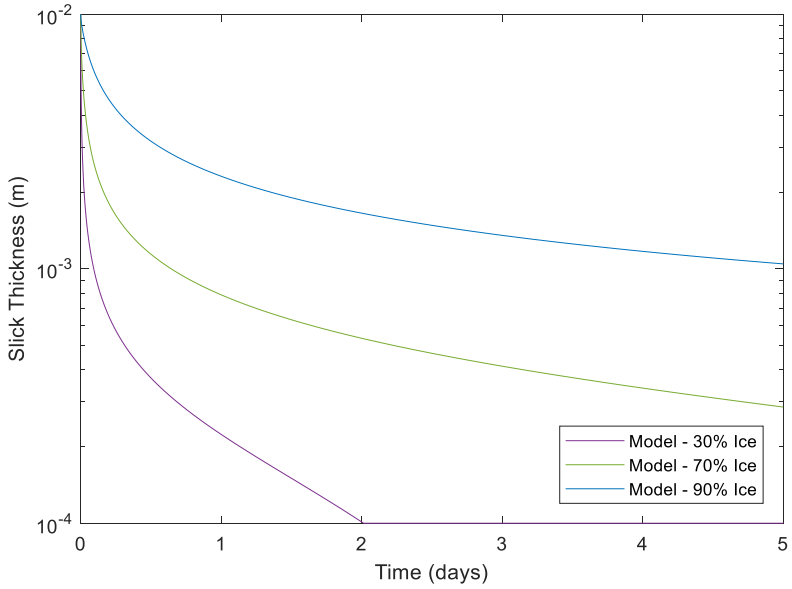

Figure 3-4: Modeled decrease in slick thickness.

Analyzing the plot, it becomes clear that the higher the ice concentration, the slower the rate of slick thinning, hence at medium to high ice coverages the final area will take longer to be reached, meaning that spreading process will persist for a longer period.

3.3.1.2 **Evaporative Loss**

On the first hours of the simulation, evaporation rate displayed a rapid increase as volatile fractions of oil are quickly lost to the atmosphere. This is in agreement with Sebastiao & Guedes (1995), which suggested that over 50% of more volatile oils are expected to evaporate in the first 24 hours after a spill in open water. After the first day, the oil slick has lost most of more volatile components and, as a result, its total vapor pressure dropped (Stiver & Mackay, 1984) and the rate of evaporative loss decreases, eventually depleting to zero.

In the simulations, the evaporative loss response to changing ice concentrations displayed a high variability. Figure 3-5 reveals that changing the ice concentration in the simulations affected dramatically the evaporation rate. Evaporative loss for the medium ice concentration case was found to be over three times greater than for the high ice concentration case and almost two times lower than for low ice concentration.

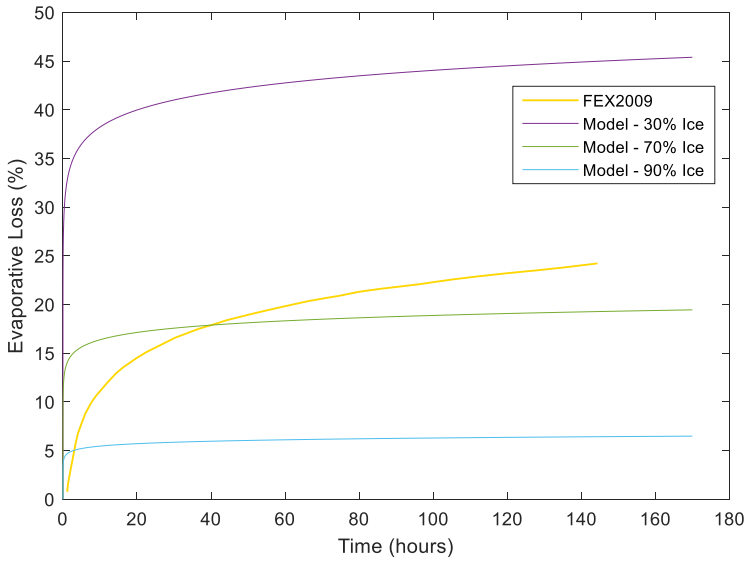

Figure 3-5: Modeled and experimental results for evaporative loss.

The model showed good correlation for 70% ice concentration, outputting similar evaporative loss to the experiment FEX2009, conducted in 70-90% ice coverage. The much higher evaporation rate observed in low ice concentration is expected, since nearly all the oil will be on the surface and ice does not represent a barrier to the process. However, the model underpredicted the evaporative loss for 90% ice coverage, when compared to previous meso-scale lab experiment carried out by Brandvik et al. (2010a). It can be considered that the model's predictions correlated well with the observations for evaporation, as the experiment was conducted in ice coverages that varied from 70 to 90% and the model's 70% curve displayed the best fit to the experimental results.

3.3.1.3 **Emulsification**

The modeled emulsification profiles varied significantly from medium to high ice coverages, both in terms of rate of water uptake and final water content. However, final water content for low and medium ice concentrations were similar. Brandvik et al. (2010a) noted that the Troll B crude has a more balanced blend of natural emulsion stabilizers (resins, asphaltenes and waxes), thus forms more stable emulsions, which may explain the lower sensitivity to ice variations at lower ice coverage.

In Figure 3-6 it can be noted that the slope of water content curves decreases with increasing ice coverage, implying that the time required for the emulsions to stabilize at its final water content is greater for high ice coverages. While for 30% ice concentration the final water content was achieved within a few hours after the release, it took over a day in 70% ice concentration and over two days in 90% ice concentration for the terminal water content to be achieved. The final water content for low, medium and high ice concentration

was 70%, 60% and 30% respectively, as expected after adjusting the final water content constant in Eq. (3.13) for each ice coverage range.

According to Brandvik et al. (2010b) the ice concentration during the experiment FEX2009 varied from 70% to 90% on the days following the oil release. The final water content for the FEX2009 curve is reached between the model's 70% and 90% curves, thus the model's estimations are consistent with the experiment's result given the variability in ice conditions in the field, although did not provide an exact prediction.

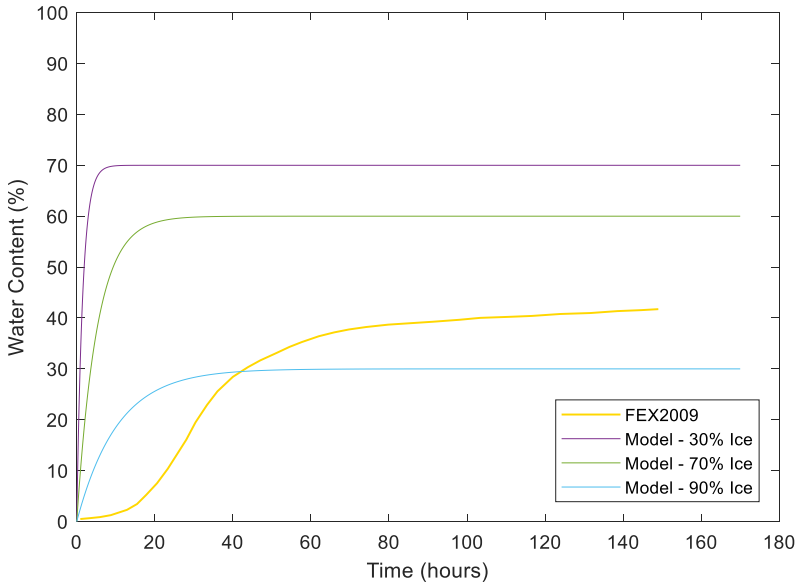

Figure 3-6: Modeled and experimental water content profiles.

The model also compared well with water content profiles from the meso-scale experiments conducted by SINTEF (Brandvik et al., 2010a) for medium and high ice concentrations. For low ice concentration, the work from Brandvik et al. (2010a) predicted lower water uptake than expected, but the authors highlighted that this was likely due to the presence of slush ice in the open water experiment.

3.3.1.4 **Increase in Viscosity**

The change in the emulsion viscosity followed the same trend as evaporative loss and water content, as connected to these processes. In the simulations, the rate of viscosity change peaked almost immediately after the release, becoming practically negligible only a few hours later. As a result, the viscosity quickly reached a more constant state in which increase is no longer significative. In higher ice concentrations, viscosity did not increase as much as in lower ice concentrations, hence the final value of viscosity was lower. In Figure 3-7 it can be seen a substantial variation in viscosity from low to high ice concentration. While viscosity increased to only about 650 cP for high ice concentration, it was as high as 2000 cP and 4500 cP for medium and low ice coverages, respectively. This high variability in viscosity range for different ice conditions was predicted by previous works (Brandvik & Faksness, 2009 and Brandvik et al., 2010) and directly influences other processes such as spreading and natural dispersion.

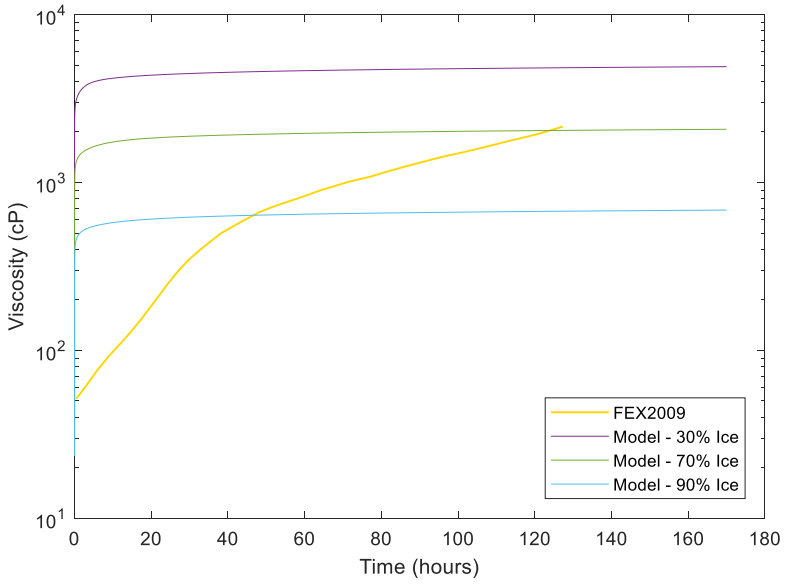

Figure 3-7: Modeled and experimental viscosity increase profiles.

The experimental curve exhibited a more gradual increase and the viscosity change rate only dropped after the first day, as opposed to a drop within the first hours in the simulations. Although a steady state was never reached in the experiment, it can be noted a decreasing trend in the rate of viscosity change indicating that, given enough time, the viscosity may become constant as in the simulations.

The model correlated well to experimental results as the FEX2009 curve remained between the 70% and 90% curves during most of the simulation time, reaching the same final viscosity (about 2100 cP) as for the 70% ice concentration case by the end of the experiment.

3.3.2 **Other Results**

The model output also included the representation of the processes of natural dispersion and entrainment in ice, as those are critical processes for the long-term oil removal from the sea surface. Additionally, the volume balance of oil in the ocean was expressed as a function of losses due to evaporation, natural dispersion and entrainment in ice. The work from Brandvik et al. (2010a) does not include consideration on these processes, thus comparison was not performed. For this analysis a time-span of 20 days was selected, in order to investigate the behavior of these processes in a longer term.

3.3.2.1 **Natural Dispersion**

Figure 3-8 shows that the amount of oil dispersed was highly sensitive to the ice concentration in the simulations. The plot indicates a significant difference in natural dispersion rates from the low to the medium ice concentration cases, which can be attributed to the inclusion of an ice correction factor in the entrainment equation (Eq. (3.5)).

The ice factor allowed the model to simulate the high variability in natural dispersion under different ice concentrations, representing an improvement to previous models that were not capable of simulating the influence of ice coverage in the dispersion rate. The plot only shows dispersion curves for 30% and 70% ice concentrations because one of the model assumptions is that for concentrations equal to or greater than 80% the ice cover will damp wind-driven waves, preventing the process to occur.

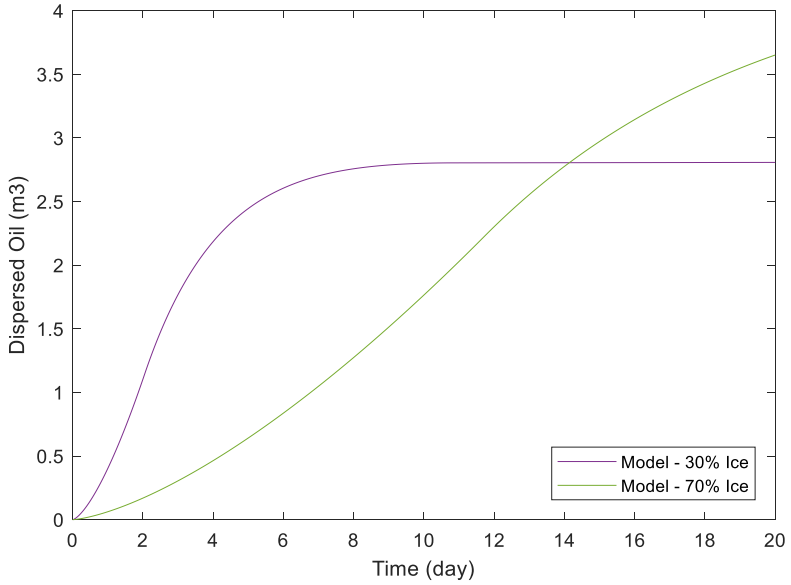

Figure 3-8: Modeled volume of oil naturally dispersed.

Besides the wind speed, oil/water interfacial tension and ice coverage, which are assumed constant in each simulation, natural dispersion is a function of decreasing oil slick thickness (aiding the process) and increasing oil viscosity (retarding it). Thus, dispersion is controlled by a balance between these two main drivers as the surface oil is gradually lost to the water column. In the simulation for 30% ice coverage, the dispersion curve's slope is greater than in the 70% case due to the higher spreading rate (Figure 3-3), resulting

in a higher rate of oil slick thinning. As oil was lost from the slick, dispersion rate decreased progressively until all the oil is consumed and, therefore, dispersion ceased. Cessation of natural dispersion occurred when the curve reached a constant value, meaning that oil was completely depleted from the slick. At 30% ice coverage, the complete consumption of oil occurred at the 10^{th} day, whereas at 70% oil was not completely consumed from the slick over the time-span of the simulation, thus dispersion continued to progress although a slight decrease in rate is observed after about the 16^{th} day, as volume of oil available for dispersion decreased.

3.3.2.2 **Entrainment in Ice**

The inclusion of an algorithm to model oil entrainment in ice represents an innovation in the current work, as previous studies on this process did not provide a formulation to describe it objectively. As a function of oil spreading, entrainment in ice displayed analogous trend to that process, although developed in much slower rate given that the two processes are correlated by a factor of 10^{-5}. The entrainment in ice in the present model is a function of growing slick area, the entrainment capacity of the underside of the ice cover and the probability of oil to be found under the ice in a given point within the contaminated area. In lower ice concentrations, less oil is expected to be under the ice, even though the contaminated area grows rapidly, reaching its terminal value much faster than in higher ice coverages. In the simulation for 30% ice coverage, the ice entrainment process ceased 2 days after the release, which coincided with the termination of spreading process, and the total entrained oil for that case was about $1m^3$. At 70% ice coverage, entrainment ceased after the 12^{th} day and total loss by entrainment was approximately 1.1

m^3. At 90% ice coverage, spreading mechanism is greatly retarded and consequently oil entrainment in ice lasts longer, thus after the 20 days of simulation the process was still ongoing and was responsible for the loss of only about 0.6 m^3 of oil from the water surface. In order to determine the time required for the termination of entrainment in ice, the time-span of the model was increased to 300 days. The entrainment process lasted for about 280 days, and the total entrained volume was 2.1 m^3. At these high ice conditions, the process took about 75 days to remove the same amount of oil as for the 70% ice case. The extremely long time required for the oil to entrain through the ice cover at heavy ice conditions reveals the persistency of oil slicks on the water surface under this scenario.

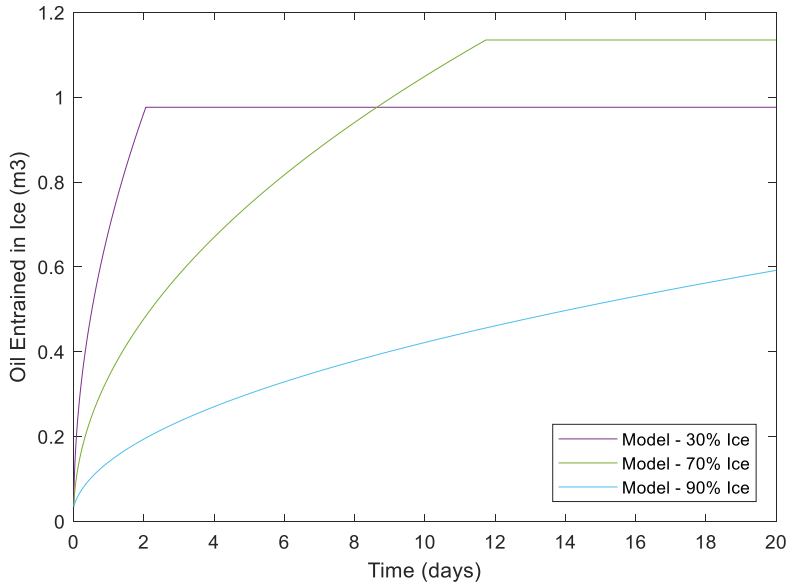

Figure 3-9: Modeled oil entrained in ice.

Overall, after the 20 days of simulation, entrainment in ice accounted for the removal of 14%, 16% and 9% of the total oil released respectively for 30%, 70% and 90%

ice coverages. When time-span was increased, entrained volume for the high ice coverage case was 30% of the total oil.

The use of a simplistic formulation to model such a complex process represents a limitation of this study as important parameters such as ice salinity, temperature and oil pool thickness under ice are not considered. However, in the present analysis this process is included as a means of better predicting the overall oil volume balance in ice-covered waters, and the model does not aim at a detailed description of the mechanisms by which it occurs, thus the simplification is justified.

3.3.2.3 **Volume Balance**

The processes of natural dispersion, evaporation and, when ice is present, entrainment in ice, are responsible for oil loss from the surface to the water column, atmosphere and ice cover, respectively. Evaporation is the dominant removal process within the first hours of a spill, after which it becomes less important. Entrainment in ice in the present model is a function of oil slick growth, and as such peaks in the first hours and ceases when the slick stops to spread. Natural dispersion is then the ultimate driver of oil removal from the surface, and the rate by which it develops eventually dictates the oil slick lifetime at the sea surface.

The oil volume thus decreases over time as a result of the mentioned processes until completely depleted from the water surface, and the ice coverage has a high influence on the time required for this removal, as illustrated in Figure 3-10. As transport and weathering processes are retarded when ice is present, the higher the ice coverages the higher the persistency of oil on the water surface.

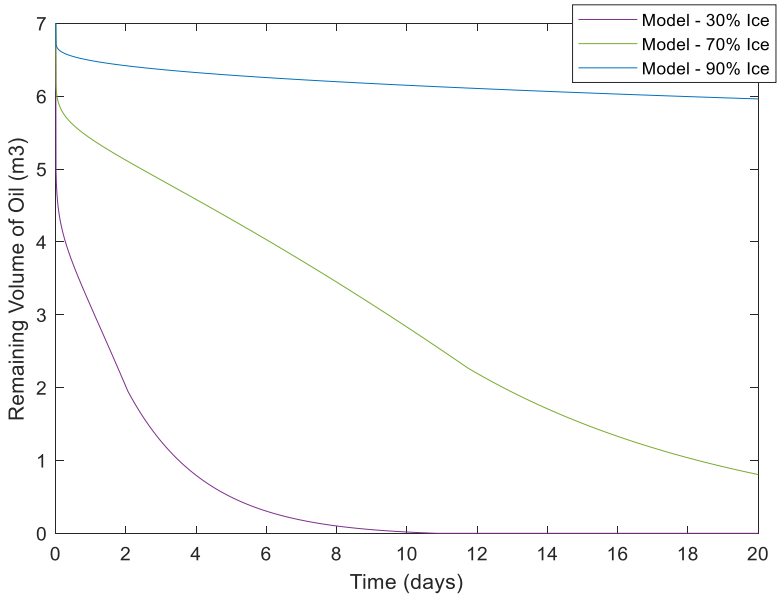

Figure 3-10: Oil volume balance.

The plot shows the great variance in oil volume balance for different ice conditions. While for the low ice coverage case all the oil was depleted in about 10 days, at the end of the 20 days of simulation there was still about 10% of the total oil volume remaining at the surface for the medium ice coverage case and for high ice coverage the slick volume was still 85% of the total release. This significant variation can be explained by the dominant process in each case. For lower ice concentrations, evaporation alone is responsible for the removal of almost 50% of the oil volume in the first hours after the spill, followed by natural dispersion which will drive the remainder of the oil volume to the water column. In this case, the loss via entrainment in ice is minor compared to the other processes playing out and oil is quickly removed as evaporation and natural dispersion occurs at high rates. The higher the ice concentration, the slower the rate of evaporation and dispersion and the more important entrainment in ice becomes. At medium ice concentrations, evaporation

and natural dispersion, though still present, are less efficient in terms of oil removal. At high ice concentrations, natural dispersion does not occur and evaporation is minor, hence entrainment in ice is the dominant process. As entrainment in ice is a very slow process, it results in a long slick lifetime on the surface, as showed in Figure 3-9.

The oil volume balance provides valuable information that can be used to assess oil spill impacts and assist in contingency planning. Oil slick lifetime can be considered as being virtually infinite for modelling purposes in some cases in which removal processes are either too slow or inexistent and weathering processes are difficulted by the presence of heavy ice, implying that oil will remain unchanged for a long time. In the simulation of 90% ice concentration for example, even after increasing the time span to 100 days oil was still not completely removed from the surface slick. In those cases, oil will be transported with the ice drift and will only be subject to weathering and loss processes after ice concentration reduces in spring and summer thaw, representing a risk to environments far from the original spill site.

3.4 Concluding Remarks

Improvements have been suggested to existing oil spill models to describe better the oil behavior in ice-covered waters, and a new formulation was proposed to predict oil entrainment in ice. The inclusion of ice correction factors of two types in the traditional transport and weathering equations yielded results that compared well to experimental results from Brandvik et al. (2010a) and allowed the analysis of each process separately for three ranges of ice concentrations (low, medium and high). Additionally, by the

adjustment of the final water content constant C_f in the emulsification equation, water uptake could be modeled with greater accuracy under varying ice conditions. Likewise, the development of a simplistic approach to model entrainment in ice led to more accuracy in the oil volume balance at high ice coverages, representing an improvement to existing models which do not include this process in their calculations. It was shown that oil mass balance in heavy ice conditions can be significantly influenced by the process of oil migration through the ice, being responsible for removal of up to 30% of oil inventory on the water surface. This can be an important route for oil transportation to locations distant from the point of release, as ice is advected with winds and ocean currents and may release the entrained oil upon spring and summer thaw long after the spill occurred.

Overall, all processes displayed a decreasing trend with increasing ice concentrations, implying that in ice conditions transport and weathering of oil will be significantly slower than in ice-free waters. While some processes such as evaporation, dispersion and entrainment in ice showed a more pronounced difference between the three ranges of ice concentrations, oil spreading was not very sensitive to changes in ice coverage although the timely change in slick thickness due to spreading was considerably sensitive to ice variations. Emulsification and increase in viscosity, as connected processes, exhibited similar trends. For those processes, a more significant difference was observed from medium to high ice concentrations than from low to medium, which might be related to chemical properties of the Troll B crude, used as the oil type in the model.

The adapted and developed algorithms could be potentially used to calibrate and update existing models, and as data becomes available, validation can be performed. As

field data on oil spills in ice-covered waters is very scarce, tests can be performed with existing programs in order to compare outputs, allowing for more meaningful conclusions. Some of the findings of the present work can help to fill identified gaps from previous models and represent one step further on the search for a better understanding of oil interaction with ice, although limitations are still present. The model performed well for the specific scenario simulated, however given that it is based in many empirical formulations without a solid physical description, care must be taken when applied to other scenarios, for which other adaptations may be required. The combination of an ice drift model with the proposed surface slick model would represent an outstanding opportunity for enhancing the accuracy of the predictions, as the permanent ice variability in real-field conditions would be addressed, providing more realistic outputs. Whenever field data becomes available, it should be used to calibrate developed models, thus it is crucial that research efforts keep on the direction of continuously testing, improving and validating newly developed models.

Chapter 4: Estimation of Ecological Risk of Oil Spills in Ice-Infested Waters: A Food-Web Bioaccumulation Model

Abstract: The complexity of the Arctic environment and the lack of knowledge on the behavior of oil when spilled in ice-infested waters hinder ecological risk assessment efforts for oil spill scenarios, and the development of tools to incorporate this complexity in models is needed. The present work introduces a fugacity-based food-web bioaccumulation model to predict the distribution of toxic components of oil in the environment after an oil spill in ice-covered waters and the associated risk level to an Arctic food web. A multi-compartment evaluative environment consisting of air, ice, water and sediment and a three-levels linear food web composed by phytoplankton, zooplankton and fish (Arctic cod) are defined and concentrations in each compartment are calculated. The concentration in fish is then used to determine the bioaccumulation potential by the analysis of the Bioconcentration Factor (BCF) for Arctic cod, selected as representative species of the Arctic ecosystem. Concentration in water is used to define the Risk Quotient (RQ) to the marine environment. Overall, the model predicted low bioaccumulation potential for fish and the risk quotient to the water compartment did not exceed the criterion for naphthalene.

4.1 Introduction

As climate change progresses and sea ice retreats, the Arctic becomes the "next frontier" for oil and gas operations and marine transportation (AMAP, 2010; Nevalainen et al., 2016). Reserves in the Arctic were estimated in 90 billion barrels of crude oil and 44 billion barrels of natural gas, accounting for 13% of all undiscovered oil and gas in the world (Camus & Smit, 2018) and 22% of the world's remaining oil and gas reserves, but the new opportunities brought about by a more accessible Arctic environment are followed by new challenges and risks. Risk is often defined in terms of the level of uncertainty associated with activities, and in the case of Arctic operations one major source of uncertainty is the lack of knowledge on Arctic environment and ecology. Moreover, the behavior of oil when spilled in icy waters is not fully understood, as limited data from real spills is available. The fate of oil in ice-covered waters may differ dramatically from spills in open waters, and the estimation of environmental damage highly depends on accurate information on oil distribution in the marine environment, as well as on ecosystem components present in potentially affected areas (Word, 2014). Another complicating factor is that, considering the harsh nature of the Arctic, oil spills may be difficult to respond due to factors such as fog, hazardously low temperatures, heavy ice conditions and extreme meteorological events like polar lows, among other circumstances that hinder cleanup efforts, thus conventional oil spill response options may not be feasible in many cases. In that scenario, oil will be left to natural attenuation processes, and the estimation of environmental risk associated with those spills will be of paramount importance for the protection of ecologically sensitive species' and habitats.

In the context of environmental risk assessment, fugacity-based models offer a simple and tangible representation of the distribution of contaminants in the environment, accounting for complex processes such as advection, degradation and diffusion (Mackay & Paterson, 1981). Considering the linear relationship between fugacity and concentration, the fugacity framework can be directly applied to study the chemical partition in a multimedia environment after a release, and concentrations in each medium can be estimated.

In multimedia fugacity modeling, evaluative environments are defined as units of study containing two or more compartments, or phases, containing the chemical of interest. There might be direct emissions within the evaluative environment or the chemical may be transported into it from sources outside this "unit world" through advection (Mackay & Paterson, 1982). Environmental compartments are defined by their physicochemical properties and volumes and are composed by the continuous (bulk) phase and dispersed sub-compartments. Water, for instance, is composed by the sub-compartments water, suspended material and biota which are summed up to form the bulk compartment.

Mackay (1979) proposed the study of chemical partition, intermedia transport and loss processes through models of four levels of increasing complexity. On Level I, all phases are in equilibrium in a closed system and have the same fugacity, from which the concentrations in each medium are calculated. Level II adds loss processes and a chemical emission source to the system, but equilibrium between bulk phases is still assumed, meaning that no intermedia transfer of chemical occurs. On Level III, the equilibrium assumption is dropped, hence equi-fugacity between phases no longer applies, although

equilibrium still exists between sub-compartments within each phase. Chemical is then allowed to migrate between phases through various processes including diffusion, deposition and advection in steady-state conditions, that is, the system is static and concentrations do not change over time. Level IV is a development of Level III to model unsteady-state systems, enabling the calculation of concentrations that change over time due to, for instance, increasing or decreasing emissions (Mackay, 2001). The chemical distribution in the evaluative environment can then be investigated and intermedia transport, as well as loss processes, can be described systematically with increased level of detail.

As an extension of the fugacity approach, bioaccumulation models can be assembled by considering the biotic media as bulk compartments in the calculations. Chemical uptake and loss processes taking place in organisms can be described in a trophic-level basis, enabling the estimation of contaminant accumulation in a given trophic level, as well as the chemical transfer throughout the food chain. In a marine ecosystem, chemical uptake and loss in organisms occur by gill exchange due to respiration, food consumption, egestion, metabolic transformation and growth dilution (Sharpe & Mackay, 2000) . These processes are quantified in each trophic level, and the transfer of contaminant to upper levels of the food web occurs by consumption of organisms situated at lower levels in the structure. The model thus provides a tool for analyzing the potential for long-term accumulation and transfer of contaminant between organisms.

Level IV fugacity models have been explored to oil spill modeling in ice-infested waters (Yang et al., 2015; Afenyo et al., 2016a & 2017b) and the methodology has yielded

representative results. Arzaghi et al. (2018) introduced a statistical treatment to the input parameters for the fugacity model using Bayesian networks to address uncertainties in the model, which represented an improvement to the use of point estimates.

In Arctic waters, ice cover is included as a bulk compartment in the multimedia evaluative environment, and chemical exchange between ice and other phases is investigated. Although previous works have made use of the fugacity framework to model oil distribution in icy waters, no studies to date included a food-web structure in the analysis. Furthermore, direct input to ice cover through brine drainage network has never been accounted for in similar works.

On the Chapter 3 of the present thesis, the fate of the surface oil slick was examined, and transport and weathering processes were simulated to obtain time-variant profiles of each process contributing to the change in position and in physicochemical properties of the oil slick. Two of the modeled processes, namely natural dispersion and oil entrainment in ice, are used as input for the fugacity model proposed in the present Chapter.

In the current Chapter, a Level IV fugacity model is applied to obtain the mass balance of oil in an evaluative environment consisting of abiotic and biotic media representing an Arctic environment. The abiotic media considered are air, water, sediment and ice cover. The biotic media is represented by a linear food chain composed by phytoplankton, zooplankton and fish (Arctic cod), in increasing order of complexity. According to Vergeynst et al. (2018), the bioavailability of hydrocarbons in the water column is determined by dispersion and dissolution, thus the input to the water column in the present work is a function of natural dispersion of oil, calculated in the Chapter 3 of the

present thesis. The evaluative environment also receives direct input to the ice cover due to oil entrainment in ice, also given in Chapter 3. After compiling all input parameters required by the model, a system of seven linear differential equations is assembled to express the mass balance of contaminant in each of the seven compartments, and the concentration profiles are given by the solution of the system of equations.

In order to examine the ecological risk represented by the distribution of oil in the environment, two endpoints are selected: the Bioconcentration Factor (BCF) and the Risk Quotient (RQ). The BCF is the ratio of contaminant concentration in fish to that in water (Arnot & Gobas, 2006) and expresses the tendency for chemical accumulation in an organism through respiration processes, that is, via gill exchange with water. The RQ is a quantity used in ecological risk assessment that compares the concentration in a medium of interest with a standard quality value for a given contaminant. It is obtained by the ratio of the Predicted Exposure Concentration (PEC), outputted by the model, to the Predicted No Effect Concentration (PNEC), derived in ecotoxicological studies (Afenyo et al., 2017b). In the present analysis, concentrations in fish and water are selected for the endpoints BCF and RQ, respectively.

The fugacity approach is only capable of handling calculations involving defined substances. As oil is a mixture of several compounds, the analysis requires the selection of one or more of oil's components to be studied separately (Nazir et al., 2007). Given that the proposed model is intended to be a tool to support ecological risk assessment, it is convenient to select components that are more soluble in water and toxic to marine organisms. As suggested by previous works (Nazir et al., 2007; Yang et al., 2015; Afenyo

et al., 2016a & 2017b; Arzaghi et al., 2018a & 2018b), naphthalene is used as surrogate for oil in the present analysis.

The following sub-chapters will present the methodology applied in the work and a case study will be introduced to demonstrate the applicability of the methodology for the scenario under investigation. Finally, the work is concluded with the findings from the case study and overall remarks.

4.2 **Methodology**

In order to represent the distribution of oil in an Arctic marine environment following an oil spill and estimate the associated environmental risk, the present work employs the Level IV fugacity framework applied to a food-web bioaccumulation model. Two outputs from the model presented on Chapter 3 are used as input for the model developed in the current Chapter: the emission of naphthalene to the water column is given by the natural dispersion of the oil slick, and the emission to the ice cover is a function of oil entrainment in ice. Emission rates in both compartments change over time, and the influence of this in the distribution of contaminant in different media is analyzed. The proposed methodology is presented graphically on Figure 4-1 and detailed in the next sub-chapters.

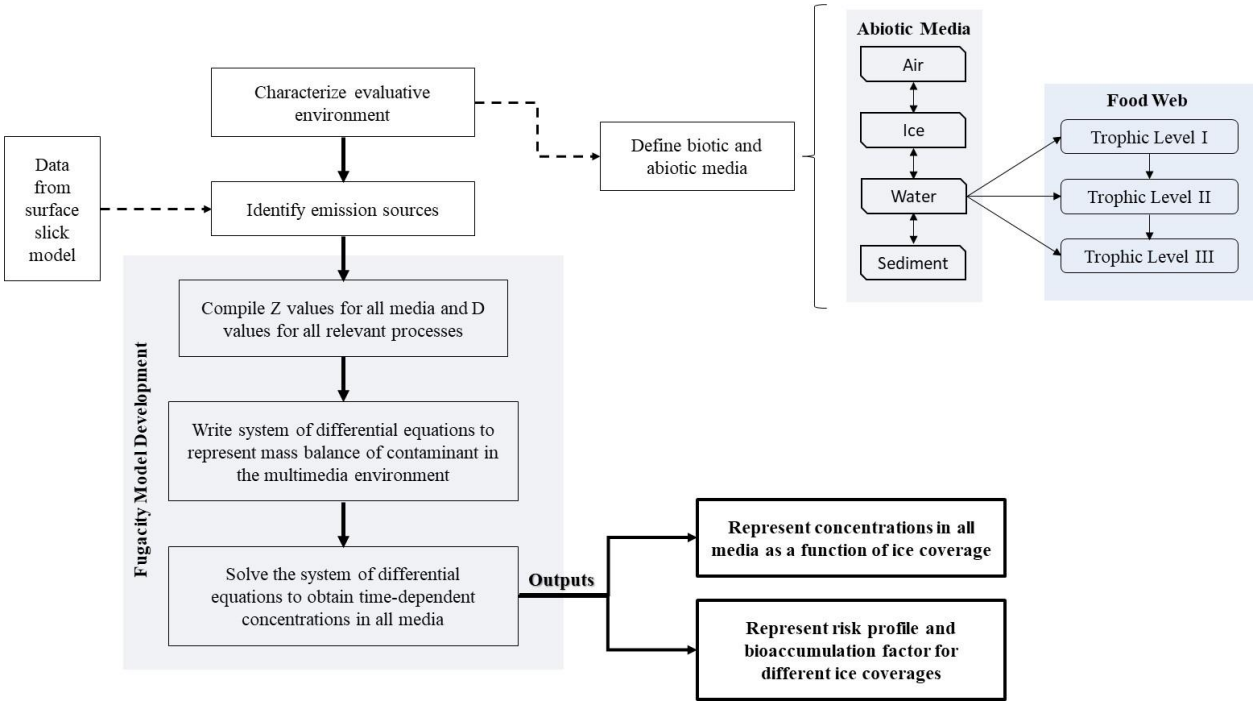

Figure 4-1: Proposed methodology for a fugacity-based food-web modeling in ice infested waters.

4.2.1 Characterization of Evaluative Environment

For the present analysis, the evaluative environment consists in biotic and abiotic media. Included in the abiotic are air, ice cover, water and sediment. A linear food chain comprising 3 levels is selected to represent the biotic media.

4.2.1.1 Abiotic Media

The abiotic media was selected to represent a marine environment away from the shore. The evaluative environment is enclosed by an ice field consisting of pack ice and is composed by four bulk compartments (air, ice, water and sediment). Each compartment contains one or more sub-compartments: air contains pure air and aerosols; ice cover

contains pure ice and organic matter[1]; water contains pure water and suspended solids (in this work, biota is treated separately as bulk compartments in the food-web model, thus it is not included as a sub-compartment); and sediment contains solids and pore water. The volume fractions of the sub-compartments in each bulk compartment is presented in Table 4-1. Other characteristics and dimensions of bulk compartments are given in Table 4-2.

Table 4-1: Volume fractions of sub-compartments in each bulk compartment.

	Bulk Compartment			
Sub-Compartment	**Air**	**Ice**	**Water**	**Sediment**
Air	1	0	0	0
Water	0	0	1	0.63
Solids	$2x10^{-11}$	$5x10^{-6}$	$5x10^{-6}$	0.37

Table 4-2: Dimensions and characteristics of bulk compartments.

Compartment	**Air**	**Ice**	**Water**	**Sediment**
Organic carbon fraction	0	0.2	0.2	0.04
Area (m^2)	$7x10^5$	$7x10^5$	$7x10^5$	$7x10^5$
Depth (m)	100	0.5	100	0.05
Volume (m^3)	$7x10^7$	$1.5x10^5$	$7x10^7$	$3.5x10^4$
Density (kg/m^3)	1.19	916	1000	2500

On Table 4-1, values for fraction of solids in air is taken from Sweetman et al. (2002) and in water and sediment are taken from Mackay & Paterson (1981). Fraction of solids in ice are assumed equal to the fraction of solids in water. Fraction of water in sediment is also taken from Mackay & Paterson (1981). The density of sediment in Table

[1]In real environments, ice cover contains fractions of liquid water and air in the pore spaces, but due to the high variability in volume fractions of those components and lack of sufficient data, these are not included in the calculations.

4-2 is taken from Sadiq (2001). In the present study, the water surface is assumed to be covered by ice in all scenarios. For lower ice concentrations, slush is assumed to be present between ice floes, impeding the direct exchange between water and air. The ice field is assumed to be composed by first-year ice with an average thickness of 0.5 m, in accordance with definition by Lepparanta (2005).

4.2.1.2 **Food-Web Structure**

The Arctic's harsh environment has a great impact on the development of its ecosystems, which are characterized by highly seasonal patterns mostly associated with ice melting periods with increased sunlight. Also, convergence zones – boundary regions such as shorelines, ice edges, polynyas and ice/water interface – represent important environmental compartments which are populated by key Arctic species, considered as valuable ecosystem components (Word, 2014). The high seasonality in Arctic biological productivity and short periods of time available for species to develop result in short food webs and low species diversity, mostly associated with heavy blooms of plankton at spring (Word, 2014).

The selection of representative species is a vital element of a food-web bioaccumulation analysis, which should reflect the level of complexity of the ecosystem under investigation. According to Word (2014), "certain taxa play a critical role in maintaining and supporting the ecosystems and other trophic levels, as well as supporting the ecosystem resources and function". In fact, Gobas (2008) suggested that food-web structures should include as few representative species as possible, and selection should be based on species of key relevance for analysis for the sake of simplicity and transparency

in the calculations. Thus, a simplistic approach considering two or three key species with linear relationships may suffice to describe short and limited food webs such as those present in the Arctic. In this context, two groups of organisms stand out as crucial to the maintenance of Arctic ecosystems. Planktonic species compose the base of the pelagic food web, responsible for the primary productivity of ecosystems in the Arctic. Phytoplankton are on the very bottom of the pelagic food chain and are the main source of food for zooplankton communities, which are critical to the Arctic's overall productivity and compose the dietary base for several species of fish, marine mammals and birds (Arctic Council, 2013) . Followed by plankton, the Arctic cod is also of great importance in Arctic ecosystems, representing a link between lower (zooplankton) and higher (marine mammals) trophic levels. Any reductions or alterations in populations of phytoplankton, zooplankton or Arctic cod may lead to damage to the entire Arctic food-web structure, impacting the resilience of those ecosystems to external perturbations.

In the present work, a linear 3-levels food-web structure is selected as representative of the Arctic pelagic ecosystem, with phytoplankton situated at the bottom of the food chain, followed by zooplankton and Arctic cod, representing the second and third trophic levels respectively. Organisms on each level feed exclusively on organisms one trophic level lower, which is a reasonable assumption for this scenario given that zooplankton species such as copepods and euphausiids are a main component in Arctic cod's diet (Rand et al., 2013) and phytoplankton consists in a critical food source for zooplankton communities (Word, 2014). Chemical uptake by marine organisms occurs by respiration through gills and by consumption of contaminated food. Clearance processes include egestion, exchange through gills as result of respiration and the self-elimination

processes of metabolism and growth dilution. Uptake and clearance processes are described in terms of D values, which can be compared to determine dominant and negligible processes. The food-web structure is represented graphically in Figure 4-2.

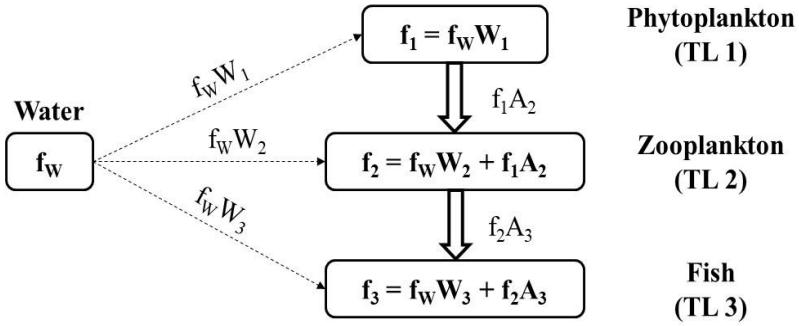

Figure 4-2: Proposed food-web structure for the present model. TL stands for Trophic Level. (adapted from Campfens & Mackay, 1997).

In the figure above, each organism takes up contaminant from water through respiration ($f_W W_1$, $f_W W_2$ and $f_W W_3$) and functions as a dietary source of contaminant for the organisms on the next trophic level ($f_1 A_2$ and $f_2 A_3$). The bioaccumulation is then expressed by the bioconcentration term (W) and the biomagnification term (A) representing contaminant uptake through respiration and food consumption, respectively.

4.2.2 Identification of Emission Sources

Upon dispersion of oil in the sea, oil droplets are transferred from the surface slick to the water column, enabling the dissolution and enhancing the bioavailability of water-soluble oil components. Additionally, in ice-covered waters oil will be pooled in under-ice roughness features, from where it will migrate up to the overlying ice cover through pore spaces known as brine channels in the process of oil entrainment in ice. These processes

can be viewed as emission sources in an evaluative environment limited by the ice field and will lead to the partition of oil components in the environmental media, contributing to the toxicity in the marine ecosystem.

In the present study, the water and ice compartments receive direct input of oil as a result of the processes of natural dispersion and entrainment in ice, respectively, which are considered as the emission sources to the evaluative environment. The emission to the water is modeled according to the dispersion algorithm by Mackay et. al. (1980), adapted to ice conditions:

$$\frac{dD}{dt} = r_{ice} V_{oil} \frac{0.11\ (W+1)^2}{1 + 50\mu^{0.5} h\ S_t} \tag{4.1}$$

Where dD/dt is the volumetric rate of oil dispersion in water; V_{oil} is the volume of oil remaining in the slick at a given time (m^3); W is the wind speed (m/s); μ is the oil viscosity (cP); h is the slick thickness (m); S_t is the oil-water interfacial tension (dyne/m); and r_{ice} is given by:

$$r_{ice} = \begin{cases} 0, & c \geq 0.8 \\ (0.8 - c)/0.5\,, & 0.3 \leq c < 0.8 \\ 1, & c < 0.3 \end{cases} \tag{4.2}$$

Where c is the ice coverage (%). The emission rate to the water compartment is then given by the volumetric dispersion rate multiplied by the initial molar concentration of the release, as suggested by Nazir et al. (2007):

$$I_w(t) = \frac{dD}{dt}\ C_i \tag{4.3}$$

Where $I_w(t)$ is the emission rate to the water (mol/h) at a given time t (h) and C_i is the initial molar concentration (mol/m^3).

A formulation to model oil entrainment in ice is introduced to calculate the emission to the ice compartment, as a function of the increasing oil slick area and of the entrainment capacity of the under-ice roughness per unit area, as follows:

$$\frac{dV_E}{dt} = 5x10^{-5} \frac{dA}{dt} \tag{4.4}$$

Where dV_E/dt is the rate of oil entrained in ice (m^3/h) and A is the slick area at any given time (m^2). The above equation assumes an under-ice entrainment capacity of 0.001 m^3/m^2 and an expected under-ice oil coverage of 5% within the contaminated area. Analogously to the emission to the water, the rate of oil entrainment in ice is multiplied by the initial molar concentration to give the emission rate to the ice compartment, as follows:

$$I_i(t) = \frac{dV_E}{dt} C_i \tag{4.5}$$

Where I_i (t) is the emission rate to the ice (mol/h) at a given time t (h) and other parameters as stated before. The above formulation implies that emissions to the ice compartment increase as the contaminated area increases, consequently allowing greater oil volumes to be in contact with the ice cover thus becoming available for entrainment. The emission to the ice cover ceases when the spreading process is terminated and, given enough time, the entrainment capacity per unit area is reached.

The rates of natural dispersion and entrainment in ice will then control the distribution of naphthalene – taken here as a surrogate for oil – in the evaluative

environment and will define the shape of fugacity curves in each compartment. The dispersion formulation includes an ice correction factor, meaning that in medium ice concentrations (>30% and <80%) the dispersion will be reduced and, in high ice concentrations (≥80%), there will be no dispersion as the ice cover will dampen the effect of waves. In this case, entrainment in ice will be the only emission source in the evaluative environment.

4.2.3 Development of Fugacity Model

Given the characteristics of the evaluative environment, the food-web structure, the oil properties and emission sources, a system of equations can be assembled to represent the unsteady-state mass balance of naphthalene in the environment. The system consists in one differential equation for each compartment describing the rate of change in fugacity as a result of changes in emission rates. Environmental compartments have fugacity capacities as defined in Table 4-3 and intermedia transport and loss processes are expressed by D values defined in Table 4-4. Intermedia processes included in the calculations are: diffusion and deposition, between air and ice cover; melting and icing, between ice cover and water; and diffusion, deposition and re-suspension, between water and sediment. Precipitation in form of rain or snow are not included in the model. Loss processes included are reaction and advection in both air and water, and reaction in sediment. No advection in sediment is assumed to occur. For the food web, phytoplankton is assumed to be in equilibrium with water, therefore equi-fugacity applies and the only source of contaminant to the organism is respiration. As a photosynthetic organism, the phytoplankton does not undergo food intake or egestion, although the self-elimination processes of metabolism and growth

dilution are present. For the other organisms in the food web (zooplankton and fish), the included uptake processes are uptake from food and gill exchange (in) due to respiration. Loss processes are egestion, gill exchange (out), metabolism and growth dilution. Intermedia processes in the food web thus take place in the form of respiration (between organisms and water) and food consumption (between organisms from different trophic levels).

Table 4-3: Definition of Z values for the proposed model.

Sub-Compartments	Z Value (mol/m^3 Pa)	Parameter Definition
Air	$Z_1 = 1/RT$	R = gas constant = 8.314 Pa m^3/mol K T = temp. (K)
Water	$Z_2 = 1/H = C^S/P^S$	H = Henry's law constant (Pa m^3/mol) C^S = aqueous solubility (mol/m^3) P^S = vapor pressure at 25ºC (Pa)
Aerosols	$Z_3 = 6x10^6/P_L^s RT$	$P_L{}^S$ = liquid vapor pressure at 25ºC (Pa)
Ice-air interface	$Z_4 = K_{ia}/RT$	K_{ia} = ice surface-air partition coefficient (m) $ln\ K_{ia} = 0.68\ ln\ K_{OW} - 19.63 + ln\ K_{WA}$ K_{WA} = water-air partition coefficient
Solids in ice	$Z_{5i} = 0.41K_{OW}/H$	K_{OW} = octanol/water partition coefficient
Solids in water	$Z_{5w} = x_w 0.41K_{OW}\rho_S/H$	x_i = organic carbon fraction in the medium i
Solids in sediment	$Z_{5s} = x_s 0.41K_{OW}\rho_S/H$	ρ_s = density of solids (kg/L)
Bulk Compartments		
Air	$Z_a = Z_1 + \phi_{3a}Z_3$	ϕ_{3a} = fraction of aerosols in air
Ice cover	$Z_i = A_{ia}Z_4 + \phi_{5i}Z_{5i}$	A_{ia} = area of ice-air interface (m^2)
Water	$Z_w = Z_2 + \phi_{5w}Z_{5w}$	ϕ_{5i} = fraction of solids in ice
Sediment	$Z_s = \phi_{2s}Z_2 + \phi_{5s}Z_{5s}$	ϕ_{5w} = fraction of solids in water
Fish	$Z_f = L_f K_{OW}\rho_f/H$	ϕ_{2s} = fraction of water in sediment
Zooplankton	$Z_z = L_z K_{OW}\rho_z/H$	ϕ_{5s} = fraction of solids in sediment
Phytoplankton	$Z_p = L_p K_{OW}\rho_p/H$	L_i = lipid fraction of organism i

In the present model, air is composed of pure air and aerosols; ice cover consists in ice surface and particulate matter; water comprises pure water and suspended particles; sediment is composed of water and solids. Organisms in the food web are treated separately as single biotic compartments with no sub-compartments.

Table 4-4: Definition of D values for intermedia transport, bulk compartment loss and biotic uptake and loss processes.

Intermedia	**Process**	**D Value (mol/Pa h)**
Air (1) – Ice Cover (2)	Diffusion	$D_v = 1/(1/K_{va}A_{ia}Z_a + 1/K_{vi}A_{ia}Z_i)$
	Deposition	$D_{di} = A_{ia}U_{di}\phi_{3a}Z_3$
	Total D (1-2)	$D_{12} = D_V + D_{di}$
	Total D (2-1)	$D_{21} = D_V$
Ice Cover (2) – Water (3)	Melting	$D_{iw} = A_{iw}U_{iw}Z_i$
	Icing	$D_{ii} = A_{iw}U_{ii}Z_w$
	Total D (2-3)	$D_{23} = D_{iw}$
	Total D (3-2)	$D_{32} = D_{ii}$
Water (3) – Sediment (4)	Diffusion	$D_y = 1/(1/K_{yw}A_{ws}Z_w + Y_4/B_{w4}A_{ws}Z_w)$
	Deposition	$D_{ds} = A_{ws}U_{dp}Z_{5w}$
	Re-suspension	$D_{ds} = A_{ws}U_{rs}Z_{5s}$
	Total D (3-4)	$D_{34} = D_y + D_{ds}$
	Total D (4-3)	$D_{43} = D_y + D_{rs}$
Bulk Compartments	**Process**	**D Value (mol/Pa h)**
Air (1)	Advection	$D_{a1} = G_1Z_a$
	Reaction	$D_{r1} = k_{r1}V_1Z_a$
Water (3)	Advection	$D_{a3} = G_3Z_w$
	Reaction	$D_{r3} = k_{r3}V_3Z_w$
Sediment (4)	Reaction	$D_{r4} = k_{r4}V_4Z_s$
Food Web	**Process**	**D Value (mol/Pa h)**
Fish (5) Zooplankton (6) Phytoplankton (7)	Uptake from food	$D_{Fi} = E_{Ai}G_{Ai}Z_a$
	Loss by egestion	$D_{Ei} = D_{Ai}/Q$
	Gill uptake	$D_{WIi} = k_{1i}V_iZ_w$
	Gill elimination	$D_{WEi} = k_{2i}V_iZ_w$
	Metabolism	$D_{Mi} = k_{Mi}V_iZ_i$
	Growth dilution	$D_{Gi} = Z_i\,(dV_i/dt)$

Z-value formulations in Table 4-3 are extracted from: Mackay & Paterson (1991), for air, water, aerosol, biota and solids in water and sediment; and Wania (1997), for solids in ice and ice-air interface. Formulation for k_{ia} was extracted from Wania et al., (1998).

D-value formulations in Table 4-4 are extracted from: Mackay (2001), for water-sediment intermedia processes and reaction and advection processes in bulk compartments; Wania (1997) for air-ice and ice-water intermedia processes; and Campfens & Mackay (1997) for food-web uptake and loss processes. Transport parameters used to calculate the D values defined in Table 4-4 are given in Table 4-5.

Table 4-5: Estimated transport parameters for the model.

Parameter	Description	Suggested Value / Formula	
k_{va}	Air-side MTC over ice cover (m/h)	2.0	**(1)**
k_{vi}	Ice-side MTC (m/h)	0.01	**(1)**
U_{di}	Aerosols deposition velocity (m/h)	10.8	**(1)**
U_{iw}	Melting rate (m/h)	3.9×10^{-5}	**(1)**
U_{ii}	Icing rate (m/h)	2.3×10^{-6}	**(1)**
k_{yw}	Water-side MTC over sediment (m/h)	0.01	**(1)**
Y_4	Diffusion path length in sediment (m)	0.005	**(1)**
B_{w4}	Molecular diffusivity in water (m^2/h)	4×10^{-6}	**(1)**
U_{dp}	Sediment deposition rate (m^3/m^2 h)	4.6×10^{-8}	**(1)**
U_{rs}	Sediment re-suspension rate (m^3/m^2 h)	1.1×10^{-8}	**(1)**
G_i	Volumetric flow rate (m^3/h)	$Z_i V_i / t_i$	**(2)**
t_i	Residence time (h)	-	
k_{ri}	Reaction rate constant (h^{-1})	$0.693/\tau_{1/2(R)}$	**(2)**
$\tau_{1/2(R)}$	Degradation half-life (h)	-	
E_A	Gut absortion efficiency (%)	0.5 (for $K_{OW} \leq 6$)	**(2)**
G_A	Gross food ingestion rate (m^3/h)	$W_i G_{Di} / \rho_i$	**(2)**
G_D	Feeding rate (kg/h)	$0.022 W_i^{0.85} \exp(0.06T)$	**(2)**
W_i	Organism's weight (kg)	-	
T	Ambient temperature (C)	-	
ρ_i	Organism's density (kg/m^3)	-	

Q	Limiting biomagnification factor	3.0	**(2)**
k_1	Gill uptake rate constant (h^{-1})	$1/k_1 = (V_i/Q_W) + (V_i/Q_L)/K_{OW}$	**(2)**
Q_W	Water phase conductivity (L/day)	$88.3\ V_i^{0.6}$	**(2)**
Q_L	Lipid phase conductivity (L/day)	$0.001\ Q_W$	**(2)**
k_2	Gill elimination rate constant (h^{-1})	$k_1/L_i\ K_{OW}$	**(2)**
k_M	Metabolic rate constant (h^{-1})	$0.693/\tau_{1/2(M)}$	**(2)**
$\tau_{1/2(M)}$	Metabolism half-life (h)	-	
dV_i/dt	Growth dilution term (m^3/h)	$W_i\ G_i/\rho_i$	**(2)**
G_i	Growth rate (g/g day)	-	

(1) Yang et al. (2015)
(2) (Campfens & Mackay, 1997)

After compiling Z values for all media and D values for all considered environmental processes and, given the emissions identified in Section 4.2.2, it is possible to write differential equations representing the unsteady-state mass balance in each compartment. The system of differential equation becomes:

- **Air (1):**

$$V_1 Z_1\, df_1/dt = f_2 D_{21} - f_1(D_{12}\, D_{a1} + D_{r1}) \tag{4.6}$$

- **Ice Cover (2):**

$$V_2 Z_2\, df_2/dt = I_2 + f_1 D_{12} + f_3 D_{32} - f_2(D_{21} + D_{23}) \tag{4.7}$$

- **Water (3):**

$$V_3 Z_3\, df_3/dt = I_3 + f_2 D_{23} + f_4 D_{43} + f_5 D_{53} + f_6 D_{63} + f_7 D_{73} - f_3(D_{32} + D_{34} + D_{35} + D_{36} + D_{37} + D_{a3} + D_{r3}) \tag{4.8}$$

- **Sediment (4):**

$$V_4 Z_4 \, df_4/dt = f_3 D_{34} - f_4(D_{43} + D_{r4}) \quad (4.9)$$

- **Fish (5):**

$$V_5 Z_5 \, df_5/dt = f_3 D_{WI5} + f_6 D_{F5} - f_5(D_{WE5} + D_{E5} + D_{M5} + D_{G5}) \quad (4.10)$$

- **Zooplankton (6):**

$$V_6 Z_6 \, df_6/dt = f_3 D_{WI6} + f_7 D_{F6} - f_6(D_{WE6} + D_{E6} + D_{M6} + D_{G6}) \quad (4.11)$$

- **Phytoplankton (7):**

$$V_7 Z_7 \, df_7/dt = f_3 D_{WI7} - f_7(D_{WE7} + D_{M7} + D_{G7}) \quad (4.12)$$

The system of equations expresses the rate of fugacity variation as a function of the environmental processes taking place in each medium. Inter-relations between compartments are expressed by the inclusion of multiplying fugacity terms to the D values. Chemical entering each compartment carries the fugacity of the medium it comes from, which is multiplied by the correspondent D values for the intermedia process involved, with positive sign. Negative signs represent chemical loss from the compartment, and D values for each process are multiplied by the fugacity of that compartment. The net chemical accumulation or loss is then given by the balance between entries and losses in each compartment and is represented by the differential term on the left-hand side of the equations. The term I_i in the mass balance for water and ice represents the direct input to those compartments. The fugacity in the medium *i* can be converted into concentration by Eq. (4.13):

$$C_i = f_i Z_i \tag{4.13}$$

4.2.4 Solution of System of Equations

The system of differential equations can be solved by analytical or numerical methods. In the present work, a combination of Excel spreadsheets and MATLAB models is used. The student version of the software MATLAB Simulink and the Microsoft Office 365 are used. The MATLAB routine ode45 is used to perform numerical integration of the system of equations, which also include the algorithms for natural dispersion and entrainment in ice. These processes are dependent on other transport and weathering processes such as spreading and increase in viscosity, which are accounted for in the calculations. Details on the calculations are given on Appendix I.

4.2.5 Outputs of the Model

4.2.5.1 Representation of Concentrations as a Function of Ice Coverage

After solving the system of equations, the output of the model is the representation of variation in fugacity – or in concentration – over time for each compartment as a result of changes in emission rates. The model is ran for three ranges of ice coverages: low (≤ 30%); medium (> 30% and < 80%); and high (≥ 80%). The outputs are then graphical representations of concentration profiles for all compartments as a function of ice coverage. In addition, rates of loss and of intermedia transport processes are estimated, allowing inference on chemical depuration times for both abiotic and biotic media.

4.2.5.2 Representation of Risk Profile and Bioaccumulation Potential for Different Ice Coverages

The fugacity data is used to perform an ecological risk analysis, using bioaccumulation potential and risk profile as endpoints. The risk profile is given by the Risk Quotient (RQ), which is the ratio between the Predicted Exposure Concentration (PEC) in the medium of interest to the Predicted No Effect Concentration (PNEC) for a given contaminant. The PNEC is determined in ecotoxicological studies and is often used as a quality criterion for water bodies, above which acute effects are expected in exposed organisms. In the present work, the PEC is the concentration in water, calculated by the model, and is benchmarked against the PNEC for naphthalene, obtained from literature. The RQ is given by Eq. (4.14) below:

$$RQ = \frac{PEC}{PNEC} \tag{4.14}$$

Afenyo et al. (2017b) defined the PEC as:

$$PEC = P_r\, C\, BAF \tag{4.15}$$

Where P_r is the exposure probability, C is the concentration of contaminant in the medium of interest and BAF is the bioavailable fraction of contaminant in the medium. In the present work, it is assumed that the organisms in the food web will be in direct contact with dispersed oil, hence the exposure probability is taken as 1. For chemicals with log K_{OW} less than 5, the bioavailable fraction is considered as being 100%, thus BAF is also 1. Thus, Eq. 4.14 can be reduced to:

$$RQ = \frac{C_w}{PNEC} \tag{4.16}$$

C_w being the concentration of contaminant in the water compartment (mg/L), outputted by the model. Anon (2007), as cited by Afenyo et al. (2017b), defined a PNEC of 0.002 ppm (mg/L) for naphthalene in marine waters, which is used in the present work. According to Afenyo et al. (2017b), the risk is acceptable to the marine ecosystem if RQ ≤ 1. Otherwise, measures should be taken to mitigate it.

The bioaccumulation potential is represented by a Bioconcentration Factor (BCF), which is the ratio of concentration in a targeted organism to that in water. In the present study, fish is selected as object of the analysis of the BCF, as it represents an important dietary component for marine mammals, birds and humans. It follows that:

$$BCF = \frac{C_f}{C_w} \tag{4.17}$$

Where C_f is the concentration in fish (mg/kg) and C_w is the concentration in water (mg/L). Both RQ and BCF are plotted against time for the three ranges of ice coverages, enabling the analysis of the influence of ice in the risk level of oil spills in the Arctic, as well as the time required for chemical depuration in the various media involved, given the ice concentration. The simulation is run for a time of 12000 hours (500 days) in order to investigate the long-term evolution of ecological risk imposed by an oil spill in the Arctic.

4.3 Case Study

The proposed methodology is exemplified by a case study involving the scenario under investigation. The proposed case study draws upon the work by Yang et al. (2015), which introduced a scenario in the Labrador Sea involving the release of 120 m^3 of Statfjord crude oil in the winter. The model assumes a sea water temperature of -1°C and wind speed of 10 m/s. Oil properties are given in Table 4-6 and naphthalene properties in Table 4-7. An initial oil slick thickness of 0.02 m is assumed, giving an initial contaminated area of 6000 m^2.

Table 4-6: Statfjord crude oil properties (Environment Canada, 2001).

Property	Value	Unit
Density at 15°C	835	Kg/m^3
Viscosity at 0°C	31	cP
Oil/saltwater interfacial tension at 0°C	2760	dyne/m

Table 4-7: Naphthalene properties (Mackay, 2001).

Property	Value	Unit
Molar mass	128.2	g/mol
Solubility at 25°C	31	g/m^3
Vapor pressure at 25°C	10.4	Pa
Henry's Law Constant	43.01	Pa m^3/mol
Log K_{OW}	3.37	-
Initial concentration	8	mol/m^3

The ice coverage is an adjusting factor in the simulations, changed in each set of simulations in order to examine how the environmental compartments respond to varying ice conditions. The transport parameters for the case study are as presented in Table 4-5.

The characteristics of the evaluative environment are as given in Tables 4-1 and 4-2 and the properties of the organisms in the food web are introduced in Table 4-8. Estimation of phytoplankton and zooplankton population volumes are based on the works from Borstad & Gower (1984) and Hunt et al. (2014) respectively. Fish population estimation is based on Yang et al. (2015). Average weight and lipid content of Arctic cod are extracted from Crawford & Jorgenson (1996) and Hop et al. (1997), respectively. Metabolism half-lives are of difficult measurement and data is scarce on this matter. Meador et al. (1995) estimated a half-life of 25 days (600 hours) for phenyl naphthalene in rainbow trout, which is used in the present work. Campfens & Mackay (1997) suggested an increase of one order-of-magnitude in metabolism half-lives for each subsequent upper level in the food chain, therefore half-lives for zooplankton and phytoplankton are assumed as being 6000 and 60000 hours, respectively. All other parameters in Table 4-8 are extracted from Campfens & Mackay (1997) and Sun et al. (2018).

Table 4-8: Properties of organisms comprising the food web.

Property	Phytoplankton	Zooplankton	Fish
Mass (g)	$4x10^{-4}$	0.1	45
Lipid fraction (%)	0.015	0.04	0.08
Water phase conductivity (L/d)	$9.04x10^{2}$	$9.12x10^{3}$	$7.13x10^{4}$
Lipid phase conductivity (L/d)	0.9	9.2	71.3
Gill ventilation rate (h^{-1})	0.547	0.116	0.029
Gut absorption efficiency	-	0.5	0.5
Feeding rate (g/g d)	-	0.2	0.02
Gross food ingestion rate (m^3/h)	-	$8.33x10^{-10}$	$3.75x10^{-8}$
Growth rate (g/g d)	0.025	0.02	0.002
Growth dilution term (m^3/h)	$4.17x10^{-13}$	$8.33x10^{-11}$	$3.75x10^{-9}$
Metabolism half-life (h)	60000	6000	600
Organism density (kg/m^3)	1000	1000	1000
Population volume (m^3)	0.05	2.31	70

4.3.1 Results and Discussion

Figures 4-3 to 4-10 show the time-variant concentration profiles for all media under investigation in three ranges of ice concentrations. Concentrations in abiotic media are given in mg/L and in biotic media in mg/kg. The shape of concentration curves is dependent on the combined effect of emissions to water and ice, and the response of each compartment to changes in emission rates depends on fugacity capacity and on predominant transport processes.

The emission rate to the water compartment depends on a balance between the increase in viscosity and the decrease in oil slick thickness. The increase in viscosity acts against the natural dispersion as the breakup of the oil slick into droplets is difficulted for viscous oils, which require higher sea energy levels to occur. In contrast, the thinning of the oil slick eases oil dispersion given the higher surface are available for breaking waves to drive the oil down to the water column. As slick thinning is a dominant process, natural dispersion rate increases up until the spreading ceases and a terminal thickness is reached, from which point the dispersion rate starts to decrease as a result of viscosity increase, eventually ceasing when the oil is completely consumed from the slick. In the simulations, a peak in emission to water is observed when the slick reaches its terminal thickness, which occurs at 140 h and 720 h for 30% and 70% ice coverages respectively. For 90% ice coverage there is no emission to the water as natural dispersion does not occur in heavy ice conditions. Emission to the water ceases at 364 h and 1800 h for 30% and 70% ice coverages respectively.

In the present model, emission to the ice cover is a function of increasing slick area, which increases with time towards a terminal value. As a consequence of increasing slick area, the emission rate also increases, assuming that oil is pooled underneath the ice for long enough to migrate through the brine channels, up until the termination of the spreading process, after which emission to the ice cover ceases. The peak in emission rate to ice is observed practically immediately after the release, following the same trend of oil spreading process. After this peak, which occurs 6 hours after the release, the emission to ice displays a decreasing trend and ceases when the oil slick reaches its terminal thickness.

Upon reaching of oil slick's terminal thickness, two important changes take place: the emission rate to ice ceases and emission to water changes its regime from an increasing to a decreasing trend. Each compartment will respond differently to this change, but all media will be somewhat sensitive to it.

The plots show a decreasing trend in concentrations with increasing ice coverage for all media, although for the air and ice compartments the concentrations for 70% coverage peaked at a higher value than for 30% coverage. This can be explained by the greater area of ice cover in contact with oil and therefore available for entrainment. Conversely, at high ice coverages the slick spreading is substantially retarded, hence the lower oil concentration. In addition, at ice coverages higher than 80% there is no oil input to the water, therefore there is a lower overall amount of contaminant in the system, also contributing to the observed lower concentration in ice.

As the only medium in contact with air is the ice cover, its concentration curves display similar trends as of those of ice, though the model outputted negligible concentrations in the air compartment (on the order of 10^{-11}).

Contaminant concentrations for 90% ice coverage in all media but air and ice were very low compared to concentrations for 30% and 70% coverages, thus those media are treated separately on Figure 4-10. The water compartment responds practically immediately to change in emission regimes, peaking when emission rates are higher and dropping quickly to reach steady-state conditions. In contrast, sediment and biotic media take longer to respond and concentrations in those compartments continue to increase for a long time after emissions have ceased or reduced. Air and ice also respond immediately to changes in emissions, but the steady state is not reached over the time span of the simulations. Overall, the higher the ice coverage the slower the response to changes in emissions and the longer the compartments take to reach maximum concentrations. Also, peak concentrations are lower the higher the ice coverage for all compartments but air and ice, as mentioned previously in this chapter. At low ice coverage (≤ 30%) naphthalene concentration in sediment peaks at the highest value amongst the abiotic media (0.032 mg/L), whereas at medium (>30% and <80%) and high (≥ 80%) ice coverages the ice compartment displayed the highest concentration peaks (0.031 mg/L and 0.019 mg/L respectively), after which there is a decreasing trend, although it does not drop significantly, reaching 0.009 mg/L, 0.011 mg/L and 0.013 mg/L for 90%, 30% and 70% ice coverages respectively at the end of the simulation. Steady-state concentrations for sediment varied in a range from $3x10^{-5}$ mg/L to $9x10^{-5}$ mg/L for 90% and 30% ice

coverages, respectively, whereas water steady-state concentrations were similar for all ice coverages, of about $1.5x10^{-6}$ mg/L.

Chemical depuration in water occurs in about 2000 h for 30%, 3000 h for 70% and 5000 h for 90% ice coverages and steady-state concentrations are in the order of $1.5x10^{-6}$ mg/L. In sediment, response times are much longer for the three ranges of ice coverages, although it can be noted that more constant steady-state concentrations are achieved earlier for higher ice coverages. Steady-state concentrations in sediment are in the order of $3x10^{-5}$ mg/L. Steady-state is not reached in air and ice compartments over the simulation's time span. This in turn explains the persistency of oil in ice.

For 90% ice coverage (Figure 4-10), concentrations in all biotic media, along with the sediment compartment, were of the same order-of-magnitude ($5x10^{-5}$mg/L) apart from zooplankton, which displayed concentrations one order-of-magnitude higher. Concentration in the ice compartment at 90% coverage (Figure 4-4) was much higher than in any other compartment, peaking at $1.9x10^{-2}$ after 121 days (2916 h). The ice cover displays this higher concentration because at 90% coverage the only emission source in the system is entrainment in ice. Emissions peaked much later for all other compartments and steady state was achieved after about 416 days (10000 h). Concentration in water compartment remained very low ($1x10^{-6}$mg/L) for the entire timespan of the simulation and achieved steady state earlier than in other compartments. This behavior is expected, given that for high ice coverages there is no chemical input to the water.

In the food-web, zooplankton displayed the highest concentrations among the three selected organisms. Phytoplankton is assumed to be in equilibrium with water, thus both

media have the same fugacity. Given the higher fugacity capacity (Z value) of phytoplankton, it shows a higher concentration than water, although the curves display the same behavior. Concentrations show a great increase from phytoplankton to zooplankton (one order-of-magnitude for medium and high ice coverages and two orders-of-magnitude for low ice coverage) given that for the latter, contaminant uptake occurs from both food consumption and exchange with water, whereas for the former only exchange with water takes place. The same trend is not observed from zooplankton to fish, and the representant of the highest trophic level in the food web displays the lowest contaminant concentration. This apparent odd behavior can be explained by two aspects. Organic chemicals with log K_{OW} less than 6 – and therefore with lower hydrophobicity – are not expected to undergo biomagnification in water, hence trophic dilution, in which higher trophic levels display lower chemical concentrations, is more likely to occur. More importantly, metabolism is the main driver of chemical loss in organisms at higher trophic levels. Chemicals with log K_{OW} lower than 4 are readily metabolized by fish, thus metabolic half-lives for those chemicals are shorter. The lower the trophic level the slower the metabolism rates, therefore loss by metabolism becomes less important, as observed in zooplankton and phytoplankton. Naphthalene has a Log K_{OW} of 3.37, hence not likely to magnify in aquatic food webs. Metabolism D values for fish, zooplankton and phytoplankton are respectively 0.35 mol/Pa h, 5.8×10^{-4} mol/Pa h and 4.5×10^{-7} mol/Pa h, thus it can be demonstrated that whereas metabolism is a major source of chemical depuration for fish, it is not relevant for organisms in lower trophic levels. If metabolism was neglected and metabolic rates are not included in the calculations, concentrations would display increasing trend from the lowest to the highest trophic levels.

The groups W and A, representing respectively fugacity factors for respiration and food uptake, provide insight on the main source of chemical for each organism and are calculated as follows:

$$W = D_{WI}/(D_{WE} + D_E + D_M + D_G) \quad (4.18)$$

$$A = D_F/(D_{WE} + D_E + D_M + D_G) \quad (4.19)$$

All parameters as stated before in this Chapter. W and A for fish are respectively 1.37×10^{-1} and 1.16×10^{-7}. For zooplankton, W and A are respectively 9.64 and 5.25×10^{-7}. For phytoplankton, respiration is the only source of chemical, thus A is zero. It can be thereby concluded that uptake from water is dominant for all organisms, which is expected for less hydrophobic chemicals of lower K_{OW}.

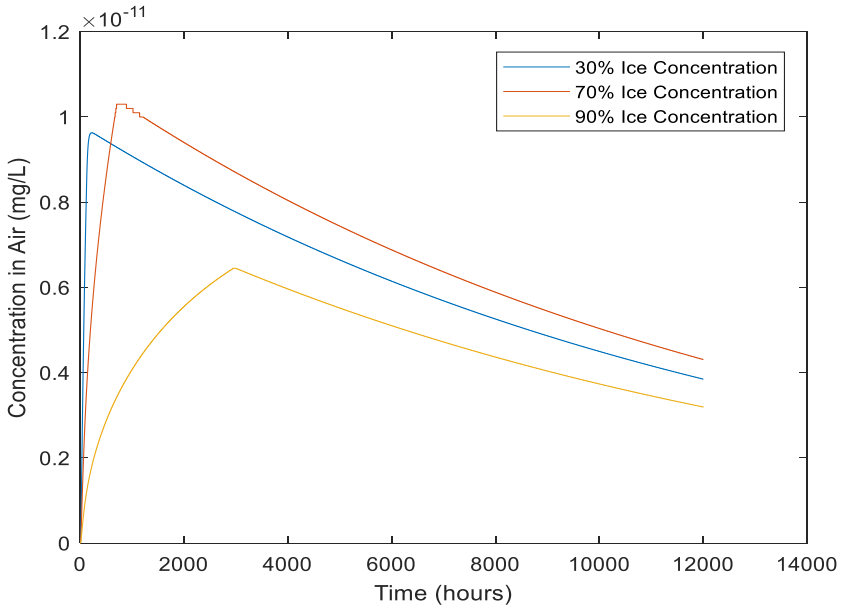

Figure 4-3: Concentrations of naphthalene in air.

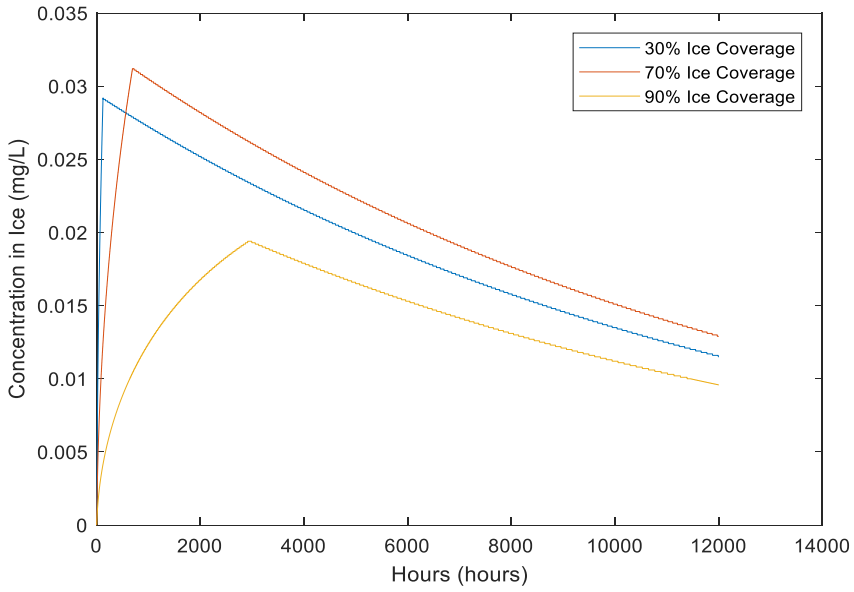

Figure 4-4: Concentrations of naphthalene in ice.

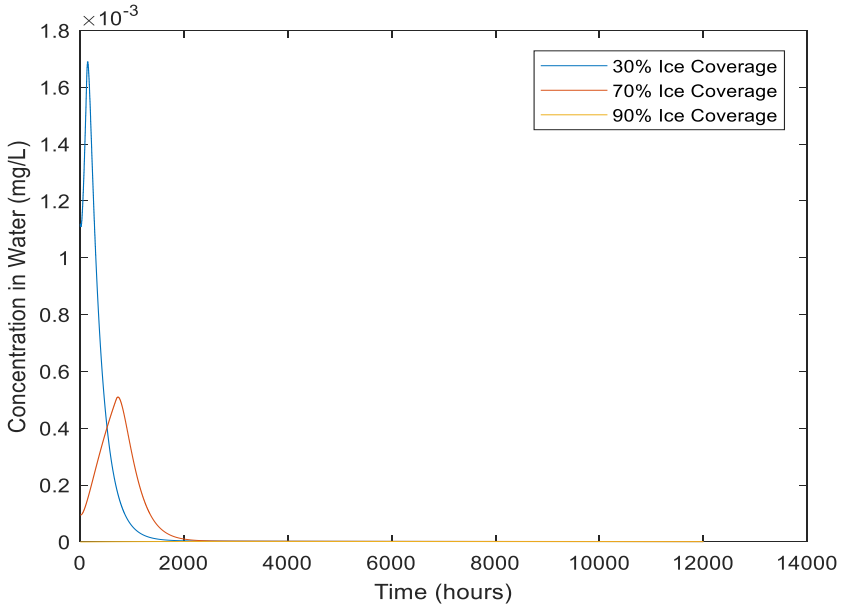

Figure 4-5: Concentrations of naphthalene in water.

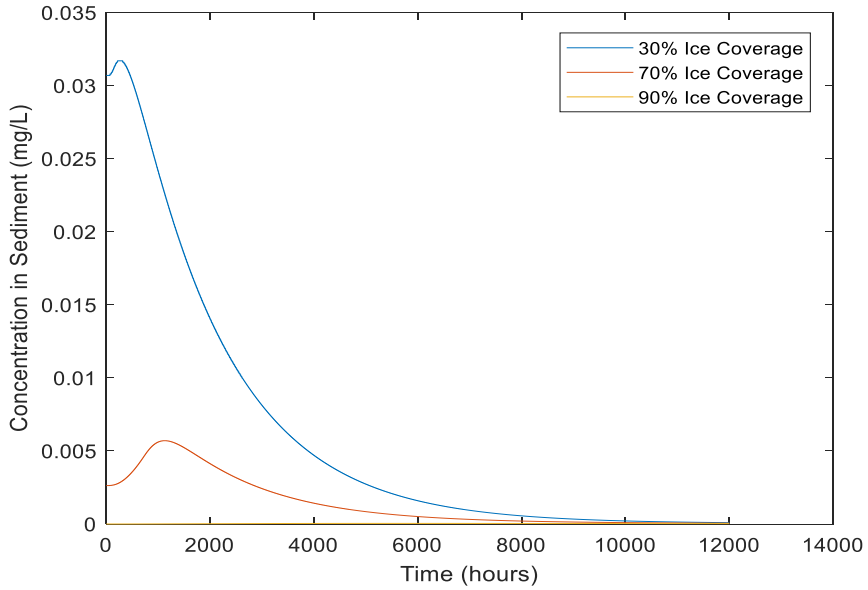

Figure 4-6: Concentrations of naphthalene in sediment.

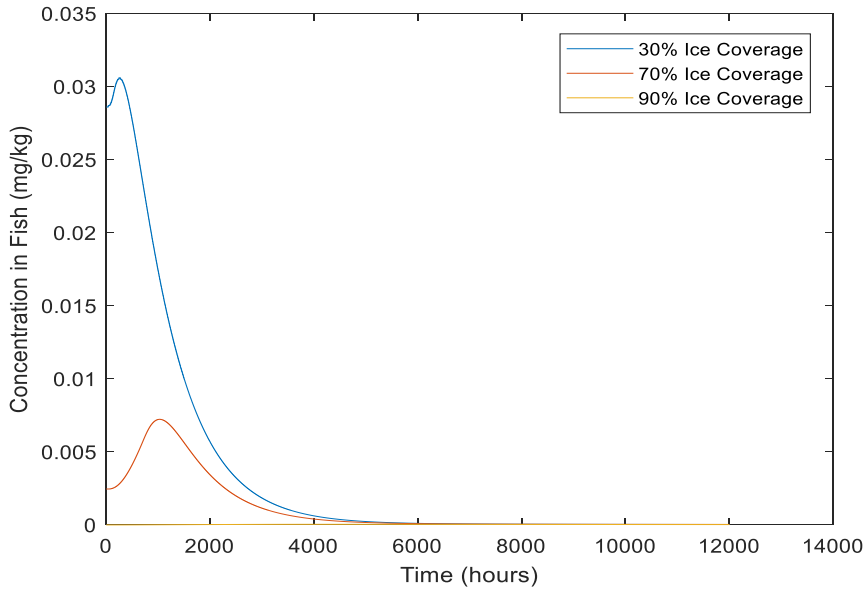

Figure 4-7: Concentrations of naphthalene in fish.

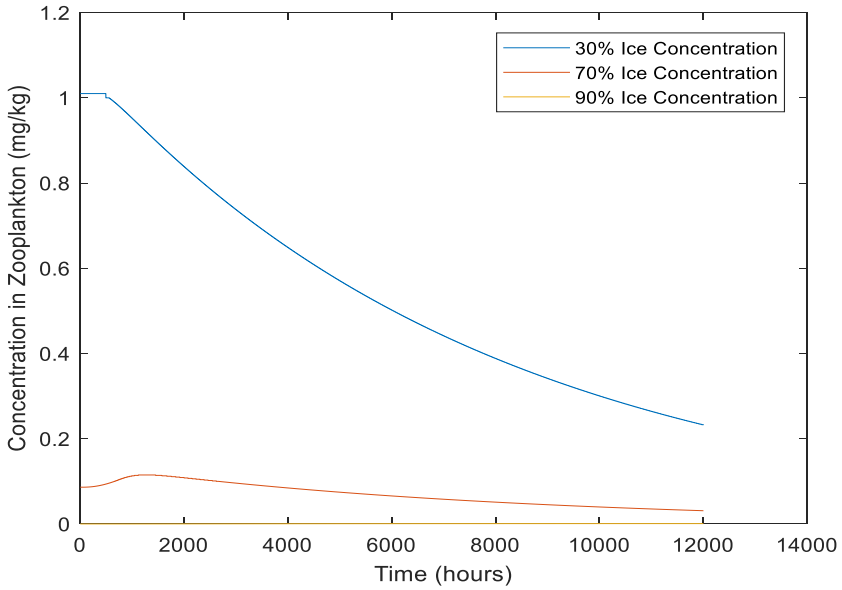

Figure 4-8: Concentrations of naphthalene in zooplankton.

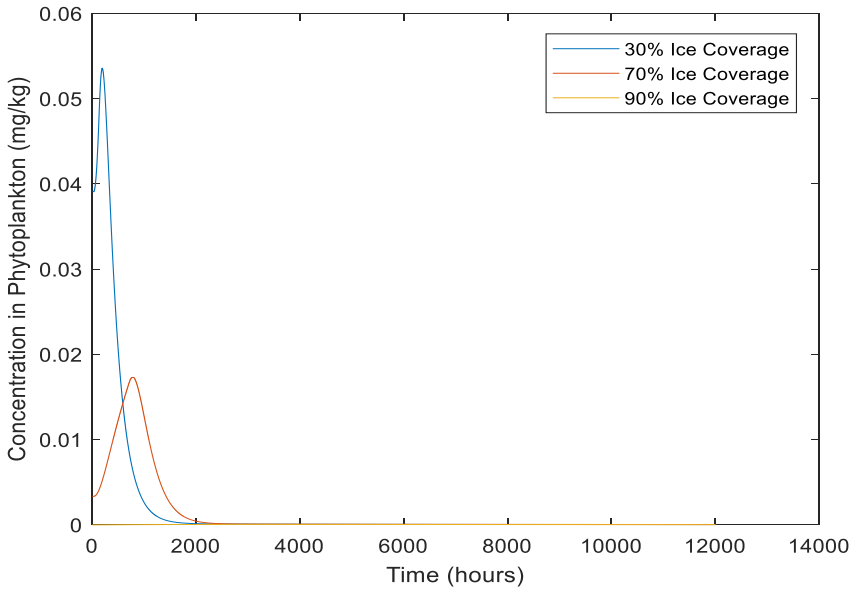

Figure 4-9: Concentrations of naphthalene in phytoplankton.

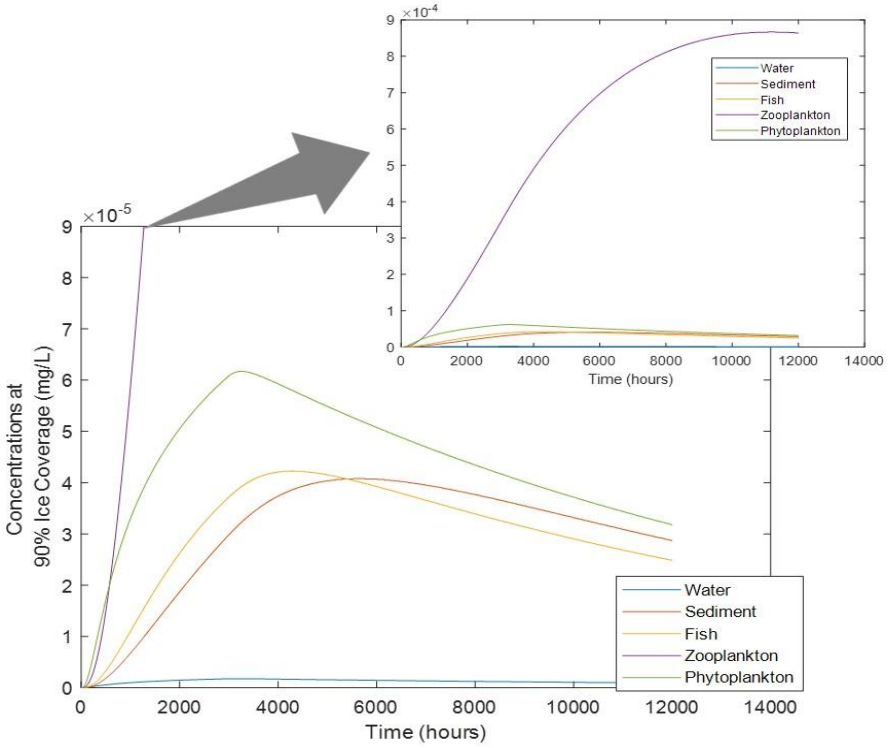

Figure 4-10: Concentrations in different media at 90% ice coverage.

Figures 4-11 and 4-12 show the Risk Quotient (RQ) and the Bioconcentration Factor (BCF), respectively. As expected, the risk quotient follows the same trend as concentration profiles in water compartment, peaking on the first days after the release and quickly dropping to very low values upon achieving steady state. In low ice coverage, the maximum risk quotient of 0.84 is reached 142 h after the release, and the steady-state RQ of 0.001 is achieved after about 2000 h. In medium ice coverage, risk quotient peaks 716 h after the release at 0.25, decreasing to the same steady-state RQ as for low ice concentration after about 3000 h. Risk quotient for 90% ice coverage remains negligible (about $8x10^{-4}$) for the entire simulation time. Consequently, according to the RQ criterion, the risk represented by the modeled spill scenario is not significative in the medium to long term, although at low ice coverage the risk quotient peaked very close to the unit 142 h

after the release, indicating that risk mitigation measures might be required within the first days of a spill to prevent the risk to reach the threshold for naphthalene. It also can be noted that the RQ decreased as ice coverage increased, thus the presence of ice may represent an attenuating factor for the risk quotient in Arctic waters.

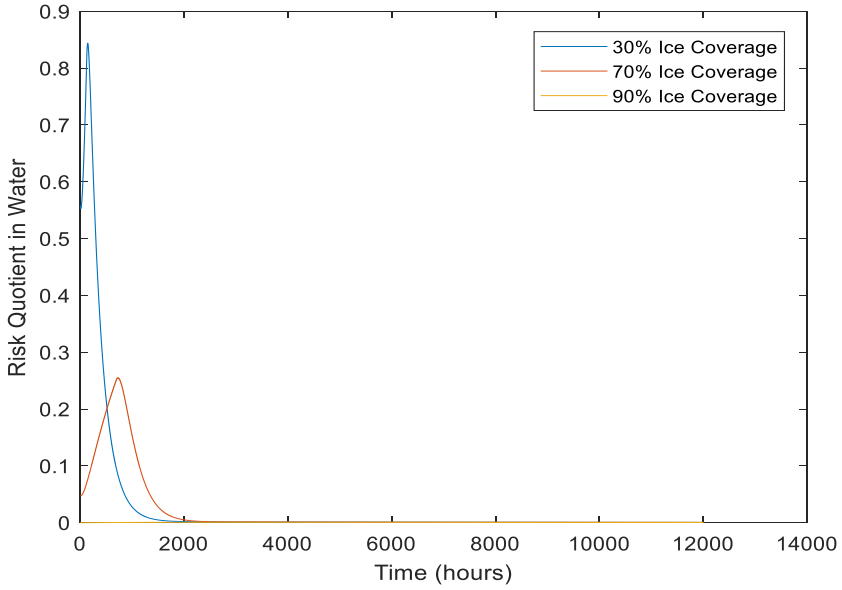

Figure 4-11: Risk Quotient for water.

The potential for accumulation of naphthalene in upper trophic levels in the food web is defined in terms of the Bioconcentration Factor (BCF) for fish. The BCF represents the balance between competing uptake and elimination processes in organisms and denotes the level in which chemical is accumulated in organism's body, when compared to water concentrations. Environment Canada defined a value of BCF of 5000 over which chemicals are deemed bioaccumulative (Anon, 1995). This value is therefore used as benchmark to compare the BCF outputted by the model.

Figure 4-12 shows the same decreasing trend for increasing ice coverages as observed in concentration profiles, although steady-state BCF values are equal for all ice coverages. Maximum BCF of 1460 and 552 are reached in 1900 h and 2470 h for 30% and 70% ice coverages, respectively. BCF for 90% ice coverage remains stable at about 25 for the entire simulation timespan, which coincides with the final steady-state BCF achieved for 30% and 70% ice coverages. By the inspection of Figure 4-12 it can be observed that the threshold BCF value used as criterion for bioconcentration by Environment Canada is not reached at any time over the simulation period. In fact, maximum BCF value achieved in the simulations was under one third of the bioaccumulation threshold, hence naphthalene is not expected to accumulate in higher trophic levels in the hypothetical Arctic food web object of the study under the scenario modeled.

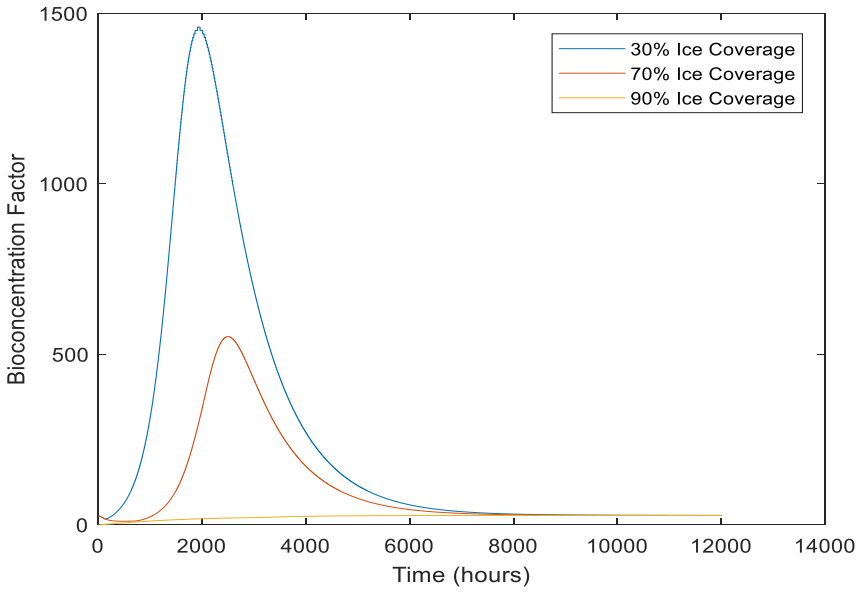

Figure 4-12: Bioconcentration factor for fish.

4.4 Concluding Remarks

The present work explored the fugacity approach to model the distribution in the environment of a toxic component of oil, namely naphthalene, as a result of an oil spill in ice-infested waters, focusing on the transfer of contaminant throughout an Arctic-specific food web. Abiotic compartments selected for the analysis were air, ice cover, water and sediment, and the linear food web was defined as consisting of phytoplankton, zooplankton and Arctic cod, in increasing order of trophic level. Emission sources to water and ice cover were determined as a function of respectively natural dispersion of oil in water due to breaking waves and entrainment of oil in ice due to migration through brine channels.

The outputs of the model showed a decreasing trend in concentration profiles with increasing ice coverages for all media, confirming findings from previous works. Excluding the air compartment, which displayed negligible concentrations over the entire simulation, water displayed the faster chemical depuration, followed by phytoplankton, fish, sediment, zooplankton and ice, the latter failing to reach steady-state over the simulation timespan. Lower contaminant concentrations in ice-covered waters confirm previous works that suggested that transport and weathering processes are retarded in those conditions. This can be advantageous in oil spill response planning, as more time is available for recovery efforts given that oil will remain un-weathered for longer periods. In addition, contaminant release from the oil slick will be reduced, hence risk represented by dissolved and dispersed toxic fractions of oil are expected to be lower. Nonetheless, chemical depuration times will be higher in ice conditions, and oil may persist much longer in the environment if response measures are not put in place.

In the food web, concentrations were the highest for zooplankton, followed by phytoplankton and fish for all ice coverages, indicating that biomagnification of naphthalene does not occur in the modeled food chain regardless of the ice conditions. Instead, it is likely that the opposite effect – trophic dilution – takes place. The Bioconcentration Factor (BCF) for fish did not reach the bioaccumulation criterion, thus accumulation in fish is not likely to occur. Likewise, the Risk Quotient (RQ) for the water compartment did not exceed the unit in any of the simulated ranges of ice coverage, meaning that concentrations in water did not represent a significative long-term risk to the marine ecosystem for the scenario under investigation, though a peak in risk quotient was observed within the first 5 days of simulations, indicating that measures should be in place to avoid a potential exceedance of risk level on the first days after a spill.

Overall, the highest concentrations were found in zooplankton (1 mg/kg) and sediment (0.03 mg/L) at low ice coverage and in the ice cover (0.03 mg/L) at medium ice coverage. The higher concentration found in the ice compartment is a result of oil migration through the ice brine drainage network, which may be a predominant process under heavy ice conditions, as other processes are substantially retarded. This may represent a risk factor to environments distant from the release point, as ice will be advected with ocean currents and winds and oil trapped in ice will be released back to the ocean upon spring and summer thaw. Also, high concentration in zooplankton might lead to further impacts to the ecosystem if organisms at higher trophic levels feeding on it do not readily metabolize or clear the contaminant, although the model suggested low accumulation potential in fish. Due to the high concentrations found in sediment, it may be important to consider the impacts on benthic food webs, along with the proposed pelagic analysis.

The model showed good agreement with previous works from Yang et al. (2015), Afenyo et al. (2016a) and Afenyo et al. (2017b), and could be potentially used in ecological risk assessments for Arctic oil and gas developments and marine shipping operations. However, the large amount of data required for the model implies that uncertainties and variability of parameters should be addressed in such studies to assure that outputs do not lead to erroneous conclusions. For some parameters only a rough estimative may suffice for the analysis whereas for some other, more precise estimations are needed. Transport rates and biological parameters such as metabolism and food ingestion rates are of difficult measurement and research is needed in these fields in order to create data bases that gather this information and are readily accessible to risk managers, thus enabling effective and reliable risk analysis. In addition, the use of naphthalene as a surrogate for oil represents a limitation in the present work, as oil is a complex mixture of components and a more realistic approach may require the assessment of concentration of other substances contributing to the toxicity of crude oil.

It is also important to note that the ecological risk characterization carried out in the present work is restricted to the selected risk endpoints – RQ and BCF – representing respectively the potential for lethality and bioaccumulation in the food chain. Other sub-lethal long-term effects such as alterations in growth and feeding, morphological deformities and damage to eggs and larvae may be playing out and influence the overall risk picture. These aspects are not addressed in the present work, thus represent opportunities for future research and improvement of existing models and other ecological risk assessment tools.

Chapter 5: Conclusions and Recommendations

The present thesis analyzed the aspects of oil spills in ice-infested waters from two different perspectives, which were combined to provide a complete picture of oil spill processes. The first part focused on transport and weathering processes, and improvements were suggested to existing models in order to obtain more accurate outputs when compared to experimental observations. The modifications were introduced by the inclusion of ice correction factors in all transport and weathering algorithms, thus enabling the representation of the influence of ice conditions in each process separately. In addition, a simplistic algorithm to model the process of oil entrainment in ice was proposed, resulting in a better estimation of oil mass balance at higher ice coverages. The inclusion of an algorithm for entrainment in ice addresses a gap in existing oil spill models for ice-infested waters, which do not account for oil migration through the ice cover. This process has been shown in the present work to be an important way of oil transport in the Arctic and may be critical at heavy ice conditions. The timely behavior of transport and weathering processes were then analyzed for three ranges of ice coverage: low ($\leq 30\%$); medium ($> 30\%$ and $< 80\%$); and high ($\geq 80\%$). The outputs of the model showed good correlation with observations from large-scale experiments carried out in the Barents Sea in ice-covered waters, and the improved algorithms displayed more accurate results than previous models.

On the second part, the outputs from the first part were used as input for a Level IV fugacity-based food-web bioaccumulation model, which aimed at the prediction of the distribution in the environment of oil toxic compounds, using naphthalene as a surrogate for the analysis. The model included a multimedia evaluative environment consisting in air, ice cover, water and sediment, and a linear food web was assembled with phytoplankton, zooplankton and Arctic cod as representative species of the Arctic ecosystem. The outputs of the model included the timely evolution of contaminant concentrations in all involved media, enabling inference on transport rates, times to reach peak concentrations, chemical depuration times and predominant uptake and loss processes for each medium. Given the predicted concentrations, the associated ecological risk was defined in terms of two endpoints: First, the Risk Quotient (RQ) was plotted as the ratio of the concentration in the water, calculated by the model, to the Predicted No Effect Concentration (PNEC) for naphthalene, taken from literature. Further, the bioaccumulation potential was expressed by the Bioconcentration Factor (BCF), defined by the ratio of concentrations in the targeted organism (in the present analysis, Arctic cod) to concentrations in water. The analysis of the BCF provides insight on the level in which the process of respiration is leading to accumulation of a chemical in the organism, when compared to the concentration in water. Both RQ in water and BCF in fish displayed values below the risk criteria for all ice coverages, indicating that the modeled spill scenario did not represent a significant risk to the ecosystem under investigation.

The present work introduced a tool for estimation of ecological risk both in terms of acute effects, through the analysis of the RQ, and of chronic effects, through the BCF. The model can be potentially used by companies and environmental protection agencies in

environmental risk assessments for developments in the Arctic and may be extended to human health risk assessments if the level of complexity of the food web is increased to include humans at the highest trophic level. Although not aimed at the definition of exact values, the model provides estimative of peak concentrations and times required for environmental compartments to reach these concentrations, thus can be applied in oil spill response decision-making to predict when contamination is expected to reach alarming levels, subsidizing timely allocation of resources for spill response. The surface slick model may be useful to determine the windows of opportunity available for each response option given oil properties and position at any given time, which will influence the feasibility and efficiency of response techniques such as mechanical recovery and chemical dispersion. In addition, rehabilitation times can be predicted for the impacted environmental compartments, aiding natural resource damage assessment efforts and enabling the quantification of compensations to stakeholders after a spill occurs. Information on chemical depuration times is invaluable when response measures are insufficient to recover all released oil and a fraction is left to natural attenuation, which is the case in many spill scenarios, especially given the complications imposed by the harsh nature of the Arctic.

Limitations of the present work are mostly due to the lack of knowledge on the Arctic environment and ecosystems. The analysis of the RQ is only possible for water because there is no data available on PNEC for other Arctic compartments, consequently the risk level for habitats in ice and sediment – which may play important roles in the ecological equilibrium – are not included in the analysis. Moreover, limited data is available on Arctic species and on rates in which processes occur, thus simplifications and generalizations are often necessary. A better understanding of the mechanism of oil

encapsulation and migration through ice sheets, and the subsequent release back to the ocean upon spring and summer thaw, is also of paramount importance to quantify more accurately the mass balance of oil at heavy ice conditions. It is also highlighted that, if used for regulatory purposes, uncertainties inherent to the model shall be addressed. Even though the present work does not offer a statistical treatment of the data, it is highly recommended that uncertainties in input data and its propagation throughout the model be properly tackled. Bayesian networks represent a useful methodology to handle uncertainties, as well as to update model's predictions as information becomes available, being very promising for Arctic applications.

Chapter 6: References

Afenyo, M., Khan, F., Veitch, B., & Yang, M. (2016a). Dynamic fugacity model for accidental oil release during Arctic shipping. *Marine Pollution Bulletin*, *111*(1–2), 347–353. https://doi.org/10.1016/j.marpolbul.2016.06.088

Afenyo, M., Khan, F., Veitch, B., & Yang, M. (2016b). Modeling oil weathering and transport in sea ice. *Marine Pollution Bulletin*, *107*(1), 206–215. https://doi.org/10.1016/j.marpolbul.2016.03.070

Afenyo, M., Khan, F., Veitch, B., & Yang, M. (2017a). A probabilistic ecological risk model for Arctic marine oil spills. *Journal of Environmental Chemical Engineering*, *5*(2), 1494–1503. https://doi.org/10.1016/j.jece.2017.02.021

Afenyo, M., Khan, F., Veitch, B., & Yang, M. (2017b). A probabilistic ecological risk model for Arctic marine oil spills. *Biochemical Pharmacology*, *5*(2), 1494–1503. https://doi.org/10.1016/j.jece.2017.02.021

Afenyo, M., Veitch, B., & Khan, F. (2015). A state-of-the-art review of fate and transport of oil spills in open and ice-covered water. *Ocean Engineering*, *119*, 233–248. https://doi.org/10.1016/j.oceaneng.2015.10.014

AMAP. (2010). *Assessment 2007*.

Anon. (2007). Risk Assessment of Naphtalene, (106), 1–246. Retrieved from https://echa.europa.eu/documents/10162/5f0beb6c-575f-4a1b-aff5-b37f06eb3852

Arneborg, L., Höglund, A., Axell, L., Lensu, M., Liungman, O., & Mattsson, J. (2017). Oil drift modeling in pack ice – Sensitivity to oil-in-ice parameters. *Ocean Engineering*, *144*(October), 340–350. https://doi.org/10.1016/j.oceaneng.2017.09.041

Arnot, J. A., & Gobas, F. A. (2006). A review of bioconcentration factor (BCF) and bioaccumulation factor (BAF) assessments for organic chemicals in aquatic organisms. *Environmental Reviews*, *14*(4), 257–297. https://doi.org/10.1139/a06-005

Arzaghi, E., Abbassi, R., Garaniya, V., Binns, J., & Khan, F. (2018). An ecological risk assessment model for Arctic oil spills from a subsea pipeline. *Marine Pollution Bulletin*, *135*(April), 1117–1127. https://doi.org/10.1016/j.marpolbul.2018.08.030

Arzaghi, E., Mahdi, M., Abbassi, R., & Garaniya, V. (2018). A hierarchical Bayesian approach to modelling fate and transport of oil released from subsea pipelines. *Process Safety and Environmental Protection*, *118*, 307–315. https://doi.org/10.1016/j.psep.2018.06.023

Boccadoro, C., Krolicka, A., Receveur, J., Aeppli, C., & Le Floch, S. (2018). Microbial community response and migration of petroleum compounds during a sea-ice oil spill experiment in Svalbard. *Marine Environmental Research*, *142*(August), 214–233. https://doi.org/10.1016/j.marenvres.2018.09.007

Borstad, G. A., & Gower, J. F. R. (1984). Phytoplankton Chlorophyll Distribution in the Eastern Canadian Arctic. *Arctic*, *37*(3), 224–233. https://doi.org/10.14430/arctic2195

Brandvik, P. J., & Faksness, L. G. (2009). Weathering processes in Arctic oil spills: Meso-scale experiments with different ice conditions. *Cold Regions Science and Technology*, *55*(1), 160–166. https://doi.org/10.1016/j.coldregions.2008.06.006

Brandvik, P. J., Resby, J. L. M., Daling, P. S., Leirvik, F., & Fritt-Rasmussen, J. (2010). Meso-Scale Weathering of Oil as a Function of Ice Conditions. Oil Properties, Dispersibility, and In Situ Burnability of Weathered Oil as a Function of Time. JIP Report no. 19 (SINTEF A15563)., 116. Retrieved from www.sintef.no/globalassets/project/jip_oil_in_ice/dokumenter/publications/jip-rep-no-19-common-meso-scale-final.pdf

Brandvik, P. J., S, D. P., Fakness, L.-G., Fritt-Rasmussen, J., Ragnhild, D. L., & Leirvik, F. (2010). Report no. 26: Experimental oil release in broken ice. A large-scale field verification of resutls from laboratory studies of oil weathering and ingitability of weathered oil spills., 32.

Brandvik, P. J., Sørheim, K. R., Singsaas, I., & Reed, M. (2006). Short state-of-the-art report on oil spills in ice-infested waters, 1–58.

Campfens, J., & Mackay, D. (1997). Fugacity-based model of PCB bioaccumulation in complex aquatic food webs. *Environmental Science and Technology*, *31*(2), 577–583. https://doi.org/10.1021/es960478w

Camus, L., & Smit, M. G. D. (2018). Environmental effects of Arctic oil spills and spill response technologies , introduction to a 5 year joint industry e ff ort. *Marine Environmental Research*, *144*(January 2018), 250–254.

https://doi.org/10.1016/j.marenvres.2017.12.008

Council, A. (n.d.). Petroleum Safety Authority Norway (on behalf of the Norwegian Ministry of Foreign Affairs) Overview of measures specifically designed.

Council, A. (2013). *Arctic Biodiversity Assessment*.

Crawford, R. E., & Jorgenson, J. K. (1996). of Arctic Studies Cod (Boreogadus saida) Schools: Quantitative in the Arctic Food Web Stores Energy Important. *Arctic Institute of North America*, *49*(2), 181–193.

Delvigne, G. A. L., & Sweeney, C. E. (1988). Natural dispersion of oil. *Oil and Chemical Pollution*, *4*(4), 281–310. https://doi.org/10.1016/S0269-8579(88)80003-0

Fingas, M. (1995). A literature review of the physics and predictive modelling of oil spill evaporation. *Journal of Hazardous Materials*. https://doi.org/10.1080/07373937.2012.696083

Fingas, M. (2015). A Review of Natural Dispersion Models. *Handbook of Oil Spill Science and Technology*, (January 2013), 485–494. https://doi.org/10.1002/9781118989982.ch20

Fingas, M. (2015). Oil and Petroleum Evaporation. *Handbook of Oil Spill Science and Technology*, *2*(3), 205–223. https://doi.org/10.1002/9781118989982.ch7

Fingas, M. F. (2004). Modeling evaporation using models that are not boundary-layer regulated. *Journal of Hazardous Materials*, *107*(1–2), 27–36.

https://doi.org/10.1016/j.jhazmat.2003.11.007

Fingas, M. F. (2015). Oil and Petroleum Evaporation. In *Handbook of Oil Spill Science and Technology*. https://doi.org/10.1016/S0304-3894(97)00051-4

Fingas, M. F., & Hollebone, B. P. (2003). Review of behaviour of oil in freezing environments. *Marine Pollution Bulletin*, *47*(9–12), 333–340. https://doi.org/10.1016/S0025-326X(03)00210-8

Fingas, M., & Hollebone, B. P. (2015). Oil Behavior in Ice-Infested Waters. *Handbook of Oil Spill Science and Technology*, (February 2015), 271–284. https://doi.org/10.1002/9781118989982.ch9

Gobas, F. A. P. C. (2008). Food-Web Bioaccumulation Models. *Encyclopedia of Ecology*, 1643–1652. https://doi.org/10.1016/b978-008045405-4.00398-0

Hop, H., Tonn, W. M., & Welch, H. E. (1997). Bioenergetics of Arctic cod (Boreogadus saida) at low temperatures. *Canadian Journal of Fisheries and Aquatic Sciences*, *54*(8), 1772–1784. https://doi.org/10.1139/f97-086

Hunt, B. P. V., Nelson, R. J., Williams, B., McLaughlin, F. A., Young, K. V., Brown, K. A., … Carmack, E. C. (2014). Zooplankton community structure and dynamics in the Arctic Canada Basin during a period of intense environmental change (2004–2009). *Journal of Geophysical Research: Oceans*, *119(4)*(7), 2518–2538. https://doi.org/10.1002/2015JC010829.Received

Johansen, Ø., Reed, M., & Bodsberg, N. R. (2015). Natural dispersion revisited. *Marine*

Pollution Bulletin, *93*(1–2), 20–26. https://doi.org/10.1016/j.marpolbul.2015.02.026

Johnsen, S., Sanni, S., & Nesse, S. (2012). MASTER ’ S THESIS.

Karlsson, J., Petrich, C., & Eicken, H. (2011). Oil entrainment and migration in laboratorygrown saltwater ice, (January 2011).

Kjær, L. K. (2014). MASTER ’ S THESIS.

Li, S. (2017). *Evaluation of New Weathering Algorithms*. Retrieved from Nova Scotia

Li, Z., Spaulding, M. L., & French-McCay, D. (2017). An algorithm for modeling entrainment and naturally and chemically dispersed oil droplet size distribution under surface breaking wave conditions. *Marine Pollution Bulletin*, *119*(1), 145–152. https://doi.org/10.1016/j.marpolbul.2017.03.048

Li, Z., Spaulding, M. L., French-McCay, D. P., Tajalli-Bakhsh, T., & Jayko, K. (2017). Validation of Oil Spill Transport and Fate Modeling in Arctic Ice. *Arctic Science*, *97*(September 2017), 71–97. https://doi.org/10.1139/as-2017-0027

Liungman, O., & Mattsson, J. (2011). Scienti c documentation Seatrack Web 1 Purpose 2 Fundamentals, (March), 1–32.

Mackay, D. (1979). Finding fugacity feasbie, *3*. https://doi.org/10.1021/es60158a003

Mackay, D. (2001). *Multimedia Environmental Models*.

Mackay, D., & Paterson, S. (1981). Calculating fugacity. *Environmental Science and*

Technology, *15*(9), 1006–1014. https://doi.org/10.1021/es00091a001

Mackay, D., & Paterson, S. (1982). Fugacity revisited. *Environmental Science and Technology*, *16*(12), 654A–660A. https://doi.org/10.1021/es00106a724

Mackay, D., & Paterson, S. (1991). Evaluating the Multimedia Fate of Organic Chemicals: A Level III Fugacity Model. *Environmental Science and Technology*, *25*(3), 427–436. https://doi.org/10.1021/es00015a008

Martin, S. (1979). A Field Study of Brine Drainage and Oil Entrainment in First-Year Sea Ice. *Journal of Glaciology*, *22*(88), 473–502. https://doi.org/10.1017/s0022143000014477

Maus, S., Becker, J., Leisinger, S., Matzl, M., Schneebeli, M., & Wiegmann, A. (2015). Oil saturation of the sea ice pore space. *Proc. of the 23st International Conference on Port and Ocean Engineering under Arctic Conditions*, (JUNE), 1–12. Retrieved from http://wxreview.org/temp/POAC15/pdf/poac15Final00244.pdf

Meador, J. P., Stein, J. E., Reichert, W. L., & Varanasi, U. (1995). *Bioaccumulation of Polycyclic Aromatic Hydrocarbons by Marine Organisms*. *Reviews of Environmental Contamination and Toxicology* (Vol. 143). https://doi.org/10.1007/978-3-319-10479-9

Nazir, M. (2007). *Quantitative Risk Assessment of a Marine Riser: An Integrated Approach*.

Nazir, M., Khan, F., Amyotte, P., & Sadiq, R. (2007). Multimedia fate of oil spills in a

marine environment-An integrated modelling approach. *Process Safety and Environmental Protection*, *86*(2 B), 141–148. https://doi.org/10.1016/j.psep.2007.10.002

Nevalainen, M., Helle, I., & Vanhatalo, J. (2016). Preparing for the unprecedented — Towards quantitative oil risk assessment in the Arctic marine areas. *Marine Pollution Bulletin*, *114*(1), 90–101. https://doi.org/10.1016/j.marpolbul.2016.08.064

Petrich, C., Karlsson, J., & Eicken, H. (2013). Porosity of growing sea ice and potential for oil entrainment. *Cold Regions Science and Technology*, *87*, 27–32. https://doi.org/10.1016/j.coldregions.2012.12.002

Rand, K. M., Whitehouse, A., Logerwell, E. A., Ahgeak, E., & Parker-stetter, R. H. S. (2013). The diets of polar cod (Boreogadus saida) from August 2008 in the US Beaufort Sea, (August 2008), 907–912. https://doi.org/10.1007/s00300-013-1303-y

Reed, M., Fiocco, R., Lewis, A., Mackay, D., Brandvik, P. J., Prentki, R., … Daling, P. (1999). Oil Spill Modeling towards the Close of the 20th Century: Overview of the State of the Art. *Spill Science & Technology Bulletin*, *5*(1), 3–16. https://doi.org/10.1016/s1353-2561(98)00029-2

Reed, M., Leirvik, F., Johansen, Ø., & Brørs, B. (2009). Numerical Algorithm to Compute the Effects of Breaking Waves on Surface Oil Spilled at Sea. Final Report Submitted to the Coastal Response Research Center. Report F10968, SINTEF, Trondheim, Norway., 131. Retrieved from https://crrc.unh.edu/sites/crrc.unh.edu/files/final_report_sintef_natural_dispersion_o

ctober-2009.pdf

Sadiq, R. (2001). *Drilling Waste Discharges in the Marina Environment: A Risk Based Decision Methodology*. *Memorial University of Newfoundland* (Vol. 84). Retrieved from http://ir.obihiro.ac.jp/dspace/handle/10322/3933

Sebastiao, P., & Guedes, C. (1995). Modeling the Fate of Oil Spills at Sea. *Science*, *2*(213). https://doi.org/10.1016/S1353-2561(96)00009-6

Sharpe, S., & Mackay, D. (2000). A framework for evaluating bioaccumulation in food webs. *Environmental Science and Technology*, *34*(12), 2373–2379. https://doi.org/10.1021/es9910208

Stiver, W., & Mackay, D. (1984). Evaporation Rate of Spills of Hydrocarbons and Petroleum Mixtures. *Environmental Science and Technology*, *18*(11), 834–840. https://doi.org/10.1021/es00129a006

Sun, X., Ng, C. A., & Small, M. J. (2018). Modeling the impact of biota on polychlorinated biphenyls (PCBs) fate and transport in Lake Ontario using a population-based multi-compartment fugacity approach. *Environmental Pollution*, *241*, 720–729. https://doi.org/10.1016/j.envpol.2018.05.068

Toz, A. C., & Koseoglu, B. (2018). Trajectory prediction of oil spill with Pisces 2 around Bay of Izmir, Turkey. *Marine Pollution Bulletin*, *126*(April 2017), 215–227. https://doi.org/10.1016/j.marpolbul.2017.08.062

Venkatesh, S., El-Tahan, H., Comfort, G., & Abdelnour, R. (1990). Modelling the

behaviour of oil spills in ice-infested waters. *Atmosphere - Ocean*, *28*(3), 303–329. https://doi.org/10.1080/07055900.1990.9649380

Vergeynst, L., Wegeberg, S., Aamand, J., Lassen, P., Gosewinkel, U., Fritt-rasmussen, J., … Mosbech, A. (2018). Biodegradation of marine oil spills in the Arctic with a Greenland perspective. *Science of the Total Environment*, *626*, 1243–1258. https://doi.org/10.1016/j.scitotenv.2018.01.173

Wang, K., Leppäranta, M., Gästgifvars, M., Vainio, J., & Wang, C. (2008). The drift and spreading of the Runner 4 oil spill and the ice conditions in the Gulf of Finland, winter 2006. *Estonian Journal of Earth Sciences*, *57*(3), 181–191. https://doi.org/10.3176/earth.2008.3.06

Wania, F. (1997). Modelling the Fate of Non-Polar Organic Chemicals in an Ageing Snow Pack. *Science*, *35*(10), 2345–2363.

Wania, F., Hoff, J. T., Jia, C. Q., & MacKay, D. (1998). The effects of snow and ice on the environmental behaviour of hydrophobic organic chemicals. *Environmental Pollution*, *102*(1), 25–41. https://doi.org/10.1016/S0269-7491(98)00073-6

Webster, E., Mackay, D., Wania, F., Arnot, J., Gobas, F., Gouin, T., … Chenier, R. (2005). Development and Application of Models of Chemical Fate in Canada Modelling Guidance Document Development and Application of Models of Chemical Fate in Canada Report to Environment Canada Contribution Agreement 2004-2005 Modelling Guidance Document, (200501).

Weetman, A. N. J. S., Ousins, I. A. N. T. C., Eth, R. A. S., Ones, K. E. C. J., & Ackay, D. O. M. (2002). A DYNAMIC LEVEL IV MULTIMEDIA ENVIRONMENTAL MODEL : APPLICATION TO THE FATE OF POLYCHLORINATED BIPHENYLS IN THE UNITED KINGDOM OVER A 60-YEAR PERIOD, *21*(5), 930–940.

Wilkinson, J. P., Wadhams, P., & Hughes, N. E. (2007). Modelling the spread of oil under fast sea ice using three-dimensional multibeam sonar data. *Geophysical Research Letters*, *34*(22), 2–6. https://doi.org/10.1029/2007GL031754

Word, J. Q. (2014). Environmental Impacts of Arctic Oil Spills and Arctic Spill Response Technologies Literature Review and Recommendations. Arctic Oil Spill Response Technology Joint Industry Programme. Literature review and Recommendations.

Yang, M., Khan, F., Garaniya, V., & Chai, S. (2015). Multimedia fate modeling of oil spills in ice-infested waters: An exploration of the feasibility of fugacity-based approach. *Process Safety and Environmental Protection*, *93*(May), 206–217. https://doi.org/10.1016/j.psep.2014.04.009

Yapa, P. D., & Belaskas, D. P. (2010). Radial spreading of oil under and over broken ice: an experimental study. *Canadian Journal of Civil Engineering*, *20*(6), 910–922. https://doi.org/10.1139/l93-123

Yapa, P. D., & Chowdhury, T. (1990). Spreading of Oil Spilled Under Ice, *116*(12), 1468–1483.

Appendix I – Model's Algorithms and Calculations

1. Algorithms

The algorithms used on the model were written on MATLAB editor as follows:

```
% Evaporative loss:
dE = (1-c)*(2.67+0.06*T)/(t*60);
% Emulsification:
dY = 2e-6*(((1-c)*Ws+1)^2)*(1-Y/C3);
% Increase in viscosity:
du = C4*dE+(0.07*u/((1-C3*Y)^2))*dY;
% Natural dispersion:
dD = r*0.11*((Ws+1)^2)*(V/3600)/(1+50*s*((u*1000)^0.5)*h);
% Spreading:
if h>0.0001
    dA = (0.5/A)*(V0^1.333)*((1-c)*6.6*(g/((u/Dw)^0.5))^0.333)^2;
else
    dA = 0;
end
% Entrainment in Ice:
if h>0.0001
    dI = 5e-5*dA;
else
    dI = 0;
end
% Volume loss due to evaporation and entrainment:
if V>0.001
    if t<=tf
        dV = -V*dE-dD-dI;
    else
        dV = -Vf*dE-dD-dI;
    end
else
    dV = 0;
end
% Slick Thickness:
if h>0.0001
    dh = (dV/A)-dA*(h^2)/V;
else
    dh = 0;
end
```

```
% Fugacity air:
df1 = (f2*D21-(f1*(D12+Da1)))/(V1*Za);
% Fugacity ice:
if h>0.0001
    df2 = ((dI*Cs)+f1*D12+f3*D32-(f2*(D21+D23)))/(V2*Zi);
else
    df2 = (f1*D12+f3*D32-(f2*(D21+D23)))/(V2*Zi);
end
% Fugacity water:
if V>0.001
    df3 = ((dD*Cs)+f2*D23+f4*D43+f5*D53+f6*D63+f7*D73-
(f3*(D32+D34+D35+D36+D37+Da3+Dr3)))/(V3*Zw);
else
    df3 = (f2*D23+f4*D43+f5*D53+f6*D63+f7*D73-
(f3*(D32+D34+D35+D36+D37+Da3+Dr3)))/(V3*Zw);
end
% Fugacity sediment:
df4 = (f3*D34-(f4*(D43+Dr4)))/(V4*Zs);
% Fugacity fish:
df5 = (f3*D35+f6*Df5-(f5*(D53+Dm5+Dg5)))/(V5*Zf);
% Fugacity mysid:
df6 = (f3*D36+f7*Df6-(f6*(D63+Dm6+Dg6)))/(V6*Zm);
%Fugacity plankton:
df7 = (f3*D37-(f7*(D73+Dm7+Dg7)))/(V7*Zp);
```

Where *E, Y, u, D, A, I, V, h, f1, f2, f3, f4, f5, f6* and *f7* are the variables of interest representing the different physical processes involved and the fugacities in the different environmental media. *T, c, g, Dw, Do, mi, Ws, C3, C4, V0, s, r, Vf, tf, uw, Cs, MW, D12, D21, D23, D32, D34, D43, D35, D53, D36, D63, D37, D73, Da1, Da3, Dr3, Dr4, Df5, Dm5, Dg5, Df6, Dm6, Dg6, Dm7, Dg7, Za, Zi, Zw, Zs, Zf, Zm, Zp, V1, V2, V3, V4, V5, V6, V7* are the input parameters of the model.

2. Numerical Solution of System of Differential Equations

The system of differential equations was solved numerically using the in-built MATLAB solver ode45, which applies the following syntax: [t, y] = ode45 (odefun, tspan, y0). For the current model, the solver was written as follows:

```
[t,x] = ode45(@Oil,[0.01  43200000], x0, [], T, c, g, Dw, Do, mi,
Ws, C3, C4, V0, s, r, Vf, tf, uw, Cs, MW, D12, D21, D23, D32, D34,
D43, D35, D53, D36, D63, D37, D73, Da1, Da3, Dr3, Dr4, Df5, Dm5,
Dg5, Df6, Dm6, Dg6, Dm7, Dg7, Za, Zi, Zw, Zs, Zf, Zm, Zp, V1, V2,
V3, V4, V5, V6, V7);
```